SURFACE ENGINEERING THROUGH LOW TEMPERATURE DEPOSITION OF WEAR RESISTANT LAYERS BY REACTIVE MAGNETRON SPUTTER ION PLATING

Present By

MICHAEL JOHN AHERN

as the fulfilment of the requirement for the degree of

MASTER OF ENGINEERING

at

DUBLIN CITY UNIVERSITY

SCHOOL OF MECHANICAL & MANUFACTURING ENGG.

ACADEMIC SUPERVISOR: Professor M.S.J. Hashmi

JULY 1991.

To Miriam

DECLARATION

I declare that all the unreferred work described in this thesis is entirely my own, and no portion of the work contained in this thesis has been submitted in support of an application for another degree or qualification of this or any other university or other institute of learning.

SIGNED: _____

Michael John Ahern.

ACKNOWLEDGEMENTS

I would like to express my very sincere thanks to Dennis Teer, who introduced me to the field of thin film technology and who helped foster and encourage that interest

To Professor M S J Hashmi a special word of appreciation both for his enthusiasm and constructive criticism and for affording me the opportunity to pursue this thesis

I am especially grateful to the following· to Donnelly Mirrors Limited for funding the work programme and for permitting publication of this work, to the EC for additional funding under BRITE P-1053-1-85 and to my BRITE partners, Philips and Siemens for their generous help and technical assistance, and, lastly, to Professor N M D Brown and Dr. B. Meenan for surface analysis studies

I would like to thank my fellow co-workers during this time especially, Declan, Denis, Elaine, Hugh, Joe, Marie, Martin, Maura, Pat, Peter, Ronan, Tom and Vikki

The utmost appreciation must go to my wife, Miriam, for her love, stalwart support and, extreme patience and for the time and effort devoted to proof-reading this manuscript A special word of thanks is due to the O'Keeffe (in particular Bradford) and Ahern families for their help and support.

Finally, I would like to offer a most sincere thank you to Yvonne Wilde who typed this manuscript Her efficiency, persistence and patience in carrying out this work could not have been surpassed

Michael Ahern

July 1991

CONTENTS

ABSTRACT

SURFACE ENGINEERING THROUGH LOW TEMPERATURE DEPOSITION OF WEAR RESISTANT LAYERS BY REACTIVE MAGNETRON SPUTTER ION PLATING

by

Michael John Ahern

The aim of this investigation was the deposition of hard, wear resistant titanium nitride (TiN) thin films, produced from a reactive magnetron sputter ion plating device, at high deposition rates and low substrate temperatures. An allied objective was the understanding and development of experimental methods which would permit the deposition of titanium nitride-type layers on plastic. The early part of the work deals with the formation of TiN layers on high speed steel, at 500°C deposition temperature Modifications in equipment design and deposition procedures aided the formation of adherent TiN layers. The routine deposition of stoichiometric titanium nitride was facilitated by a control feedback network The use of graded interfaces between the film and the substrate improved adhesion. Total gas pressure and the level of substrate bias affect film hardness and wear resistance.

The next stage of the development process was the deposition of TiN at approximately 250°C substrate temperature. The main source of substrate heating, in the case of an indirectly cooled magnetron, was identified as the heat liberated from the target The use of a directly cooled magnetron configuration resulted in lower substrate temperatures With this device, TiN films were formed on high speed steel at high deposition rates and with good adhesion The increased ion current to the substrate is, tentatively, attributed to an extended

plasma region associated with the directly cooled configuration Metastable Ti_2N phases are formed from the combination of high deposition rates, low substrate temperatures (250°C) and increased ion bombardment to the substrate These TiN films, however, are softer and less wear resistant than those produced at 500°C

The final part of the investigation centred around the deposition of TiN type layers onto plastic Ti-TiN and Al-Ti-TiN layered structures were deposited onto polycarbonate plastic at 100°C An experimental design approach was employed to develop adhering coatings A slight partial pressure of oxygen during the initial Ti deposition improves film adhesion The use of the aluminium interface improves film reflectivity, cosmetic appearance and adhesion This aluminium interface makes the multilayer structure more susceptible to physical and chemical attack The wear resistance of the coated plastic is 2 to 4 times greater than the base plastic material

BIBLIOGRAPHY OF ABBREVIATIONS

amu	Atomic Mass Units
CVD	Chemical Vapour Deposition
EHT	Extra High Tension
EPMA	Electron Probe Micro Analysis
esu	Electro Static Units
DCM	Directly Cooled Magnetron
fcc	Face Centred Cubic
ICM	Indirectly Cooled Magnetron
KE	Kinetic Energy
KH	Knoop Hardness
m/e	Mass to Charge Ratio
MFC	Mass Flow Controller
MS	Mass Spectrometer
PC	Polycarbonate
PECVD	Plasma Enhanced Chemical Vapour Deposition
PVD	Physical Vapour Deposition
RMSIP	Reactive Magnetron Sputter Ion Plating
SCCM	Standard Cubic Centimetres per Minute
SEM	Scanning Electron Microscope
SIMS	Secondary Ion Mass Spectroscopy
VH	Vickers Hardness
XPS	X-Ray Photoelectron Spectroscopy
XRD	X-Ray Diffraction

CHAPTER I

INTRODUCTION

1 1 INTRODUCTION

At present there exists a wide variety of thin film deposition and thin film characterisation techniques In general, these deposition methods can be divided into two classes One class depends on the physical evaporation or ejection of material from a source, generally termed Physical Vapour Deposition (PVD) The second class depends on the deposition of a film on a surface by means of a chemical reaction occurring in a gaseous phase Usually the deposition surface is hotter (~1000^{o}C) than its surroundings so that a heterogeneous chemical reaction occurs at that surface, otherwise the reaction may take place in a homogeneous manner in the gas phase. Such chemical reactions from the vapour phase are termed Chemical Vapour Deposition (CVD). Since CVD techniques preclude low temperature deposition, no further consideration of these or allied film fabrication techniques will be pursued

Although application of the sputtering process to the deposition of thin films has been known and practiced since the first observations of Grove [1] as reported in 1852, it is only in the last two decades that this method has become a serious competitor to vacuum evaporation The long delay for sputtering to mature as a routine method in thin film deposition has been primarily the result of contamination in sputtered films and the lack of reproducible process control The latter issue will be more fully expoused in relation to this investigation, in Chapter II The focus on sputtering processes will be specifically related to the deposition of films. A broader discussion on sputtering can be found in reviews [2-7] A brief overview of glow discharges as applied to sputtering phenomena is contained in Appendix A to which the reader is referred

1 2 MAGNETRON DISCHARGES

Central to the interaction of a charged particle with a magnetic and electric field is the Lorentz Equation [8] viz ,

$$F = M \frac{dV}{dt} = q(E + V \times B)$$

F is the force on the particle, V is its velocity, q its charge, E the electric field and B the magnetic field qE is a vector parallel to E The magnetic force is given by qV x B = /V//B/SinΘ, and is directed mutually perpendicular to V and B

Consider the simple case of a charged particle moving into a constant, uniform magnetic field, such that V and B are perpendicular Since V is perpendicular to B the particle undergoes circular motion The radius described by the particle is determined by equating the magnetic force to the centrifugal force encountered in such motion, viz ,

$$Rg = (mV_+)/B\ [(Ze/c)^{-1}]$$

where m is the mass of the particle in grs, V_+ is the perpendicular velocity component cm/s, B the magnetic field in Gauss, Z the integer value of the electronic charge, e the electronic charge (e s.u statcoulombs), c velocity of light cm/s Rg is called the radius of gyration or the Larmor radius. Since the Larmor radius of the argon ion is much greater than that of the electron, it is assumed that in magnetron discharges electron motion is magnetic field dependent while ion motion is unaffected by the field Thus, ion bombardment which produces sputtering, is very similar to that which occurs in the DC diode discharge case, but electron motion is substantially changed [8]

When an electron enters a constant uniform magnetic field at an oblique angle its velocity can be separated into V_+ and $V_{//}$ components, + (perpendicular) and // (parallel) to the B field The V_+ component induces the circular motion (Lorentz Force) of the electron. The $V_{//}$ component causes the centre of rotation of the electron (termed the guiding centre) to drift with a velocity of $V_{//}$, since $V_{//}$ is unaffected by B Electrons are now confined to move along magnetic field lines with kinetic energies (KE) ½ Me ($V_+^2 + V_{//}^2$). These fields do no work on the electron and, hence, do not change its KE The electron moving in an orbiting manner produces a magnetic field which is in opposition to the B field (Lenzs Law) [9] As a consequence the plasma is strongly diamagnetic in nature

When an electron enters a mutually perpendicular E and B field the Larmor radius decreases as the electron approaches the target surfaces

and increases as the electron moves away from the target (as a result of the orientation of the electric field in the magnetron device). This motion is the **E** to **B** drift (sometimes called the electron cycloid gyration movement).

A drift, similar to the above, which is also prevalent in planar magnetron discharges is the Grad **B** drift As the magnetic field strength increases near the target surface (Grad B), the electron producing the circular motion of radius Rg is subjected to a changing magnetic field The stronger the field the smaller the Larmor radius The particular cycloid gyration (or drift) induced by this motion is mutually perpendicular to both **B** and Grad B

Finally, a particle motion associated with magnetron discharges is the "magnetic mirror" effect, which is an electron reflection that occurs when a spiralling electron moves into a strongly converging magnetic field [8] The electron moving into the converging field reduces its drift motion along the magnetic flux line, while tending to increase its rotation (so that magnetic moment is conserved). Consequently $V_{//}$ is reduced to zero resulting in the reflection of the electron out of the high flux regions of the magnetic field

The cathode/target is planar with a configuration of magnets behind the target face as depicted in Fig 1 1 This arrangement yields a tunnel-like magnetic field configuration which has the following features

a. Mid-way between the magnet poles, the magnetic field lies parallel to the plane of the cathode face Since the electric field is perpendicular to the target face, this creates an **E** to **B** region wherein the magnetron drift is created

b The **E** x **B** field formed closes on itself forming a continuous path This is a basic characteristic of magnetron discharges.

c Since the magnetic field is created from a source located behind the cathode face, the field converges near the cathode face, and further converges near the pole regions. This configuration induces both a Grad B drift and a magnetic mirror effect

d Over the magnet poles, the magnetic and electric fields are virtually parallel There is no effective electron confinement in these regions The plasma density in the region is very low, and no net sputtering occurs from this part of the cathode face

e The plasma density is maximum where the E x B field maximises This region is called the race-track Sputtering is very rapid in the race-track region

Figure 1 2 shows the electron motions which occur in the magnetron discharge In the race-track region, the electron motion is governed by the E x B drift The maximum excursion of the electrons from the cathode face is approximately 0 5 cm at the centre of the race-track The E x B drift velocity is 3 x 10^8 cm/sec The configuration confines this drift motion in a closed loop path until ionising collisions occur This is the cycloidal hopping motion indicated in this Figure Further away from the target face, the discharge electrons move in a plasma region which is substantially free of any electric field Here the electrons tend to spiral around lines of constant magnetic flux. The gradient in the magnetic field induces a drift in the race-track direction, and a magnetic mirror effect causes some electrons to be scattered back into the race-track as they approach the pole regions of the magnet configuration However, some electrons escape near the poles These electrons are accelerated by the electric field which exists here, and, since the magnetic field is parallel to the electric field in this region, the electrons can escape It is for this reason that a flux of high energy electrons escapes from the plasma in these pole regions This electron escape can be artificially enhanced by unbalancing the magnetic field with stronger magnets in these pole regions (colloquially termed "unbalanced magnetrons") These electrons can contribute to substrate heating and further gas ionisation

Sputtering of the target material in the race-track area is increased by the magnetron configuration Because of the electron trapping phenomenon magnetron discharges can be created at lower pressures (0 001 to 01 mbar) compared to DC discharges (> 0 02 mbar).

In addition to metals being deposited on the substrate surface, compounds are readily deposited upon the introduction of a reactive gas, namely nitrogen, oxygen, and hydrocarbons (producing nitrides, oxides and carbides) The technique is called "reactive magnetron sputtering" and is widely used in this investigation to deposit titanium nitride (TiN) [10,11].

1.3 ADSORPTION AND NUCLEATION PROCESSES

Adsorption of atoms onto a substrate surface may occur with (a) the partial transfer of electrons (called chemisorption) or (b) without such electron transfer (termed physisorption) Physisorption is the most basic phenomenon and adsorption occurs via unspecific and undirected weak Van der Waals forces This behaviour is reversible and typical of inert gas adsorption onto metals [12]. Mechanistically, physisorption is a prerequisite to chemisorption. Chemisorption produces a surface compound derived from the chemical reaction (through partial electron transfer) of the adsorbate with the surface Binding energies are greater than in the case of physisorption and reactions tend to be non-reversible [7]

Real surfaces are far from perfect, containing a distribution of ledges, kinks, dislocations and point defects, in addition to perfect terraces These imperfections can influence the binding of single atoms and small clusters, to the substrate and, consequently, can influence adsorption, diffusion and nucleation behaviour It is generally accepted [13] that there are three modes of film growth on surfaces, which are illustrated schematically in Fig 1.3 In the island, or Volmer-Weber model, small clusters are nucleated on the substrate surface and then grow into islands of the condensed phase. This occurs when the intra-molecular bonds between the atoms of the deposit are stronger than the inter-molecular bonds existing between the film and the substrate. This mode of growth is displayed by many systems of metals growing on insulators The layer, or Frank-van der Merwe model, displays the opposite characteristics Because the atoms are more strongly bonded to the substrate, the initial adsorbate layer condenses to form a complete monolayer on the surface which then becomes deposited with a more loosely bound layer This type of growth mechanism is observed in the case of inert gas adsorption on graphite

and in semiconductor growth on semiconductors The intermediate case of layer plus island growth is called the Stranski-Krastanov model Upon formation of the initial monolayer, or a few monolayers, subsequent layer growth is unfavourable and islands are generated on this intermediate layer Virtually any factor which disturbs the monotonic decrease in binding energy, characteristic of layer formation, may give rise to this film growth regime, e g , it may not be possible to continue the symmetry, molecular orientation or lattice parameter of the monolayer into the bulk of the deposit This results in a high free energy of the deposit-intermediate-layer interface in which subsequent island formation is preferred

1 4 STRUCTURE OF THIN FILMS

The microstructure of sputtered thin films depend on many factors some of the more important of which are.

- Deposition rate of condensing atoms
- Pressure of working gas
- Temperature of substrate
- Substrate surface roughness
- Bombardment of substrate with ions or electrons

1 4 1 Deposition Rate

It is experimentally very difficult to isolate the influence of deposition rate on film morphology from other deposition variables The sputtering rate can be increased by raising the energy of the bombarding inert gas ions producing an increase in the kinetic energy of the ejected species [14] which will be more mobile on the substrate surface The whole effect is similar to increasing the substrate temperature The continuous increase in deposition rate of Al films leads to the burial of mobile adatoms thus impeding grain growth [14] The occurrence of voided structures in metal films deposited at low deposition rates is rare because the adatom surface mobility is adequate to prevent hole formation The texture of metallic thin films is related to the kinetic energy of the incident particles or to the deposition rate Preferred orientation becomes more pronounced as the kinetic energy of the condensing atoms increases [15, 16]

1 4 2 Pressure, Temperature and Surface Roughness

In the classic article by Thornton [17] the influences of pressure, temperature and surface roughness on film structure are considered In general, higher inert gas pressures are considered to limit the mobility of surface adatoms, because adsorbed inert gas atoms limit the surface diffusion of incident species. Increased substrate temperature enhances surface mobility and conventional bulk diffusion Thornton's Model is depicted schematically in Fig 1 4. In Zone 1, surface roughness features preferentially collect incident atoms which, because of the low substrate temperature have insufficient energy to diffuse and form a continuous layer structure (the substrate temperature to substrate melting point ratio, T/Tm, is <0 2) Typical Zone 1 growth yields open, porous grain boundaries In Zone T, the surface temperature is insufficient to promote, adatom diffusion at significant rates but the surface is sufficiently flat because enough diffusion has occurred to overcome the main surface irregularities The dense, fibrous structure is identical to that generated in the open grains of Zone 1 Inert gas adsorption at increased pressure and the subsequent porous film morphology are low temperature effects Zone 2 is dominated by surface diffusion processes and the film comprises columnar grains with fully dense boundaries The high temperatures found in Zone 3 produce substantial bulk diffusion, recrystallisation and grain growth

1 4 3 Substrate Bias

Ion bombardment of a growing film can densify an otherwise porous layer [18-20] Ion bombardment invariably leads to inert gas incorporation [21,23] at high bias potentials (>150V) Low voltage bombardment generates an atomic peening effect, which produces a fresh surface, whereas high voltage bombardment increases surface roughness. For a particular film morphology, substrate temperature and bias are inversely related "high temperature" deposits may be obtained at low substrate temperatures when a substrate bias is employed [24].

1.5 STRESS IN THIN FILMS

Virtually all metallic and compound films are in a state of stress [25] The total stress is composed of a thermal stress and a so-called intrinsic stress The thermal stress is due to the differences in the thermal expansion coefficients of the coatings and the substrate materials The intrinsic stress arises from the accumulating effect of crystallographic flaws which are incorporated into the film during deposition While the intrinsic stress is a function of the deposition process, the thermal stress only forms when the film-substrate combination cools down from the deposition temperature [14] The thermal stress induced in the film is given by

$$\sigma_{th} = E_f(\alpha_f - \alpha_s)\ (Ts-Ta) \qquad 1.5\ 1$$

where E_f is the Youngs modulus, α the coefficient of thermal expansion, Ts the temperature during deposition and Ta is the temperature during measurement Subscripts f and s refer to film and substrate, respectively [26] A positive value of σ_{th} corresponds to a tensile stress

Intrinsic stresses are more complex in nature and can arise for a number of reasons [27-30]·

(a) Lattice mismatch between the substrate and film producing interfacial disorder

(b) Incorporation of impurities in the growing film which precludes the formation of a stress-free deposit.

(c) Rapid film growth leading to the deposition of the kinetically more accessible rather than the thermodynamically more stable form

(d) Forward sputtering and ballistic recoil mixing (at high bias potential) leading to vacancy and interstitial sites

The intrinsic stress in the film increases with layer thickness thus stress cracking, buckling and poor adhesion are observed when film

thickness increases such that the film substrate bond cannot withstand the force produced by the integrated stress throughout the deposit [25]

1 6 ADHESION

One of the main reasons for the failure of hard wear resistant coatings during service conditions is the lack of sufficient adhesion Adhesive strength is a function of the type of bonding across the interfacial zone [31] This bonding may be due to van der Waals forces, ionic, covalent or metallic bonds However, no predicative theory of chemical adhesion exists [32] A practical definition of adhesion states that the interfacial region does not fail under test conditions The interface is of paramount importance both in the development of the adhesive bond and in the quality of the bond between film and substrate [33]

1 6 1 The Interface

Interfacial regions may be classed as mechanical, monolayer to monolayer, compound, diffusion or pseudo diffusion and combinations of the above, as outlined in Fig 1 5 [34, 35] A mechanical interface is characterised by the mechanical interlocking of the film material with a rough surface In monolayer to monolayer (abrupt) type of interface the transition from substrate to film composition occurs over 2-5Å Such an interface forms when negligible diffusion occurs A chemical compound may form at the interface in which case a compound interface several angstroms thick is generated In diffusion interface layers, there is a gradual change in composition and lattice parameter Diffusion layers can act as transitional regions between materials possessing different mechanical and chemical properties

Ion bombardment, prior to film deposition, can increase interfacial solubility by creating high concentrations of point defects or stress gradients which enhance diffusion, resulting in the formation of pseudo-diffusion interfaces A single isolated type of interface is not generally found, combinations of the various interfacial layers are often formed simultaneously. The interface which forms is a function of the surface topography, level of contaminants, chemical reactivity

of the film and substrate material in concert with the energetics of the deposition process [7]

1.6.2 Control of Adhesion

(a) Surface Contamination

Cleaning of the substrate prior to film deposition reduces the level of surface contamination which can be detrimental to good adhesion [36] In the PVD area the substrate is commonly ultrasonically degreased in an organic solvent prior to in-situ Ar sputter etching It is also possible to remove the surface contaminants (especially oxides) by dissolution in a labile intermediate layer Several materials - notably Ti, Al, Zr - are capable of readily forming solid oxide solutions In addition, the oxides present in a surface can be used to form a chemically graded interface through the formation of chemical compounds having mutual affinity for the film and substrate. Examples of such intermediates include spinels (AB_2O_4 e g , $NiFe_2O_4$ and $MgAl_2O_4$) or ilmenites (ABO_3, A Fe, Co, Ni, Cd, Mg and B · Ti, Rh, Mn) Most of these oxides are formed in high energy deposition processes

(b) Film-Substrate Material Properties

The movements of the film will follow the elastic movements of the substrate since the coating is thin However, because of the differences in elastic moduli between the film and the substrate a stress concentration is generated at the interface [37] In applications with high loading intensity, e g , wear resistant cutting and machining tools, the stress concentration can cause cracking in the film, delamination and premature adhesion failure, and, possibly, crack initiation and propagation through the tool material. The, ab initio, matching of film substrate elastic properties or the generation of intermediate layers greatly reduces this abrupt stress gradient [32, 38].

(c) Intermediate Layers

To improve adhesion, an intermediate layer of a material which will react with both the film and the substrate is commonly employed The mechanisms of such adhesion enhancement are not fully understood [39-41], however intermediates are quite widely used In the deposition of TiN by reactive DC magnetron sputtering onto high speed steel, Ti has been used as an intermediate layer [42]. Ti can react with 34 atomic % of oxygen, therefore the weak iron oxide present on the steel can readily react with the intermediate Ti thus improving adhesion However, if this reaction temperature exceeds 400^{o}C, the adhesive strength decreases because of the reaction of the Ti with the C of the steel [43] If the Ti interface layer is excessively thick (generally >0 2-0 3μm) the adhesion strength is reduced [44] Since the capacity of Ti to withstand a shearing stress is low, thicker Ti interfaces easily fail in performance assessment tests when the applied load to the film has a shearing component

1 7 TITANIUM NITRIDE COATINGS

During the last few years there has been an increasing interest in TiN thin films deposited by various PVD methods Because PVD methods permit growth of TiN films at low temperature, a large section of the literature concentrates on deposition temperatures of 550^{o}C. The most successful application area for TiN so far is that of coatings onto various high speed steel tools Coatings with thickness of 2-10μm are found to increase tool life by many hundred per cent [45]. The use of TiN films as diffusion barriers in contact structures to silicon integrated circuits [46] and solar cells [47] have been investigated In addition, TiN has been studied for selective transparent films and for high temperature photothermal conversion [48]

Optically TiN is similar to gold in the visible region and is also used for decorative purposes [49] However, TiN has been studied in view of its other applications as single phase selective solar absorbers for high temperature use and as selective transparent films or "heat mirrors" [50]. However, in spite of the many application areas, there is still a lack of knowledge of how these films grow and of how the resulting structure and properties depend on the growth conditions.

Even though TiN is stable over a broad range of composition [51] its structure and properties depend critically on the actual composition For single phase TiN the variation with composition is mainly due to the high vacancy concentration on either the metal or the metalloid sublattices In thin film samples these effects are often more pronounced than, and different from, those in bulk materials since thin films are grown under non-equilibrium conditions [52]

It can be seen that for understoichiometric films two trends can be distinguished either the hardness increases up to a value of 3500 ± 500 kg mm^{-2} or it decreases and reaches a value of 1500 ± 200 kg mm^{-2} at a nitrogen-to-titanium ratio of 0 6 For overstoichiometric films all results show decreasing hardness values as the ratio of nitrogen to titanium increases and values as low as 340 kg mm^{-2} are reported [37, 53]

Since the dislocation mobility is low for carbides and nitrides below 1000°C the strength of the grain boundaries is an important factor in determining the hardness of polycrystalline films Also for the bulk materials, voids or microcracks have been found to be a weak point initiating crack propagation and fracture when external forces are applied [51] Films possessing voids which are located in grain boundaries thus have lower strength and lower hardness This is the case for overstoichiometric films, thus explaining the rapid decrease in hardness above (N)/(Ti) = 1 However, for films with strong grain boundaries, the plastic deformation during a hardness indentation occurs through a dislocation movement characteristic of f c c materials [51]

An increased ion bombardment during growth can result in an increased hardness mainly because of a reduction in grain size It has also been shown that the ionisation efficiency during ion plating processes should be as high as possible in order to obtain films with maximum hardness [54, 55] This implies that not only the energy of the incident particles but also the particle flux are important The ratio between the ion and metal fluxes should thus be kept as high as possible

Not only do such growth parameters as substrate temperature or ion bombardment affect the structure of the deposits, but also, for example, the substrate material itself is of importance This is especially important if the substrate contains different phases, e g a high speed steel The vanadium carbide particles in these steels have the same structure as TiN and the lattice mismatch between the two phases is only 1 6% [56] A localised epitaxial growth can then occur on these particles, resulting in a microstructure with large grains surrounded by small grains The shape of these large grains is markedly influenced by the temperature of deposition.

1 8 THE OBJECT OF THE PRESENT INVESTIGATION

Currently, deposition of TiN coatings is technically possible at various temperatures (500-800^{o}C), depending on the fabrication process employed Many technologically important substrates are damaged when exposed to these high temperatures Relatively little work has been done in the area of low temperature deposition of TiN as wear resistant layers on bulk substrates Work to date has shown that thickness distribution, adhesion stoichiometry and morphology of films are important for many industrial applications [57-59] The object of the present project is to develop the reactive magnetron sputter ion plating process to permit the deposition of

(i) hard, wear resistant TiN films on steel at deposition temperatures between 250^{o}C and 550^{o}C, and

(ii) golden coloured TiN films on polycarbonate plastic at approx. 100^{o}C substrate temperature These films would infer a wear resistance property to the plastic and also have a decorative/cosmetic appeal

Plasma enhancement of the deposition process together with modifications to the thermal impedance of the magnetron target are seen as the keys to lower temperature deposition The uniqueness of a plasma to create chemically reactive species at low temperatures is due to the non-equilibrium nature of the plasma state whereby free electrons within the plasma exhibit temperatures of tens of thousands degrees Kelvin, while the free atoms, radicals and molecules remain at

only hundreds of degrees Kelvin Plasma enhancement is common in physical vapour deposition (PVD) whereas plasmas play a key role in various ion plating configurations and allow substantial reduction in the substrate temperatures associated with traditional deposition methods

The initial part of this thesis will concentrate on depositing well adherent hard TiN layers at approx $550^{o}C$ on steel substrates The subsequent section will deal with design changes both in the deposition equipment and in the method of deposition which allow film formation at approx $250^{o}C$ on steel substrates The final section gives details of a Taguchi experiment focused on the formation of anti-scuff, decorative, golden-coloured TiN layers on plastic substrates

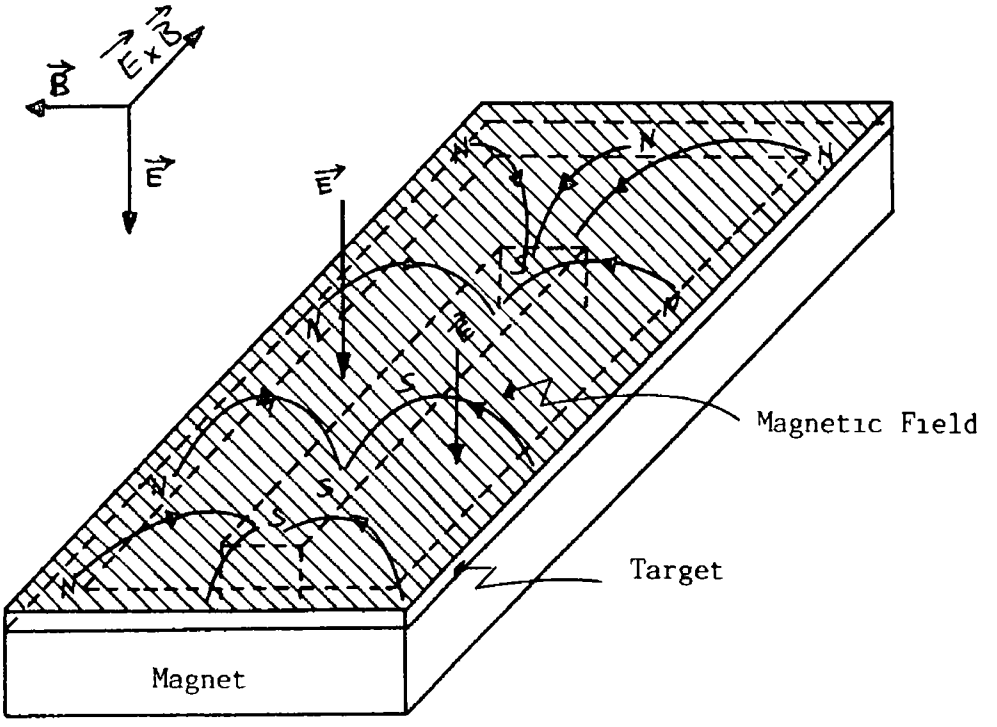

Fig 1 1 Planar magnetron configuration

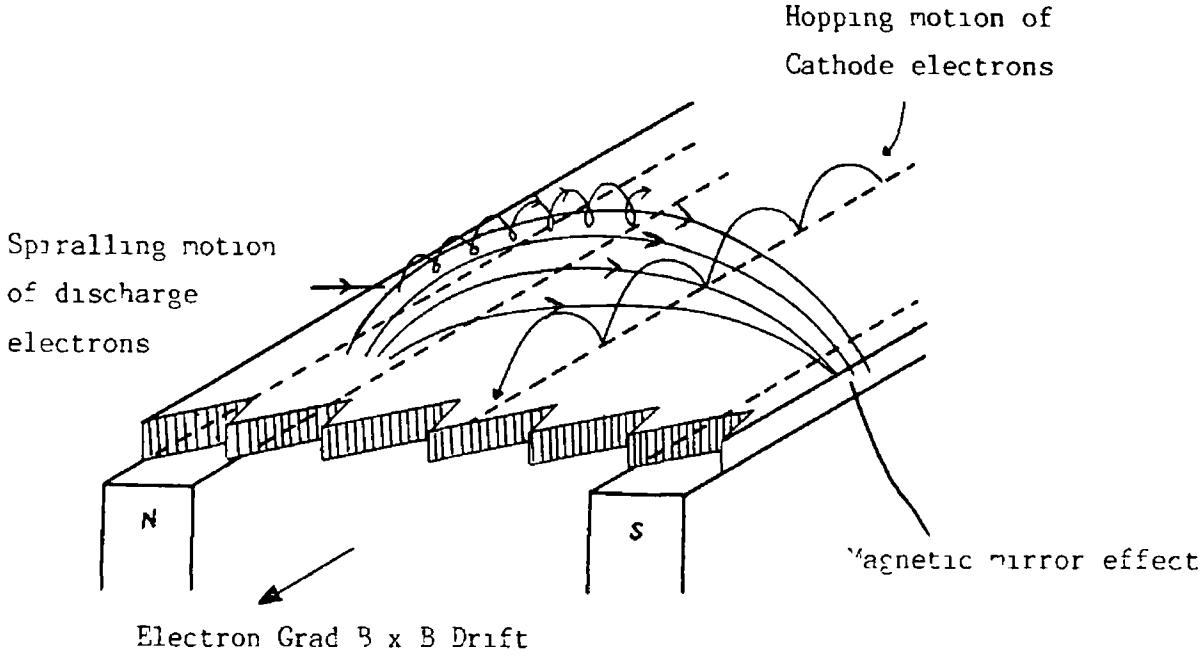

Fig 1 2 Electron motions in the planar magnetron configuration

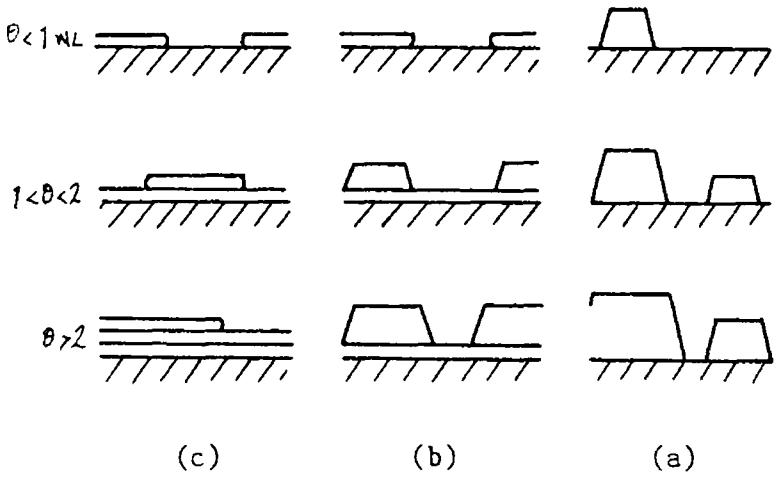

Fig 1 3 Schematic representation of the three crystal growth modes A, island or Volmer-Weber, B, layer plus island or Stranski-Krastanov, C, layer or Frank-van der Merwe mode θ represents the coverage in monolayers (ML)

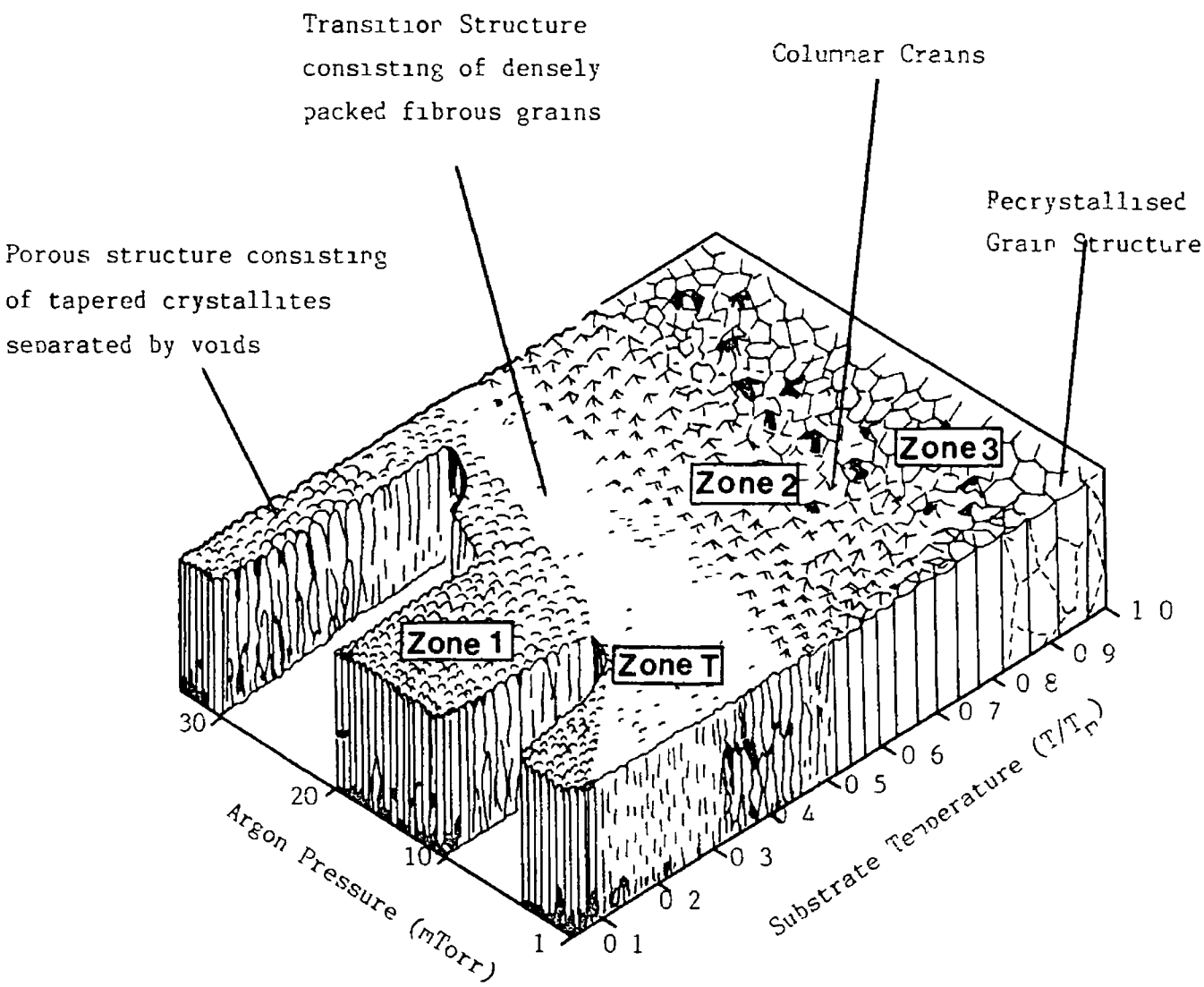

Fig 1 4 Influence of substrate temperature and Argon pressure on microstructure of sputtered films

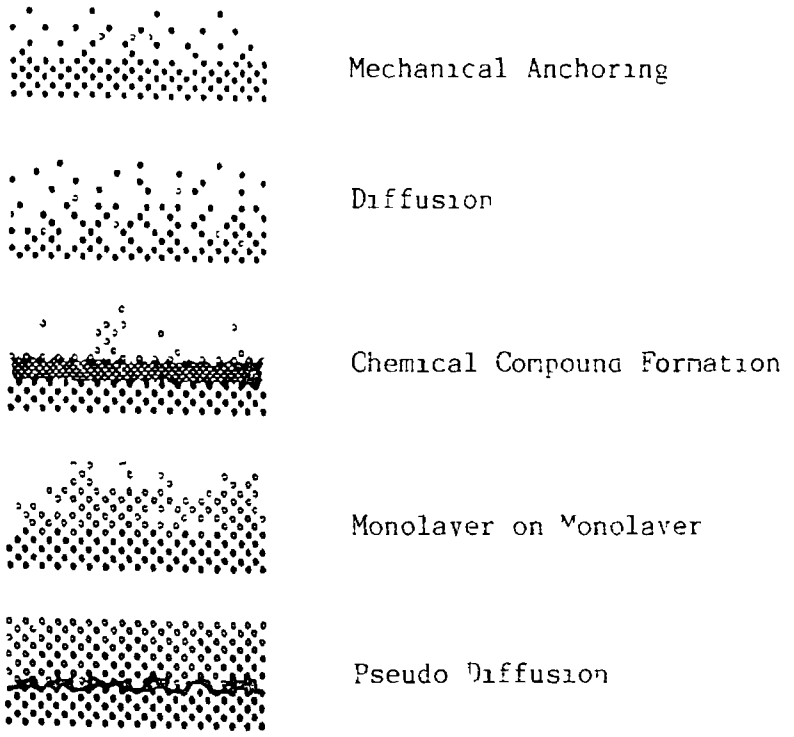

Fig 1 5 Different types of interface layers formed between film and substrate

CHAPTER II

EXPERIMENTAL EQUIPMENT PROCEDURES

2.1 REACTIVE MAGNETRON SPUTTER ION PLATING (RMSIP)

The operating principles of diode and magnetron discharge systems can be found in Appendix A and in the Introduction Chapter and, hence, will not be discussed in this chapter

2 1 1 PVD Deposition Equipment

The laboratory scale deposition apparatus, pictured in Fig 2.1, was designed, constructed and commissioned at Teer Coating Services Limited, Hartlebury, U K The vacuum chamber (A) and pumping set (B) are mounted on a tubular steel frame The chamber comprises an aluminium alloy (2042 Duralloy) top-plate (C), steel (304 stainless) base plate (D) and cylindrical stainless steel walls. The 1" thick top-plate houses two 8" x 4" magnetron cathodes (E) and two rotatable magnetron shutters (F) The substrate holder consists of an electrically isolated web of 6 x 60^{o} stainless steel sector plates (G) whose distance from the sputtering sources is adjustable A 1/6 horse-power variable speed AC motor, attached to the substrate holder through a water cooled 3" feed-through (centrally positioned in the base-plate), permits controlled rotation of the substrate at a minimum frequency of 1Hz An electrically operated screw hoist, which is fully interlocked with the pressure gauges, permits both the top-plate and chamber walls to be raised independently The liquid nitrogen cooled Edwards CR160/700 Diffstack (700l/s), backed by an Edwards E2M18 rotary pump ($40m^{3}$/hr), is mounted from an 8" port (H) in the base-plate.

5KW and 3KW Eratron DC magnetron power supplies were employed to operate the two magnetron targets (E) These generators incorporate both open-circuit and short-circuit protection together with arc suppression capabilities A 1 2KW Eratron RF (13 56 MHz) power supply with automatic load match tuning capability is used to bias insulating substrates The substrate biasing of conducting samples is achieved with an AEI 450W EHT DC (constant power) generator capable of delivering -3KV at 150mA

The working gas, usually Ar, is admitted into the deposition chamber via a Nupro needle valve (I) with vernier type readout. The flow rate of the reactive gas is controlled by a Tylan FC 260 mass flow

controller (MFC) (J) (calibrated from 0-50 standard cm^3/min , SCCM, with dry nitrogen) The total pressure in the chamber is monitored by a Balzers ionisation gauge and an Edwards pirani gauge All shut off valves and the quarter swing baffle valve are electropneumatically operated

The flexibility in design of this vacuum coater permits the deposition of a range of thin films from a number of target compositions. The substrate holder can be biased with an RF potential. This allows the deposition of thin films onto non-conducting substrates such as plastics or glass with the substrate being ion bombarded The thin films themselves, can also be non conducting, such as, silicon carbide, silicon dioxide, alumina, titania etc With the RF potential applied to the substrate, ion-plating can be achieved In this particular configuration insulating films can be ion-plated onto insulating substrates The ion-plating of conducting films onto insulating substrates e g TiN on plastic or insulating films onto conducting substrates is also possible. When the DC bias is applied to the substrate only conducting films can be ion-plated onto conducting substrates e g TiN onto HSS In this present investigation both RF and DC ion-plating were employed

The deposition of a compound film (i e a chemical compound is formed on the substrate material) can be carried out by (i) reactive magnetron sputtering and (ii) sputtering from the compound target (i e the target is the same material as the proposed thin film) Method (i) underpins the entire work of this thesis and is discussed in the relevant sections However, method (ii) has not been employed in this investigation Considering the deposition of silicon carbide, the target material comprises hot pressed silicon carbide particles when the deposition is carried out by method (ii) Since silicon carbide is, essentially non-conducting, the RF power source is connected to this magnetron target and sputtering occurs Changing the stoichiometry of the thin film requires the composition of the target material to be altered which leads to levels of inflexibility. Deposition rates are, typically, 2-3 μm/hr for insulating targets because of their low thermal conductivity and, hence, the reduced input power which can be accommodated. However, this configuration, has two main advantages The first advantage relates to the fact that this may

be the only method to deposit a film, e g such films would include PTFE (polytetrafluoroethylene), titanium dioxide, aluminium oxide, etc The second advantage is based on the fact that many ceramic oxide are non-conducting and the metal component in the ceramic is very reactive In the reactive DC magnetron deposition of such films, indium tin oxide is a particular example, target poisoning converts the target properties from those of a metallic conductor to those of an insulator from which the target does not recover When the reactive magnetron deposition is powered by an RF source this target poisoning has a minimum effect With the combination of RF and DC magnetron sources and RF and DC ion-plating capabilities a large range of substrates can be coated with a variety of films

The position of the magnetron targets can be adjusted so that multilayered coatings or three dimensional films can be deposited The multilayer coatings can be deposited from the magnetron configuration outlined in Fig 2 1 Three dimensional geometries, whose maximum volume envelope is approximately 125cm^3, can be coated by placing the magnetron on the top right hand side of the chamber directly beneath the magnetron on the top right hand side of the chamber directly beneath the left hand magnetron

The ability of the PVD coater to use RF biasing on the substrate permits limited use of the instrument as a Plasma Enhanced Chemical Vapour Deposition (PECVD) unit In this instance, the RF plasma cracks a gas or a mixture of gases and the products of the deposition fall on the substrate This instrument has been used in this configuration to deposit diamond-like-carbon (DLC) from a gaseous mixture of methane/hydrogen and acetylene/hydrogen The hybrid nature of the PECVD/PVD apparatus finds use in depositing diamond like films and boron nitride type films onto steel substrates through the use of PVD intermediate layers

The power supplies, vacuum gauges, flow monitors and all controls are fully rack mounted in an ergonomically convenient arrangement The coating unit is safety interlocked against operator misadventure, mains water, electricity and gas failure

2 1 2 Feedback Control Network

As both an aid to process parameter control and to enable stoichiometric TiN to be consistently and reproducibly deposited, a VSW 0-100 amu differentially pumped mass spectrometer (MS) was installed (refer to item K in Figure 2 1) The computer controlled mass spectrometer was used as a quantitative sensor for the presence of reactive gas in the chamber The computer then controlled the admittance of this gas through the MFC to a preset level An IBM AT computer with a Graphitek A/D card was employed in the gas control network The overall system was designed, installed and commissioned to meet specific requirements of the project [60] The feedback control and monitoring system can be briefly described as follows

The computer (refer to item L in Fig. 2 1) comprising a colour monitor, OKI printer and Graphitek A/D card was interfaced both to the MS and the MFC valve The computer is also used as a monitoring system in parallel with its control functions Magnetron current and voltage, RF forward and reflected power, total pressure, partial pressure of any gaseous species in the chamber, time, complete 0-100 a m u mass spectrographs, flow rate in SCCM are the variables which are monitored during a typical coating experiment

The facile operation of reactive processes with the RMSIP device is compounded because of the reaction occurring at the sputtering target surface in the reactive gas [61,62] When the partial pressure of the reactive gas reaches the correct level to form the stoichiometric compound on the substrate surface, a compound is also formed on the surface of the target, and a "poisoned" target surface results [63] Increasing the partial pressure of the reactive gas further increases the relative proportion of the target surface which poisons, thus resulting in reduced metal coating flux from the target In the absence of any remedial action a completely poisoned target ensues. The following mechanisms were adopted to minimise such poisoning effects

A gas separation principle was applied At coating pressures of 0.005 mbar the mean free path for nitrogen is approximately 1cm [64]. Therefore, to a first approximation the nitrogen gas inlet must be more than 1 cm from the titanium target surface In practice, the nitrogen inlet was positioned near the substrate, which is 7 cm from the target surface The argon gas inlet is located near the target surface This system exhibited greater stability with less compound formation on the magnetron target surface In addition, the amount of reactive gas in the sputtering process was controlled by the automatic feedback loop between the MS and the nitrogen (MFC) valve During the formation of a poisoned target surface, under constant current operating conditions, the potential of the magnetron undergoes changes because of differences between the electron emission coefficients of the unpoisoned and poisoned target surface The level of nitrogen in a given titanium magnetron discharge is incremented from 0 SCCM (to levels where stoichiometric and non-stoichiometric films are formed) while monitoring the target potential A typical magnetron poisoning curve is illustrated in Fig 2 2

It was observed that increasing amounts of nitrogen were required for stoichiometric TiN formation as targets aged, presumably because of the increase in the surface area of the racetrack Fine adjustments to the preset levels of nitrogen were carried out on a regular basis Computer control of the admittance of nitrogen, via the MFC valve, prevented initial nitrogen flow overshoot which was found to lead to abrupt and poorly adhering interface regions. Ramping the nitrogen admission rate improved adhesion and facilitated the formation of a graded interface The MS-MFC valve system is particularly useful at the low target sputtering currents used to achieve low substrate deposition temperatures

2 1 3 Pumpdown System

The diffusion and rotary pump combination is capable of pumping the steel chamber (approx. volume $0.1m^3$) to a base pressure of 5×10^{-5} mbar in 25 min without the aid of the cryogenic trap. The rotary pump evacuates the chamber to 0 07 mbar in 5 min at which point the diffusion pump is employed to reduce the pressure to the 10^{-5} mbar range At these pressures the main residual gas is water vapour which

pumps slowly out of the chamber, as depicted in Fig 2 3 The base pressure may be reduced to 1 x 10^{-5} mbar through the use of the liquid N_2 trap The chamber is not bakeable but after a deposition experiment where the substrate reaches 500°C the chamber subsequently pumps down to $<10^{-6}$ mbar Any air leaks in the system are noted by observing the m/e at 28 to m/e at 32 ratio When this ratio is 6 . 1 an air leak exists Leaks are located by a He sniffer with the MS tuned to mass 4

2 1.4 Magnetron Design

The housing of the magnetron is fabricated from Duralloy (2042) of side wall thickness 8 mm Cooling water inlets and outlets are located in the base-plate Ferrite magnets are placed in the water cooled cavity and oriented as outlined in Fig. 1 1 such that an outer loop of similar magnetic orientation is formed on the internal perimeter of the cavity. The central magnet is oriented in the opposite sense to those on the peripheral loop To achieve a balanced magnetic field configuration, exposed geometrical surface area of the peripheral magnets should equal that of the central magnet (In practice this is rarely achieved). In the balanced configuration the penetration of stray magnetic field lines into the vacuum chamber (and hence the bulk plasma) is reduced Such a design enables increased target usage, higher deposition rates and less electron bombardment of the substrate surface thereby reducing uncontrolled substrate heating [65] Two particular magnetron targets were employed, namely, the indirectly cooled magnetron (ICM) target and the directly cooled magnetron (DCM) target arrangement. In the ICM a 6 mm copper backing plate is fixed over the water cooled cavity Onto this backing plate a target of dimensions 7 3/4" x 4" x 3/8" is mechanically secured In Fig 2 4(A) an ICM with a slightly used Ti target is illustrated. When higher deposition rates and reduced substrate temperatures are required (as discussed in Chapter IV) the copper plate is replaced by a plate machined from a sheet of the target material An unused DCM with a Ti directly cooled target is pictured in Fig 2 4(B)

2 1 5 Sample Preparation and Pretreatment

(a) Steel Samples

Ground M2 high speed steel (HSS) and mild steel platelets, 2 5 x 2.5 x 0 3 cm, were continuously polished with silicon carbide paper, varying systematically in grit size from 400-1200 (Buehler-Met) The polishing residues were removed by ultrasonic agitation in ethanol at room temperature After hot air drying, the platelets were progressively polished on 6μm, 3μm and 1μm diamond lapping wheels (Buehler-Met) until the steel surface had a mirror finish This surface was necessary so that true adhesion effects could be studied in the absence of gross substrate roughness effects Average surface roughness (Ra) values for the polished substrates were less than 0 3μm The polished samples were ultrasonically degreased in 1,1,1, trichloroethane The air dried samples were placed on the substrate table and the chamber pumped to base pressure, and backfilled with Ar gas to a pressure of 0 02 mbar. The sputter etching of the samples was accomplished by igniting a -2kV DC Ar diode discharge between the grounded parts of the steel chamber and the steel substrate holder which acted as cathode. The temperature of the substrate was monitored by thermocouples placed in the body of the substrate table near the samples A typical sputter etch step of 30 min. duration produced a temperature increase in the steel samples of $180^{o}C$

(b) Plastic Samples

Polycarbonate (PC) samples (2 5 cm x 2 5 cm x 0.3 cm) were washed in a hot soapy aqueous solution, dried, transferred to methanol and cleaned ultrasonically for 20 min and subsequently air dried Substrates to be coated were dusted (the PC was observed to electrostatically attract fine dust particles) and placed on the rotatable substrate holder (see item G in Fig 2 1) The chamber was pumped to below 2×10^{-5} mbar before in-situ cleaning commenced at 80W RF power to the substrate holder in the presence of 0 015 mbar of Ar gas The temperature achieved by the plastic samples was related to the duration of the etch time The precise experimental details are discussed, at length, in Chapter V

2 1 6 General Description of TiN Deposition Technique

A poisoning curve similar to that outlined in Fig 2 2 is obtained by incrementally increasing the level of N_2 into a magnetron discharge, operated under the conditions necessary for the experiment In general, the current to the target, the type of target arrangement, the total gas pressure and the level of substrate bias are fixed parameters during the poisoning experiments TiN films, produced when the N_2 flow is held so that the magnetron voltage lies at position A, are under-stoichiometric in N (silver coloured), at position B the films are stoichiometric (golden coloured), and at position C the films are over-stoichiometric (copper coloured) It was necessary to operate at region B of the curve to produce stoichiometric TiN layers. The position of B in terms of the partial pressure of N_2 in the vacuum system is noted for each experiment The feedback network controls the level of N_2 gas to this fixed partial pressure

(a) TiN Formation on Metallic Substrates

In the case of steel samples, the latter were placed on the substrate arm 55-70 mm directly beneath the magnetron target surface A shutter was rotated into position between the magnetron target surface and the substrates. Upon chamber pump down to 5×10^{-5} mbar a -2KV DC potential was applied to the substrates in the presence of 0.02 mbar of Zero Grade argon gas A diode discharge was established between the substrate and the earthed walls of the vacuum chamber This sputter etching continued for 30 min and the substrate temperature increased to between $180^{o}C$ and $200^{o}C$ as measured by a thermocouple fixed to a dummy sample Since Ti has excellent gettering properties the Ti target was sputter cleaned before film formation commenced The magnetron was operated at 2 5 Amp with the coating flux being intercepted by the shutter The initial arcing (due to charge accumulation on oxidised titanium sites of the target) abated after 5 min whereupon the potential of the magnetron was approx -270V. It is evident from the poisoning curve of Fig. 2 2 that the target is oxide or nitride free and only metallic Ti is being sputtered The shutter is removed and the Ti flux is deposited on the substrates After a few minutes (typically 2-5 min) of Ti interface formation, the total Ar gas pressure is adjusted to that required for the bulk deposition

(typically between 5 to 15μbar) and the bias potential is reduced (typically about -50V to -800V) The magnetron sputter current is increased to 3 0 Amp and the automatic N_2 gas admission is activated The N_2 (99 99% pure) gas is slowly ramped to the level preset from the magnetron poisoning curve It was observed that the partial pressure of N_2 (PPN_2) in the chamber during stoichiometric TiN deposition was approx 0 9 to 1 μbar, across a broad range of coating conditions Significantly altering the magnetron current gave rise to a similar shift in the PPN_2 required for stoichiometric film formation The TiN deposition continued for 30 min with deposition rates of >1000Å/min All discharges were extinguished, the chamber was pumped to base pressure, and the samples were allowed to cool in-vacuo for 2 hours The temperature of the dummy substrate was monitored during deposition The chamber was vented to air and the coated samples removed (these samples were at a temperature of approx $50^{o}C$)

(b) TiN-Al Formation on Plastic Substrates

In the case of deposition onto plastic substrates, the chamber was pumped to below 2×10^{-5} mbar before in-situ sputter etching commenced at 80W RF power which was capacitively coupled to the substrate holder A self-biasing potential of -300V was generated on the substrates The aluminium target was sputtered at 3 Amp (from a DCM system) onto a shutter before deposition onto the PC Etching and precleaning of the aluminium target occur simultaneously for 5 min at 0 015 μbar argon pressure at the end of the etch phase The subsequent sequences in the deposition procedure are dictated by the Taguchi experiments which are discussed in detail in Chapter V The total pressure was adjusted to the required level and the Ti or Al deposition was initiated to produce the interface Overlap of the etching phase and the initial Ti interface formation improved adhesion Nitrogen gas was slowly admitted to a fixed partial pressure (as determined from the poisoning curve) via the MS-MFC network After deposition for a known period the substrates were cooled in-vacuo for 2 hrs

2 2 THIN FILM CHARACTERISATION

The characterisation of thin films can be broadly categorised into three main groups, namely, the Physical, Mechanical and Compositional characteristics

2.2.1 Physical Characterisation

(a) Crystal Structure

X-ray diffraction (XRD) studies were carried out on a JEOL JDX diffractometer employing Cu Kα(λ=0 154nm) radiation A special sample holder was fabricated such that the complete substrate is at the correct orientation to the x-ray beam The scan was operated at 1^{o}/min with medium slit size Intensities, registered as counts/sec, were plotted against 2θ in degrees The absolute peak intensities and peak intensities relative to the highest peak (taken as 100%) were noted The peak positions, reported with respect to $2\theta^{o}$, were converted to d spacings from the Bragg formula

$$d = \frac{\lambda}{2 \sin\theta}$$

These d spacings were compared with the Miller indices of TiN, Ti_2N and Fe, etc

(b) Thickness

The thickness of the deposit is routinely measured on a ball-cratering device [66] pictured in Fig 2 5 The 50 mm diameter steel ball sits in a "V" groove on a 15 mm diameter axle The speed of rotation of the shaft is variable A small amount of 1μm diamond paste is placed on the ball which is friction driven and wears a hemispherical taper section in the sample The lengths a and b are measured at 200X on an optical microscope to yield the thickness, t, of the coating as outlined in Fig 2 5 Comparison of results obtained from this evaluation compared to direct scanning electron microscope (SEM) observation of the cross sectional thickness of the film suggest that thickness data obtained from the ball cratering device are correct to within 5%. SEM thickness evaluation was primarily employed in the case of metallic coatings on plastic substrates 1 μm diameter latex

spheres (Agar Aids) were used to calibrate the SEM image when thickness measurements were performed A typical image of a metal film on plastic together with the calibration spheres is illustrated in Fig 2 6

(c) Morphology and Topography

Samples were notched from the backside in a low speed diamond saw (Behuler), then snapped, and mounted with silver dag (Agar Aids) on an SEM 45° angle stub The steel substrate - TiN film combination were electronically conducting and warranted no further treatment The TiN-Al layers on plastic substrates were coated with approx 100Å of Au in a diode sputtering device (Agar Aids) The sample temperature was <50°C during Au deposition The sample was placed at 45° to the incident electron beam and the secondary electron image detector of the SEM (JEOL-JXA 8600 Superprobe) The morphology and topography of the sample can be analysed simultaneously, as evidenced from Fig 2 6

(d) Surface Roughness

Surface texture is quantified by parameters which relate to certain characteristics of the topography The universally recognised parameter to quantify the amplitude of vertical displacements of the surface profile is the surface roughness, Ra Ra is the arithmetic mean of the departures (all departures taken as positive) of the profile from the mean line It is usually determined as the mean asperity height over several sampling intervals, n, along a length l of the specimen i e.,

$$Ra = (1/n) \{Y_1+Y_2+Y_3+. \quad Y_i+ \quad Y_n\}$$

where Y_i is the amplitude on the interval $1 < i < n$. If there is any distortion of the test sample, roughness measurement cannot be taken, due to the fact that the experimental values will not be on scale Ra values of samples were routinely measured on a profilometer.

2 2 2 Mechanical Characterisation

(a) Hardness Measurements

Hardness is defined as the resistance of a material to deformation and is usually measured by indenting a diamond stylus of known shape under load into the specimen and measuring the size of the resulting deformation Common practice among workers in the coating field is to minimise the size of the indentation in an attempt to ensure that only the hardness of the coating is measured, i e , there is no contribution to the measured hardness from the substrate In order to achieve this a criterion is often adopted in which the indentation depth for an indenter must be less than one tenth of the coating thickness [67-70], a criterion which is difficult to fulfil using standard microhardness equipment since wear resistant coatings are often deposited as layers only 3-5 μm thick

With the Vickers indenter the depth of indentation is about one-seventh of the diagonal length of the indentation The Vickers hardness number (VH) is the ratio of the load applied on the indenter to the surface area of the indentation

$$VH = (2P\sin\theta/2)/d^2$$

where P is the applied load, in kilograms, d is the mean diagonal of the square indentation in mm, and θ is the angle between opposite faces of the diamond indenter (136°) [71]. In order to keep the zone of plastic deformation caused by the indenter completely within the thin film layer the indentation diagonal, in the case of Vickers hardness measurement, must be less than the thickness of the film [37,72-74] The use of small indentations less than a few μm, places severe requirements on the resolution of the microscope optics used for the measurement In this project hardness measurements were carried out with a Knoop indenter

Knoop indentation testing is performed with a diamond ground to a pyramidal form that produces a diamond-shaped indentation having an approximate ratio between long and short diagonals of 7 to 1 The pyramid shape thus employed has an inclined longitudinal angle of 172° 30′ and an included transverse angle of 130°. The depth of indentation is about one thirtieth of its length Because of the shape of the

indenter, indentations of accurately measurable lengths are obtained with low loads The Knoop hardness number (KH) is the ratio of the load applied to the indenter to the unrecovered projected area of indentation

$$KH = P/A = P/(Cl^2)$$

where P is the applied load in kilograms, A is the unrecovered projected area of indentation, in square millimetres, l is the measured length of the long diagonal in millimetres, and C is 0 07028, a constant of the indenter relating projected area of the indentation to the square of the length of the long diagonal [69, 72] To define the reproducibility and precision of calculated hardness measurements initial tests were carried out with the Knoop indenter at different mass loadings on 10μm thick TiN films coated on HSS The results of 30 such readings at 25 gram force (grf), at 50 grf and at 100 grf are tabulated in Table 2 1 At 100 grf load the measured hardness of the 10μm thick TiN layer was 3110 Kg mm^{-2} +/- 2% at 50 grf the Knoop hardness was calculated to be 3471 Kg mm^{-2} +/- 5% and at 25 grf load 4182 Kg mm^{-2} +/- 19% Because of the geometry of the Knoop diamond the indentation depth is less than that of the Vickers diamond at the same mass loading [70] Knoop indentations from 10 grf - 500 grf loads were studied in the SEM It was evident that film penetration occurred at 500 grf load At 300 grf and less the thin layer was not pierced In Fig 2 7 an SEM of the indentation at X3000 produced by a 300 grf load is displayed Further hardness measurement determinations were performed at 100 grf loads This value was chosen because the 2% degree of reproducibility is acceptable, see Table 2 1, and provides an acceptable basis for measuring hardness of layers of 5-8μm thickness Values of Knoop and Vickers hardness at various mass loadings were correlated using the above TiN layer. Hardness calculations were performed on 10 indentations per loading in the same general area of the deposit Fig 2 8 depicts the variation of Knoop and Vickers hardness values with indenter mass loading The apparent increase in hardness with decrease in load is primarily caused by two factors [75]; these are errors in the determination of the size of the indentation and in the elastic recovery of the indentation The latter is a factor with Knoop values, but experimental studies [75] have indicated that elastic recovery of Vickers indentations is too small to explain load dependence completely In the case of Fig 2.8 it is clear that under given load/sample conditions Knoop hardness values may be related to

those of Vickers In agreement with the work of Kinosita et al [76] the hardness measured at low loads is approximately proportional to the square-root of load Fig 2 8 could be used as a method of correlating Knoop hardness to a Vickers equivalent for these films

(b) Adhesion Measurements

Among the various techniques used to examine the adhesion of thin hard films the one most widely referenced is the "scratch tester" (see Fig 2 9) The scratch test deforms the coating by drawing a hard indenter across the coated surface under an increasing normal load L as outlined schematically in Fig 2 9 The load at which the coating "flakes" (adhesive failure) or "clips" (cohesive failure), the critical load L_C as observed via an optical microscope is taken as a measure of the adhesion Critical loads for ceramics coatings on hard steel substrates are usually 40-50N [77] A hemispherical scratch diamond, which has a radius of 200 μm, initiates plastic deformation in a ceramic at a load of approx 5N and causes full plastic deformation at a load of approx 200N Critical loads are always measured where deformation under normal load would be partially or fully plastic Therefore, the indenting diamond leaves a permanent groove in the surface, which has the effect of transferring the full load to the front half of the indenter resulting in a stress increase of a factor of 2 in this region There is plastic accumulation of material ahead and to the sides of the indenter and the resulting bending of the coating causes the surface to be in tension

Partial ring cracks curved in the same sense as the front of the indenter are often observed in the scratch as can be seen in Chapter III, Fig 3 13 These cracks first form ahead of the indenter and pass beneath it on continued sliding It is commonly observed that "chipping" occurs at the edge of the scratch due to delamination of the deposit at the tensile cracks This delamination spreads both inwards and outwards under the tensile stresses which arise at the interface when the cracked material passes out of the loaded region Such stresses arise from the difference in elastic recovery of the coating and substrate Furthermore, it is likely that these failure processes are further augmented by the presence of defects and any resulting stress concentrations at the interface Substrate-film adhesion

evaluations were performed on a scratch adhesion tester (Teer Coating Services, UK) at a loading speed to traverse speed ratio of 10N/mm with an hemispherical diamond indenter of tip radius 200μm

(c) Abrasive Wear Resistance

The abrasive wear resistance of coated substrates was assessed on a modified ASTM G65 rubber wheel abrasion tester pictured in Fig 2.10 A rubber wheel tester was constructed in-house and modified to suit the measurement of abrasive wear of thin films This involves the abrading of the specimen with an abrasive grit (8μm diameter Al_2O_3 powder) which is introduced between the test specimen and the rotating rubber wheel The test specimen is pressed against the wheel at a specified force by means of a weighted lever arm while the grit abrades the surface Wear resistance is quantified in terms of the number of revolutions of the wheel, per micron thickness of the coating, which are required to achieve penetration of the film A water based slurry is used to abrade the surface less severely as the lubrication dulls any sharp surfaces of the abrasive An 8 litre water slurry of Al_2O_3 abrasive was prepared by mixing 65g Al_2O_3 in 1 litre of deionized water 14 l of this solution was placed in a container and fitted snugly beneath the rotating wheel and specimen holder The specimen was completely submerged in the slurry The moment of penetration of the abrasive wear scar into the steel substrate was particularly difficult to observe The Ti interface of the TiN deposit exhibited the same colour as the steel substrate. (In the case of the clear polycarbonate plastic substrate, film penetration was plainly visible) A 1 mol/l $CuSO_4$ solution acidified with H_2SO_4 to pH 2 was spotted onto the wear scar If an electroless deposit of Cu metal formed in the well of the wear scar then the Fe rich substrate had been exposed. This sample test was employed to determine the end of the wear test

The rubber wheel (as depicted in Fig 2 10) consists of an aluminium disc (220 mm diam x 12 mm) with a 5 mm outerlayer of chlorobutyl rubber (as defined in ASTM D2240) chemically anchored to the outer rim of the disc The wheel is driven by a 1 horse power variable speed DC motor whose rate of revolution (0-> 200 r p m) must remain constant under

load The abrader is equipped with a wheel revolution counter which is used to give the total elapsed revolutions of the wheel The counter has the ability to cut off the motor after reaching a pre-selected number of revolutions The specimen holder is attached to the lever arm to which weights may be added At the base of the machine is a basin and stirrer in which the Al_2O_3-water slurry is contained (not shown in Fig 2 10) A typical specimen is rectangular in shape, 25 x 76 mm and between 3 2 to 12 7 mm thick The size of the specimen is variable but its geometry must allow a planar face, 10 x 10 mm, to be presented to the abrading wheel

Abrasion resistance of a thin film on plastic substrates proved to be more difficult to measure in absolute terms The rubber wheel abrasion test was not discriminatory Eventually a pencil eraser was used as the abrading element, and the number of rubbing passes was counted until the coating was penetrated This test is subject to inconsistancies in human operation However, if all the tests are carried out by the one individual, then reproducible results are obtained

(d) Corrosion Resistance

A qualitative measure of corrosion resistance of TiN films coated on steel substrates was obtained from a 10 day salt spray test A 5% w/v NaCl aqueous solution, held at 35°C, is continuously sprayed over the test pieces for 10 days A gray sliding scale between 0-10 is used to access the corrosion resistance of the samples TiN films coated onto PC plastic were subjected not only to the above corrosion test but to a number of chemical corrosion tests The test pieces were submerged in concentrated acetic acid, concentrated hydrochloric acid, concentrated sulphuric acid, concentrated nitric acid and 20% w/v sodium hydroxide for given lengths of time and the condition of the test piece then noted

2 2 3 Compositional Characterisation of Thin Films

(a) Electron Microprobe Analysis

Electron Probe Microanalysis (EPMA) is a technique used to determine the local composition of solids in the near surface region The principle underpinning the technique is the excitation of characteristic X-rays by a finely focused electron beam The popular application is local analysis on regions down to a volume of approximately $1\mu m^3$, where secondary electron imaging is frequently used to select the position of analysis EPMA can be exploited to determine the elemental composition of films as thin as 0 5μm The JEOL JXA-8600 Superprobe with two wavelength dispersive spectrometers and with a LINK AN10,000 energy dispersive spectrometer is employed to carry out the EPMA investigations Within the sequence of ultra-light elements B, C, N and O, nitrogen presents particular difficulties to quantitative EPMA because (i) the N K_α radiation falls on the K-absorption edge of carbon and (ii) interference from higher order metal lines frequently occurs

(b) Secondary Ion Mass Spectroscopy

The Secondary Ion Mass Spectroscopy (SIMS) technique is a surface analytical method which employs a beam of ions to sputter secondary ions (neutrals and electrons are also produced) from a sample surface These positive and negative ions so produced are mass detected in a quadrupole mass spectrometer adjacent to the sample normal SIMS has a surface sensitivity in the ppm range and can be operated in either a "static" mode, where only the uppermost layers of the sample are sputtered, or a "dynamic" (or depth profiling) mode which implies that a fresh surface is exposed to the beam and is continually eroded away The rate of this process is a function of the incident ion beam (spot size, energy, current etc) which is under the control of the operator The mass scans, as recorded, give the intensity (count rate) of a particular mass This is not a true measure of the surface composition with regard to the particular element or fragment, since matrix (surface structural) effects determine sputtering yields for particular ions In order to produce a more quantitative picture of the surface composition it is usually necessary to use standards in order to

determine the sputtering yields for different elements in the matrix environment of interest

The ion source used for the dynamic SIMS work was a VSW DPS10 duoplasmatron system operating on oxygen focused to a 10μm spot size with an O_2^+ beam current of 75nA and beam energy of 5kV The quadrupole mass spectrometer was a Balzers QHS 511, 0-500 amu system. The necessary control, data acquisition and processing was achieved via a PC-driven software package

(c) X-ray Photoelectron Spectroscopy (XPS)

When X-rays impinge upon matter, electrons may be ejected from the material. When monoenergetic x-rays are used, the kinetic energy of the ejected electrons, E_k, is determined by the difference between the binding energy of the electron, E_b, and the energy of the x-ray photon, hυ If, then, the kinetic energy of the ejected electrons is determined, the binding energy of the electrons can be evaluated from the relationship

$$E_b = h\upsilon - E_k$$

Since the binding energies of electrons in the outer region of the atomic core depend upon the chemical environment, this method can be used to analyse several materials which are chemically similar In practice, the samples are irradiated by monoenergetic x-rays and the emitted electrons are analysed by an electron spectrometer The XPS method of analysis is primarily suitable for surface analysis because the ejected electrons are easily stopped, thus the analysis is characteristic of the top few monolayers of a surface All elements except hydrogen may be identified, and the oxidation state and bonding of the element is usually determinable The XPS spectra were obtained using a VSW twin anode TA10 x-ray source with the AlKα anode operating at 12mA and 10KV The energy analysis system comprises a VSW HA100 hemispherical analyser with a HAC5000 control unit The system is driven by a PC host computer with control of all data acquisition, storage and processing functions Binding energy calibration is based on the measurement of the Au $4f_{7/2}$ line at 83 8 eV with the resolution, at a pass energy of 25eV, typically 2 0eV

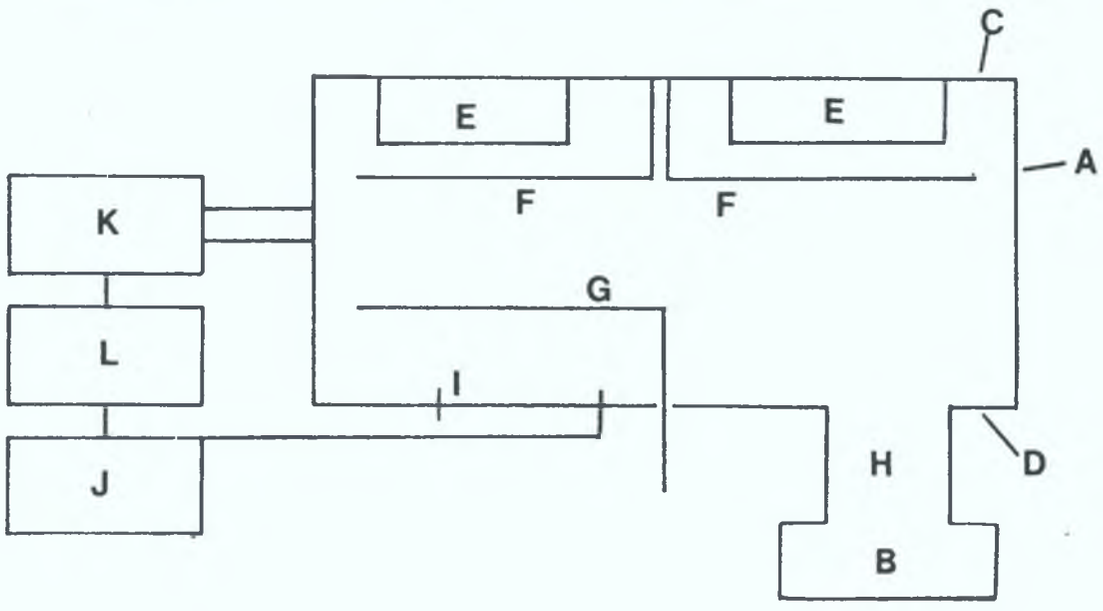

Fig. 2.1 Picture and schematic of reactive magnetron sputter ion plating equipment incorporating the mass spectrometer - mass flow controller feedback system. The key to the schematic is as follows: A, cylindrical steel vacuum chamber; B, diffusion pump and rotary pump; C, top-plate of vacuum chamber; D, steel base plate; E, magnetron cathodes; F, magnetron shutters; G, substrate table; H, pumping port and baffle valve; I, Ar gas admittance valve; J, mass flow controller; K, mass spectrometer; L, computer.

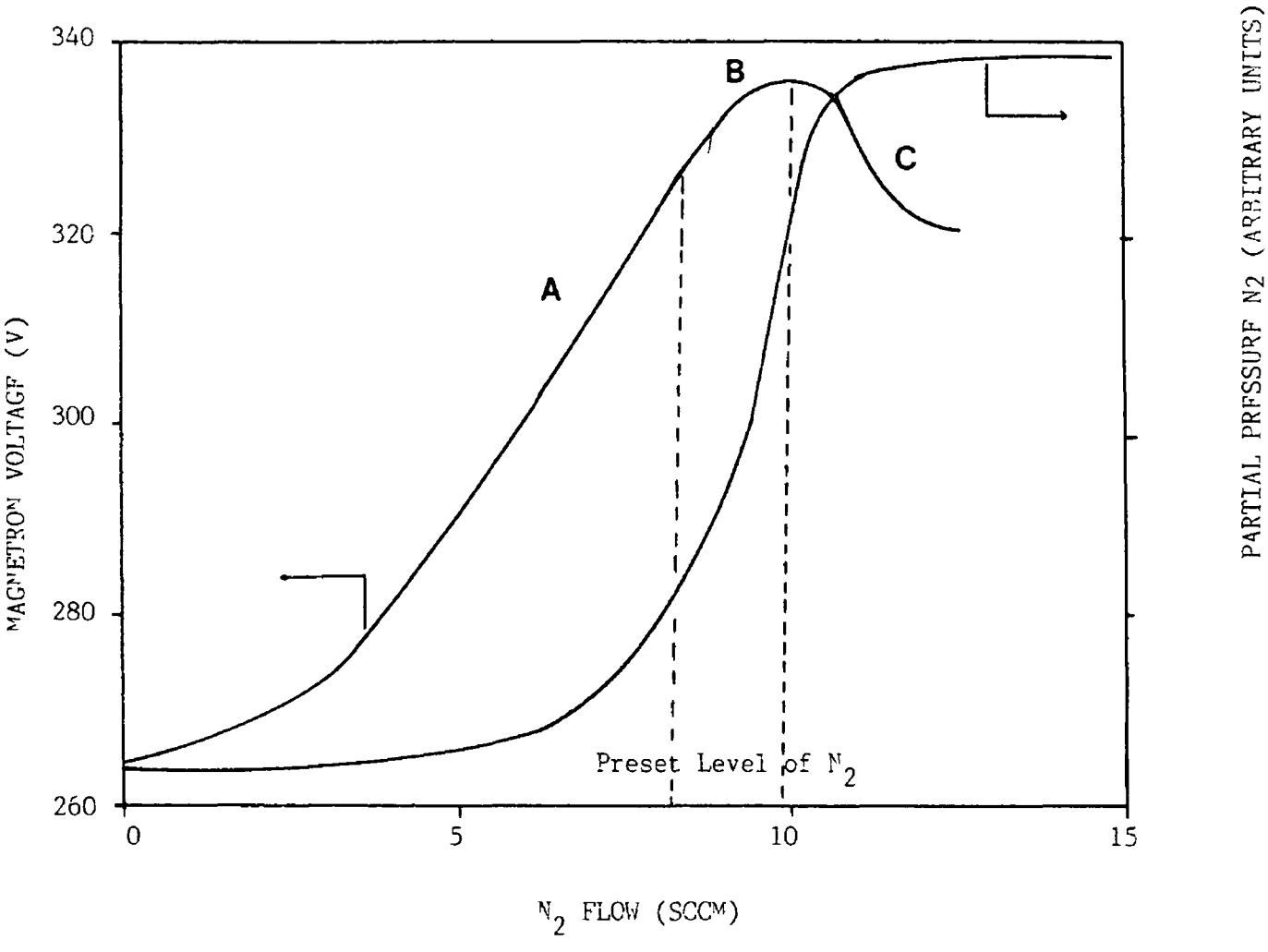

Fig 2 2 Magnetron poisoning curve for a Ti target in the presence of N_2 gas The change in magnetron voltage and N_2 partial pressure is monitored with respect to the N_2 flow-rate Regions A, B, and C are discussed in the text Total pressure was 8 μbar, 2 5 Amp magnetron current and -200V bias voltage

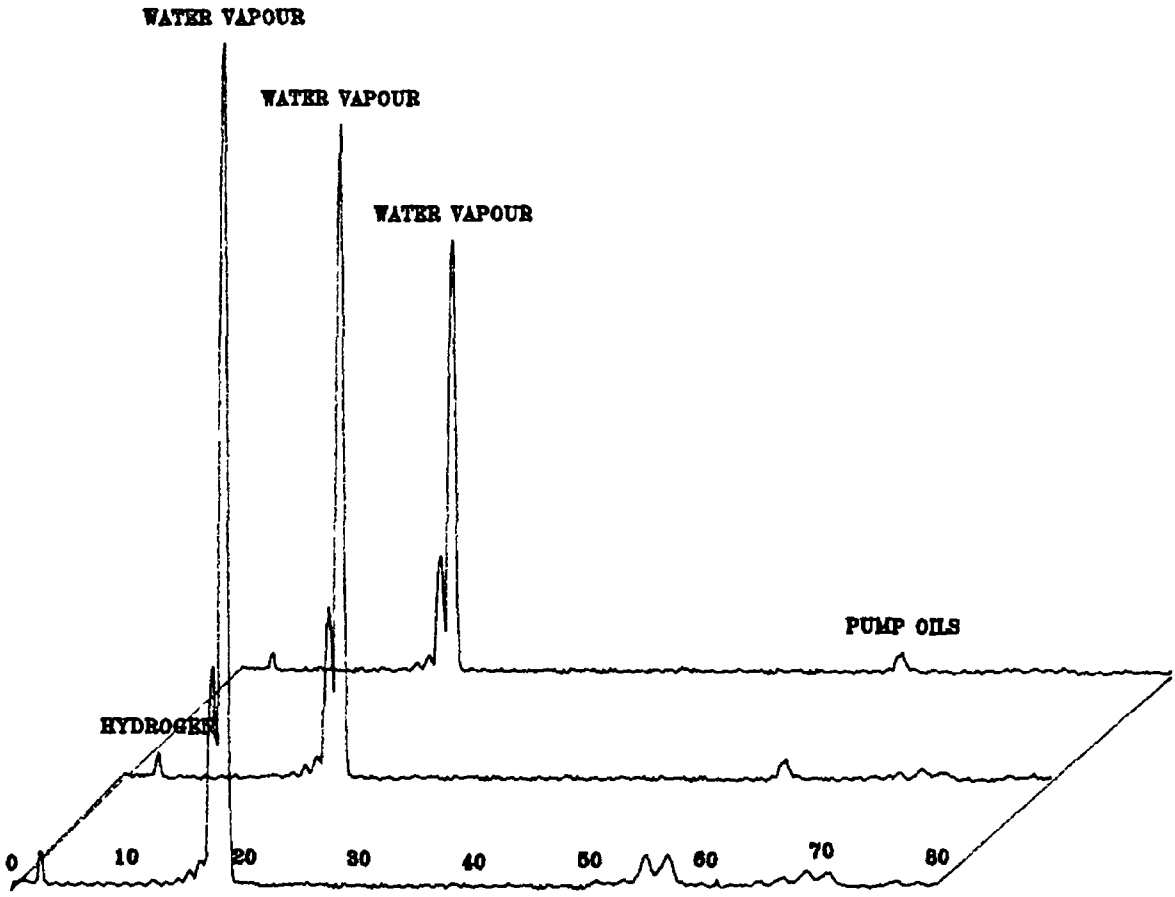

Fig 2 3 The change in the profile of the mass spectrum obtained from the vacuum chamber during diffusion pump operation The three mass spectra were taken 5, 10 and 15 min after the initiation of diffusion pumping The peak at 18 amu (assigned to water vapour) clearly decreases with pumpdown time

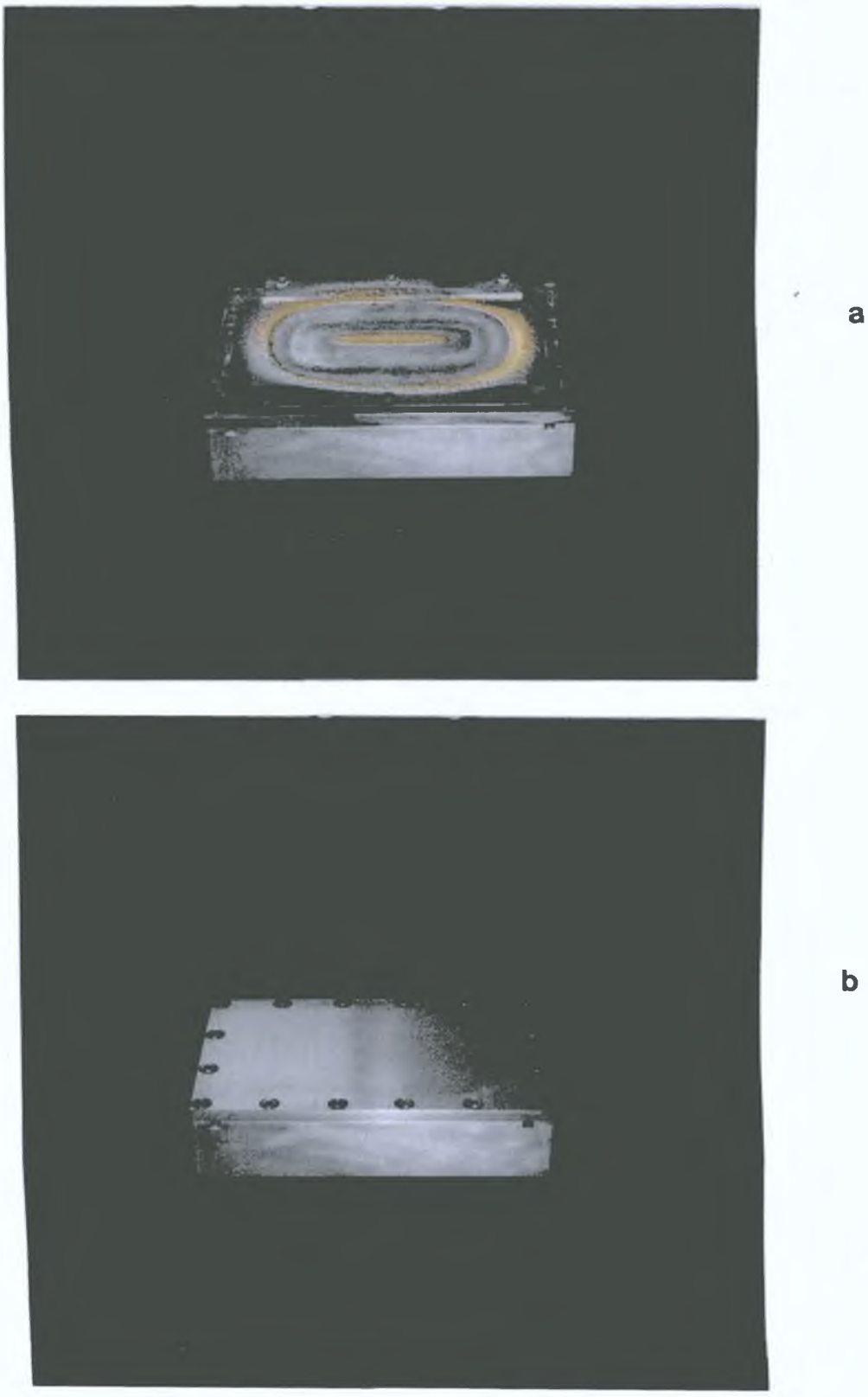

Fig. 2.4 A: Picture of the ICM with the erosion zone of a Ti target clearly visible.

B: Picture of a DCM containing an unused Ti target.

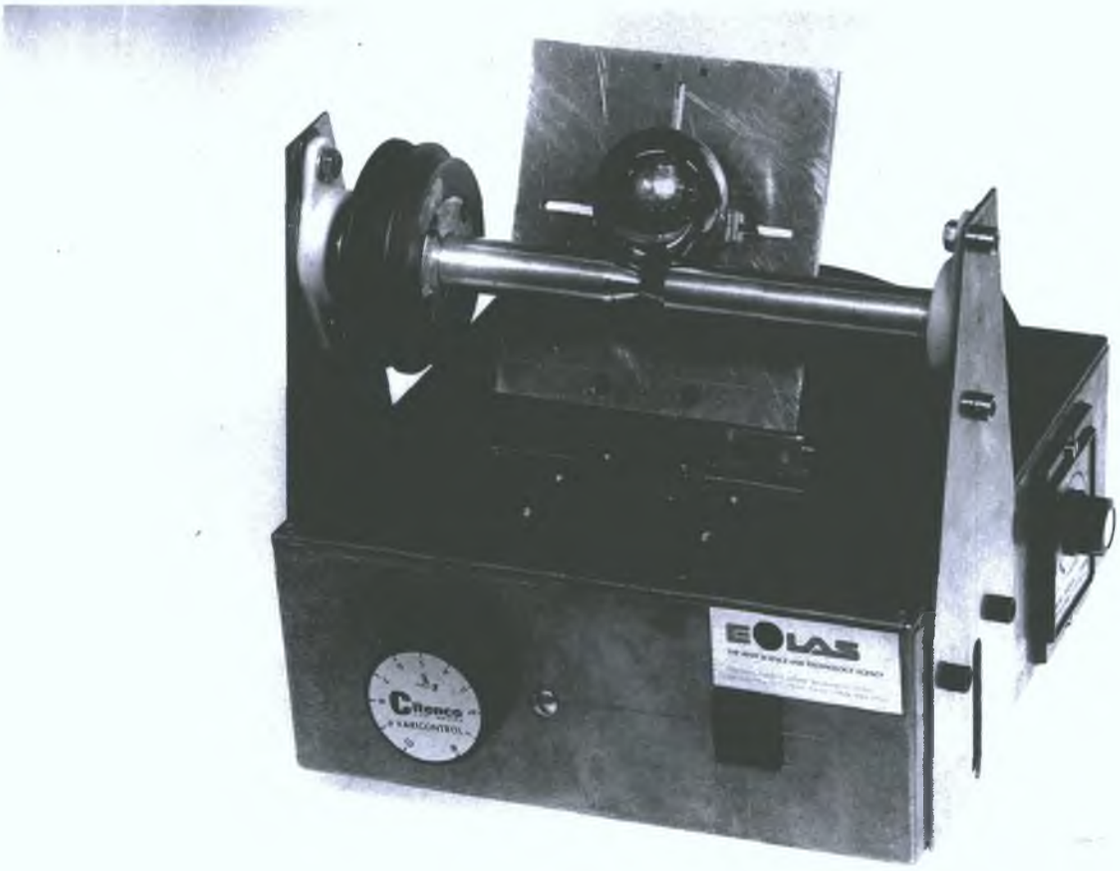

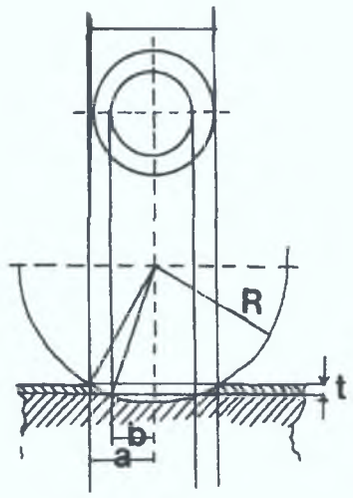

$$t = (R^2-b^2)^{\frac{1}{2}} - (R^2-a^2)^{\frac{1}{2}}$$

or

$$t = R\ (1-\frac{b^2}{R^2})^{\frac{1}{2}} - (1 - \frac{a^2}{R^2})^{\frac{1}{2}}$$

since a^2/R^2 and $b^2/R^2 \ll 10^{-3}$

then the following simplification can be used:

$$(1 - e)^n = 1 - ne$$

Therefore

$$t = \frac{1}{2R}(a^2 - b^2)$$

Fig. 2.5 Picture of the ball cratering device used to routinely and quickly measure the thickness of thin films. Distances a and b are measured with the aid of an optical microscope. The radius of the ball R, is 50,320 μm. If a, b and R are in μm the the thickness of the film, t, can be calculated in μm.

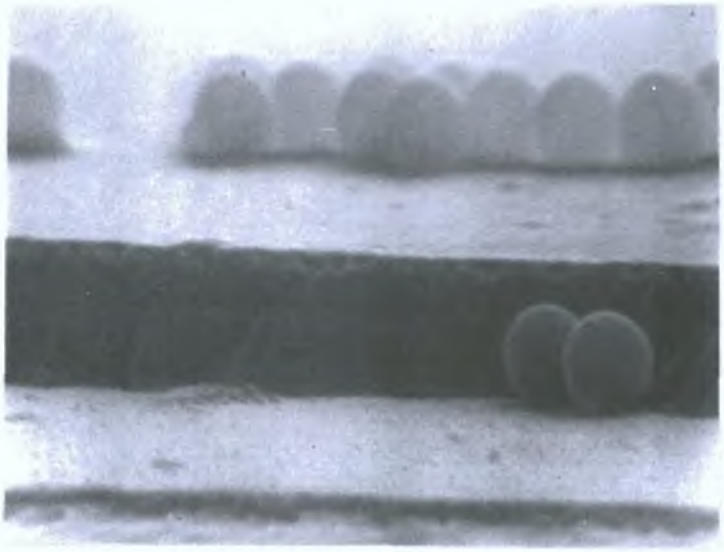

Fig. 2.6 SEM cross-section of fractured edge of metal film on which some 1μm diameter latex spheres were placed. The sample was gold coated to a thickness of ca. 100Å to reduce charging effects on the surface x 10,000.

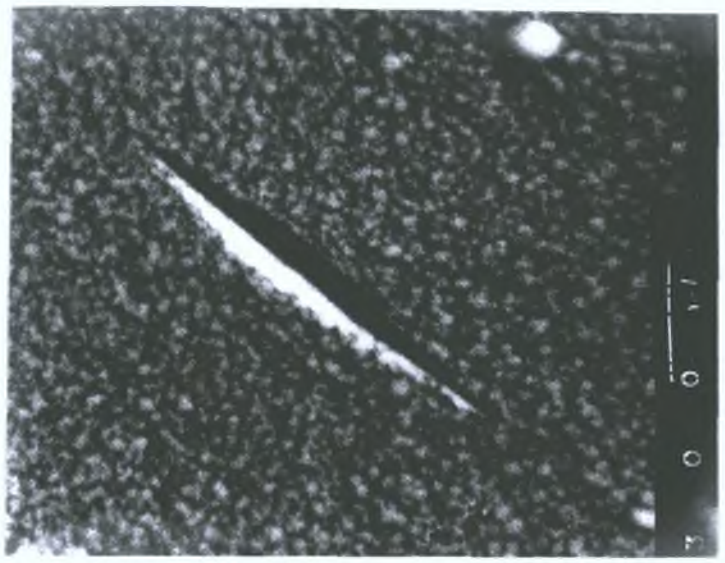

Fig. 2.7. SEM, x3000, of the surface of a TiN film showing the indentation produced by a Knoop indenter at 300grf load. The 10μm thick film was produced at -200V bias, 0.014 mbar, 480°C and 2.5A magnetron current. Substrate: HSS polished with 0.25 μm diamond paste.

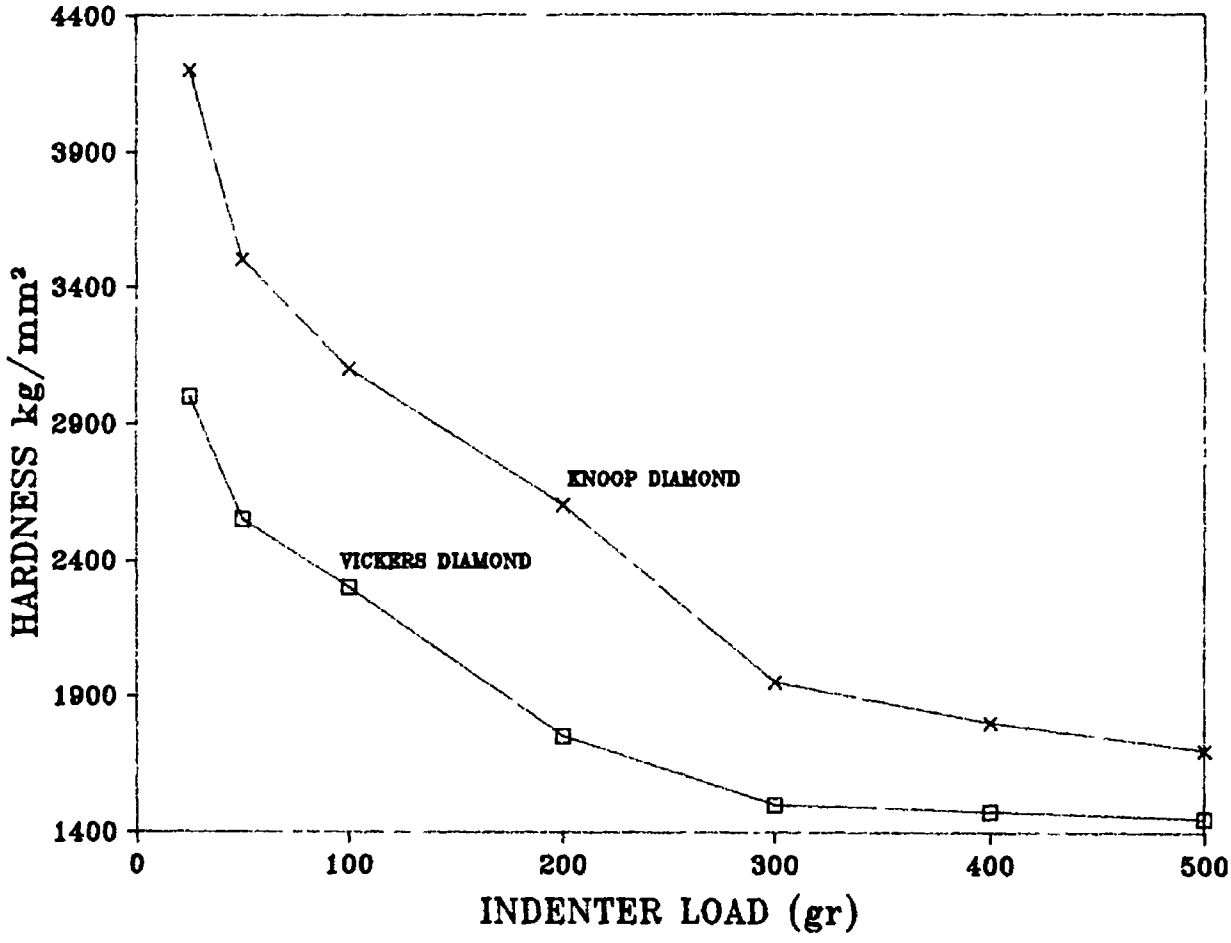

Fig 2 8 Effect of mass loading the indenting diamond, in grf, on the observed Knoop and Vickers hardness of the TiN film described in Fig 2 7. The hardness values depicted are the average of 10 readings per mass loading Indentations were localised over a small area of the film to minimise errors due to inherent variations in film hardness

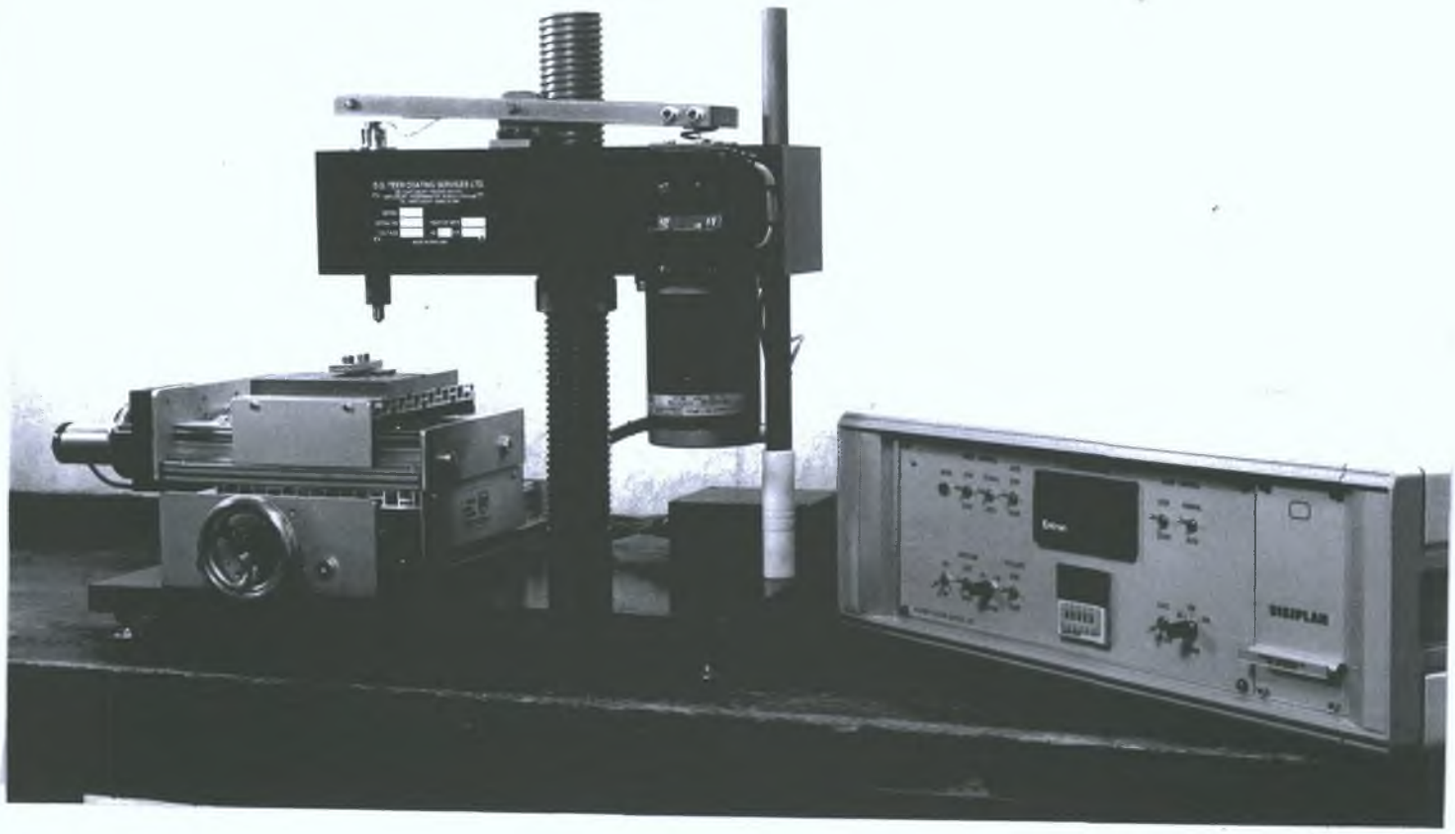

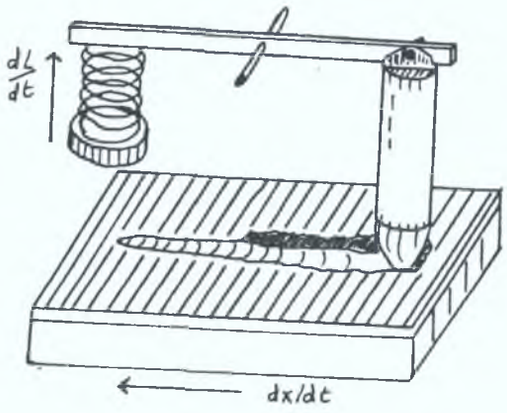

Fig. 2.9 Picture of scratch adhesion tester together with schematic view of the scratch region.

Fig. 2.10 Picture of ASTM G65 rubber wheel abrasion tester.

EXP	25 gr LOAD		50 gr LOAD		100 gr LOAD	
	DIAGONAL	KH	DIAGONAL	KH	DIAGONAL	KH
NUMBER	µm	kg/mm²	µm	kg/mm²	µm	kg/mm²
1	8 3	5164	14.8	3248	21 1	3196
2	8.4	5041	14 2	3528	21 4	3107
3	9.2	4203	14 3	3479	21.5	3078
4	10.6	3166	14.7	3292	21.5	3078
5	8 9	4491	14.7	3292	21 2	3166
6	8.4	5041	13.9	3682	21.4	3107
7	8.2	5290	14.7	3292	21.6	3050
8	10.3	3353	13.9	3682	21.5	3078
9	8.8	4593	14.2	3528	21 7	3022
10	10.2	3419	14 5	3384	21 3	3136
11	11.1	2887	14.3	3479	21	3226
12	10.8	3050	13 8	3736	21.4	3107
13	9.6	3860	13.2	4083	21 5	3078
14	9	4392	14.6	3338	21.2	3166
15	8.3	5164	13.7	3791	21 6	3050
16	10	3557	14.1	3578	21.6	3050
17	9.2	4203	14 3	3479	21.3	3136
18	8 4	5041	14 4	3431	21	3226
19	10	3557	14.9	3205	21.1	3196
20	10.6	3166	14 7	3292	21 8	2994
21	8.9	4491	14 3	3479	21.3	3136
22	8.2	5290	14.3	3479	21.5	3078
23	8 8	4593	13.9	3682	21.6	3050
24	9.6	3860	13.9	3682	21 3	3136
25	9	4392	14.8	3248	21 2	3166
26	8.9	4491	14 7	3292	21.1	3196
27	10	3557	14.1	3578	21.2	3166
28	8.3	5164	14.2	3528	21.3	3136
29	9.5	3941	13.8	3736	21 6	3050
30	10.8	3050	15	3162	21.6	3050
AVERAGE		4182		3490		3114
DEVIATION		759		206		61
% DEVIATION		18.15		5 90		1.97

Table 2 1 Knoop Hardness results at different mass loadings for 10 µm thick TiN on polished HSS Deposition conditions -200V bias, 8 µbar pressure and 2 5 Amp magnetron current

CHAPTER III

EXPERIMENTAL RESULTS AND DISCUSSIONS

THE DEPOSITION OF TIN FILMS AT APPROXIMATELY 500°C SUBSTRATE TEMPERATURE

3 1 INTRODUCTION

Titanium nitride (TiN) thin films have been studied extensively for the last decade because of their properties which find applications, primarily, as wear protective layers on cutting tools [78-81], as diffusion barriers in the semiconductor industry [82], or as low friction couples for space applications [78]. In addition, the golden appearance of TiN coatings is employed in decorative applications [53,83] Plasma assisted vapour deposition techniques (200-500^{o}C) are more suitable than chemical vapour deposition (CVD) (800-1000^{o}C) for the deposition of TiN onto hardened steels The lower substrate temperatures associated with the former method greatly increase the number and type of candidate substrate materials. The reduced substrate temperature does not degrade the mechanical properties of the steel and helps to minimise thermal stresses between the surface coating and the substrate

Reactive sputtering is widely used to deposit TiN, however, it suffers one major disadvantage When the partial pressure of the reactive gas (i e N_2) reaches the level required for stoichiometric TiN to form on the substrate a similar reaction occurs on the Ti magnetron target [63] In this "poisoned" state, increasing the partial pressure of the reactive gas further increases the relative proportion of the target surface which poisons thus resulting in reduced metal coating flux to the substrate Literature states [63,79] and experience has demonstrated that stoichiometric TiN films are readily produced on that portion of the poisoning curve where the reactive gas partial pressure increases rapidly, the so-called "transition" region Manual gas flow control can only maintain the reactive gas partial pressure in the transition region if the vacuum chamber is substantially over-pumped If target poisoning occurs the deposition rate decreases Automatic feedback control permits both high deposition rates and control of reactive gas partial pressure [61,63,84]

To obtain good adhesion between a deposited coating and a metal substrate any surface contaminants which would limit diffusion and reaction at the interface must be removed [36] In general, a degreasing step in chlorinated organic solvents removes the more loosely bound carbon based contaminants The tightly bound organics

and oxide layers are, more commonly, removed from metal substrates through an in-vacuo sputter etching process prior to reactive sputter deposition In the case of TiN deposition at 450°C, it is necessary to overlap the sputter etching process with that of the initial stages of interfacial Ti layer production. This technique ensures the formation of a continuum between the cleaned metal surface and the Ti interface layer in preparation for the TiN deposition, thus providing the graded interface necessary for improved film-substrate adhesion

TiN is widely used as a coating material for high speed cutting tools where film-substrate adhesion and high hardness are important TiN has been deposited onto M2 steel by reactive magnetron sputtering The combination of (a) the control of the rate of admission of reactive gas and (b) the control over the etching/deposition bias potential enables the facile deposition of a graded substrate-film interface The variation of film hardness with substrate bias voltage and the total gas pressure are discussed in terms of film morphology and gas scattering effects

3 2 RESULTS

A typical poisoning curve from an indirectly cooled magnetron is displayed in Fig. 2.2 showing the flow rates of N_2 which produce various levels of stoichiometric titanium-nitrogen films To obtain reproducible operating conditions producing high deposition rates and stoichiometric TiN films, the feed back control system must operate in the transition region of the poisoning curve A poisoning curve is obtained, for each given set of TiN deposition parameters, and the appropriate level of N_2 partial pressure (PPN_2) is determined to produce stoichiometric TiN This PPN_2 is used as a set point for the automatic feedback control mechanism

Three sets of thin films of TiN were produced on HSS by fixing the PPN_2 at position A, B and C of the poisoning curve displayed in Fig 2 2 The experimental conditions are outlined in the legend of Fig. 2 2 The TiN layers which were formed are photographed in Fig 3 1 The cross-sectional morphology of these films were studied in the SEM and the images recorded in Fig 3 2 The control feedback system was designed and fabricated in a separate sub-project [60] However, the

device was commissioned during the present investigations of TiN film formation at approximately 500°C It was observed that some of the early TiN films exhibited poor adhesion as evidenced from the spalling effects observed in Fig 3 3 EPMA analysis indicated that the initial Ti layer was adherent to the HSS but that the TiN layer spalled at the Ti/TiN interface Upon investigation of the rate of N_2 admission to the deposition zone there appeared to be a high degree of initial overshoot in the profile of the N_2 admission, see Fig 3 4 This overshoot was rectified by increasing the time-constant and slowing down the rate of initial N_2 injection into the deposition zone The controlled injection of N_2 and the corresponding change in PPN_2 in the chamber is depicted in Fig. 3 5 Subsequent TiN films deposited via the controlled injection of N_2 i e controlled to the level indicated from the poisoning curve in Fig 2 2, were found to be adherent to HSS and produced no evidence of delamination

The temperature acquired by the HSS substrate during a typical TiN coating deposition was monitored by means of a thermocouple fixed to an adjacent HSS dummy sample The temperature of the substrate during the Ar etch phase increased from room temperature to 180°C over the 30 min etch time, Region I of Fig 3 6 A rapid increase in substrate temperature to 420°C accompanied the deposition of TiN, refer to region II of Fig 3 6 The in-vacuo cooldown period of 2 hrs permitted the substrate temperature to decrease to approximately 100°C, see region III of Fig 3 6 A slight increase in peak substrate temperature was noted on increasing the bias voltage, but at no stage did the substrates temperature increase above 480°C

To confirm that the HSS did not soften during the TiN coating procedure, Knoop Hardness (KH) assessment of the M2 HSS before and after TiN coating was performed M2 HSS begins to soften at 550°C hence reducing the hardness of the steel [85] HSS samples were polished on both flat surfaces and the KH was evaluated at 100grf load The reverse side HSS was coated under the conditions described immediately above for the substrate temperature measurement The KH of the uncoated side of the HSS was determined at 100grf load and the results are tabulated in Table 3 1 demonstrating that no softening of the HSS occurred during RMSIP.

XPS investigation of the TiN films indicated that O, Ti, N and C were present as outlined in Fig 3 7 The relative intensities of the Ti and N bands give a value for the Ti N ratio near the film surface of close to unity

The hardness of a series of TiN films, produced on polished HSS, employing substrate bias potentials varying from -50V to -800V at a total pressure of 0 014 mbar, was investigated Six Knoop indentations at 100grf were taken for each sample and the results are displayed in Fig 3 8 Each of the coatings were a minimum of 5μm and a maximum of 8μm thick The indentation size effect [70] was minimised and could be considered negligible [67,86,87] with the combination of substrate and thick TiN film employed It was observed that the film produced at -100V bias was quite brittle and when subjected to indentation loads of 300grf developed considerable cracks about the indentation

Thickness measurements, from a ball cratering device, were routinely carried out on six locations of the coated HSS platelet One such crater is depicted in Fig 3 9 Hemispherical craters formed on the more brittle coatings displayed severe chippage on the edge of the depressions The SEM fracture cross-section of TiN films formed at -800V and -100V are detailed in Fig 3 10a and Fig 3 10b, displaying columnar and dense amorphous structures, respectively The influence of total gas pressure on the apparent hardness of TiN films was carried out at -100V bias The apparent hardness decreases as the total gas pressure is increased Fig 3 11 The structure of the deposit is altered as evidenced when Fig 3 12 is compared to Fig. 3 10b. It was observed that the critical load (Lc) tends to decrease with increasing gas pressure

Scratch adhesion measurements were carried out for each TiN layer but the results are, somewhat, inconclusive It is widely reported in the literature [88-91] that parameters such as hardness, coating thickness, substrate and coating roughness and friction coefficient affect the interpretation of the critical load results In general, the critical load values produced by adhesive failure were greater than 65N, as illustrated in Fig 3 13 Fig 3 14 shows the abrasive wear resistance of the TiN layers deposited at approximately 420-480^{o}C from the ICM target system as a function of their Knoop Hardness at 100grf load

The abrasive wear resistance is linearly related to the KH value from 2000 to 4000Kg/mm^2 but appears to deviate from linearity at 1800Kg/mm^2 Fig 3 15 displays the types of wear scars produced by the rubber wheel abrasion tester The wear scars show no obvious signs of gross film delamination or cracking In effect, a slow polishing (or mild abrasion) has taken place which did not disrupt the remainder of the film

A polished edge of a TiN coating, formed at -200V bias, was subjected to analysis by SEM X-ray wavelength spectrometry The resulting energy dot density map produced in Fig 3.16 clearly shows a gradual build-up of Ti at the interface The lack of an abrupt interface is confirmed by a O_2^+ SIMS depth profile in Fig 3 17 where a level of Ti is observed in the surface of the steel

3 3 DISCUSSION

3 3 1 The Deposition of Stoichiometric TiN

In agreement with the work of Howson [61] it was observed that the "transition" stage of the TiN poisoning curve can be made less pronounced if the magnetron is operated at high sputtering rates in a vacuum chamber pumped at high speed In Fig 2 2, the typically steep A-B transition occurs over a gradual sloping interval of 2 SCCM N_2 flow TiN films, produced when the N_2 flow is held so that the magnetron voltage lies at position A, are under-stoichiometric in N (silver coloured), at position B the films are stoichiometric (golden coloured), and at position C the films are over-stoichiometric (copper coloured) Photographs of these films are displayed in Fig 3 1 Their SEM cross-sectional morphology is clearly Zone 2 type as evidenced from Fig 3 2 As the PPN_2 increases (i e. from A-B-C) the level of columnar structure of the coatings increase (A-B-C) of Fig 3 2) in agreement with the general considerations outlined in the Thornton Diagram in Chapter I Section 1 4 2 The increase in PPN_2 increases the level of adsorbed nitrogen on the substrate thus limiting adatom surface mobilities and promoting the growth of island structures resulting in the columnar morphology observed

During the commissioning of the feedback control system, it was observed that the TiN films (deposited at approx 480°C onto HSS) delaminated, as evidenced from Fig 3 3 EPMA investigations of the spalled regions indicated that the exposed surface was Ti with no nitrogen content Thus the delamination had occurred at the interface of the initial Ti deposit and the subsequent TiN layer This type of delamination indicated that an abrupt interface had formed. The analysis of a typical N_2 admission curve can be viewed in Fig. 3.4 The level of initial overshoot of the N_2 flow rate compared to the required steady state is significant This overshoot may have generated an abrupt interface with Ti due to the formation of an over stoichiomatic TiN layer. The initial rate of N_2 admission was decreased by a software adjustment which prevented the overshoot problem The rate of admission of N_2 gas is followed closely by a concomittant increase in the PPN_2 in the vacuum chamber see Fig 3 5 On attainment of the steady-state condition, the feedback network easily controls the PPN_2 to the desired level. The gradual addition of the N_2 gas to the Ti deposition zone is intended to build a graded interface region between the initial Ti metal deposit (as described in Section 2 1 6) and the final ceramic TiN layer This graded interface would have material properties intermediate between those of Ti metal and TiN ceramic TiN films on HSS, deposited under the above regime, displayed no premature delamination

The temperature profile of the HSS substrate during a deposition cycle is outlined in Fig 3 6 The softening point of M2 HSS is 550°C therefore it is imperative that the substrate is not subjected to such temperatures during PVD deposition The 2KV Ar etch increases the substrates temperature from room to 180°C On exposure to the magnetron source (operated at 2 5 Amp) the temperature of the HSS quickly rose to 380°C and equilibrated at 420°C The in-vacuo cool down to approx 100°C was required especially with high hardness TiN films When a high hardness (i e >4200Kg/mm^2 KH at 100grf load) TiN film was taken out of the chamber immediately after deposition, the film-substrate bond broke as a result of the rapid cool down The high level of thermal stresses in the brittle TiN coatings was alleviated via the in-vacuo cool down The precaution of a 2 hour cool down period was employed as a general rule.

As a check on the deposition temperature, the KH of a sample before and after deposition was analysed From Table 3 1 it is clear that, within the error of the measurement, the KH of the steel substrate did not change during the TiN deposition process The latter indicates that the maximum temperature attained by the HSS during TiN deposition did not approach 550^{o}C [85]

XPS studies of the films (refer to Fig 3 7) revealed that the TiN stoichiometry was close to unity for all the layers produced at position B of the poisoning curve An interesting feature of this XPS investigation is that curve fitting of the Ti 2p atomic orbital region indicates the presence of three distinct Ti environments The mass spectrometer registered large levels of oxygen in the magnetron discharge immediately after switch-on Hence, the magnetron is sputter cleaned onto a shutter for some minutes to reduce the oxygen level in the initial Ti layers The presence of oxygen in the TiN layers as evidenced from XPS results in Fig 3 7 means that, in the absence of an air leak, oxygen must be generated in the plasma from the decomposition of residual water vapour (refer to Fig 2.3) and thereby incorporated into the growing TiN film The low levels of C in the film can be attributed to C species entering the plasma as a result of backstreaming of the pump oil or by the presence of advantitious carbon

3 3.2 The Effect of Deposition Parameters on TiN Film Properties

The effect of bias potential on the hardness of TiN films, produced from region B of the poisoning curve was investigated Knoop indentations at 100 grf load were studied At bias potential values greater than -100V (in a positive sense) the ion current density to the sample was >0 5 mAcm^{-2} At less than -100 volts bias the ion current density approached 1 to 1 25 mAcm^{-2} Freller [92] states that ion current densities of the order of 1 5 mAcm^{-2} and low bias voltages are required to generate hard films At these low voltage levels, high energy neutrals impinging on the growing film may sputter-forward surface atoms or etch the surface through an "atomic peening effect", thus densifying the layer [25]

At high bias voltages back sputtering (or re-sputtering) may be the more dominant mechanism At low bias voltage settings the temperature of the substrate was near 400°C As the bias was increased the substrate temperature increased The shape of the curve depicted in Fig 3 8 originates from the underlying morphology of these TiN films The Knoop hardness of 4000 Kg mm^{-2} is generated by a TiN film whose cross-sectional morphology is outlined in Fig 3 10b This particular film while apparently very hard, is also quite brittle, and hence of limited technological importance In subsequent TiN deposits produced at higher bias voltages (Fig. 3 10a is a typical example) a columnar fibrous structure is observed in the cross-sectional SEM investigation. The indentation size effect [67,86] cannot be invoked to offer an explanation to the observed hardness variation of these films, since, the thickness of these coatings lies between 5-8μm. A hemispherical indentation dimple (depression) is diagrammed in Fig 3 9 for the TiN layer produced at -200V The initial Ti deposit and subsequent TiN layer are clearly visible Thickness measurements indicate a Ti layer thickness of 1μm with a TiN layer thickness of 4μm In the case of harder films, produced with bias voltage settings of -100V, cracking at the edge of the crater was observed lending further evidence to the brittle nature of such films

The effect of total gas pressure on the resulting hardness of the TiN deposit was investigated from 5 to 40 x 10^{-3} mbar, while keeping the bias voltage at -100V At total gas pressures between 5 to 15 x 10^{-3} mbar the hardness of the TiN layer appears constant, however, the hardness of the deposit decreases dramatically at higher pressures, as shown in Fig 3 11 This is probably due to the formation of a more open columnar morphology as a result of collisional scattering and reduced surface adatom mobility These pronounced morphological changes can be clearly seen from Fig 3 12 The topography of this sample is relatively smooth as a result of the rather low bias voltage (viz , -100V) employed These films display properties of toughness with a reduced level of brittleness These films are the subject of continuing research.

The TiN films which were the subject of the graph in Fig. 3 8 were tested for their wear resistance on the ASTM G65 modified rubber wheel abrader The wear scars depicted in Fig 3 15 are typical of the

abrasive tracks produced on the TiN/HSS combinations. It must be remarked that brittle films whose hardness exceeds 4200 Kg/mm^2 possessed areas of delamination in the wear scar consistant with films having high levels of stress The variation of wear resistance with TiN film hardness is seen, from Fig 3 14, to be directly related to film hardness confirming the theory of Tabor [71] and discussed in Appendix B This decrease in slope suggests that a change in wear mechanism may have occurred The criterion, that the hardness of the abrading particle be approximately 0 8 times that of the abraded surface, may not hold when the TiN films hardness is 1800 Kg/mm^2 (refer to Appendix B for a more complete discussion of abrasive wear) In this instance severe wear of the TiN surface may occur and instead of a polishing action, associated with films whose hardness is greater than 2000 Kg/mm^2, the film surface may be subjected to a deep ploughing action from the abrasive alumina grit

3 3 3 Adhesion of TiN to High Speed Steel

In general, the Lc observed for TiN coatings on steel, produced at various substrate bias, was 50-70N These films, with Knoop hardness less than 3000 $kgmm^{-2}$, failed the scratch adhesion test by the same adhesive failure mode, see Fig 3 13 The broken rings on the indentation track being consistent with the film piling up ahead of the indenter and passing beneath it on continued sliding A more complete description of this phenomenon can be found in reference [93] In the harder TiN films, the scratch failure mode was cohesive, indicating the higher levels of stress in these thin films. It is difficult to draw firm conclusions about the level of adhesion of these coatings to the steel substrate because the scratch test results are influenced by the thickness of the coating, its coefficient of friction against the indenter and the morphology of the layer, etc [88] Those films which failed by an adhesive failure mechanism produced critical load values of 65-70N The TiN layer formed at -200V bias and 14 x 10^{-3} mbar was fractured, mounted in bakelite, and polished with diamond paste A Ti distribution density map (obtained by x-ray wavelength spectrometers in the SEM) was taken of the polished region and is reproduced in Fig 3 16 It is clear that an indistinct interphase region exists between

the steel substrate and the TiN layer (Extreme precautions were taken during the polishing procedure to minimise spill-over of the Ti into the steel) This investigation was further embellished by submitting the same TiN film to an O_2^+ ion SIMS depth profile from the top of the TiN surface through to the steel substrate Two interface regions can be clearly distinguished in Fig 3 17, namely, the TiN/Ti and the Ti/steel In the case of the TiN/Ti interface, it appears that the gradual addition of N_2 gas into the Ti sputtering flux produces the desired graded interface (Note, also, the differences in the Ti ion yield in the TiN and Ti layers) This may be related to the sputtering yield of Ti form both of these matrices when an O_2^+ ion beam is employed. Based on a composite film thickness of 5μm and an O_2^+ etch rate of approximately 100Å/min , the TiN/Ti interphase layer approximates to 0 4μm in thickness In a similar manner, the Ti/steel interphase can be measured as approximately 0 3μm in thickness The embedding of the Ti into the steel is clear from the onset of the Fe profile which indicates the beginning of the steel surface, thus, confirming the earlier Ti density map studies of Fig 3 16 By overlapping the plasma etching/cleaning conditions with the onset of initial Ti deposition, a graded interface was formed which produced improved film-substrate adhesion

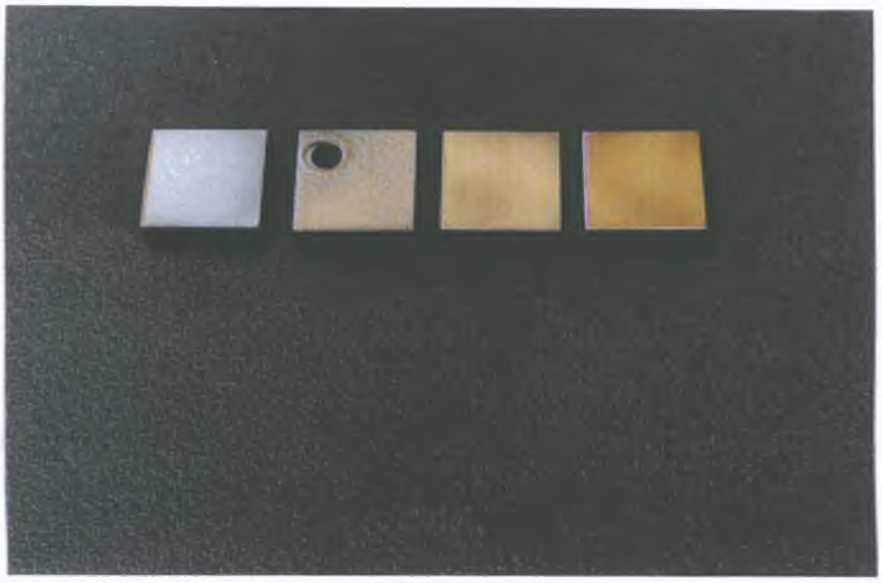

Fig. 3.1 Photograph of (from l to r): polished 2.5 x 2.5 x 0.3 cm M2 HSS; A, under-stoichiometric TiN film; B, stoichiometric TiN film; C, over-stoichiometric TiN. A,B and C refer to regions of Fig. 2.2 and are discussed in the text.

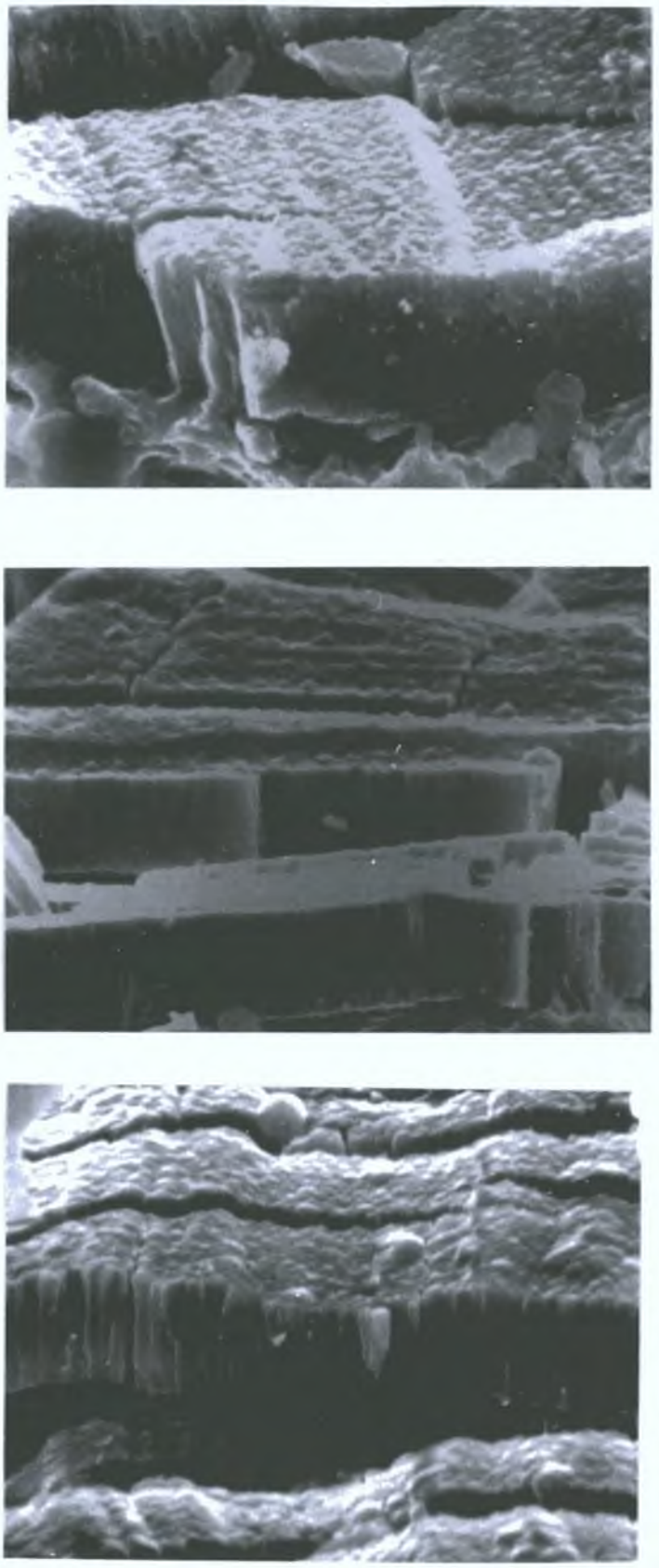

Fig. 3.2 SEM cross-sectional morphology of the films outlined in Fig. 3.1 (x4000).

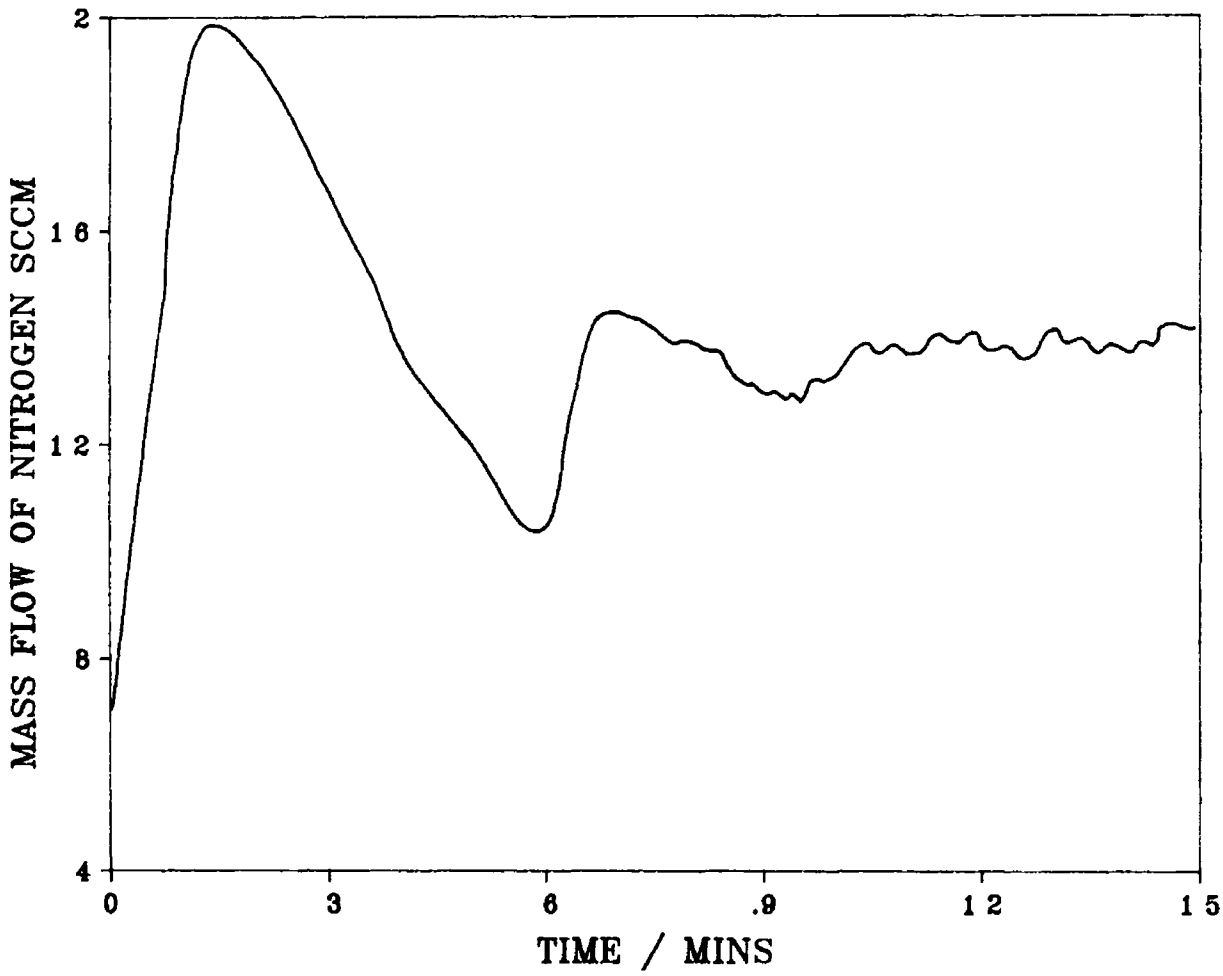

Fig 3 4 Variation of flow of N_2 with time for a typical TiN reactive magnetron deposition, showing the overshoot feature discussed in the text

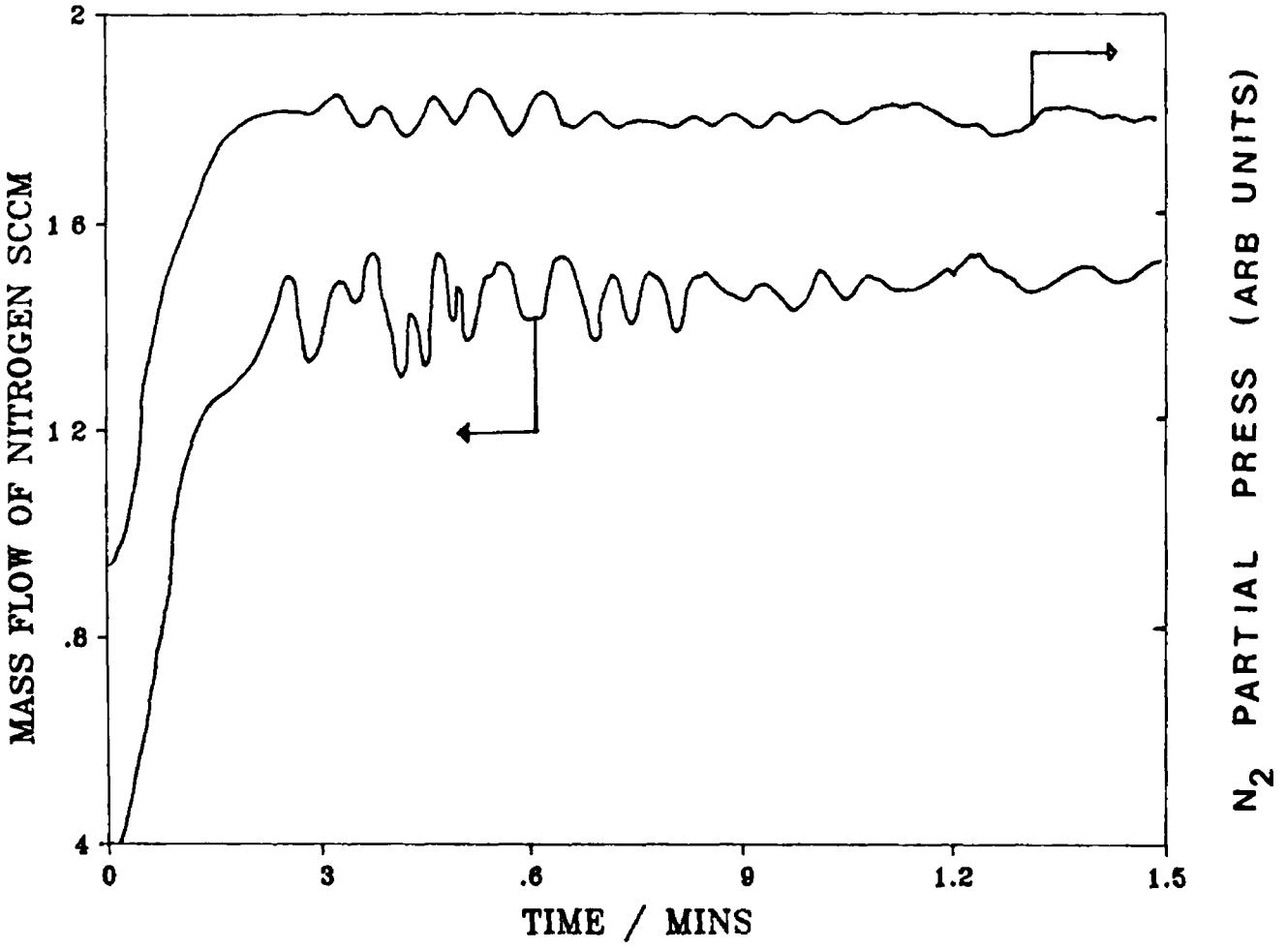

Fig 3 5 The variation in the controlled levels of N_2 admission and the corresponding change in PPN_2 after the software correction to prevent the overshoot

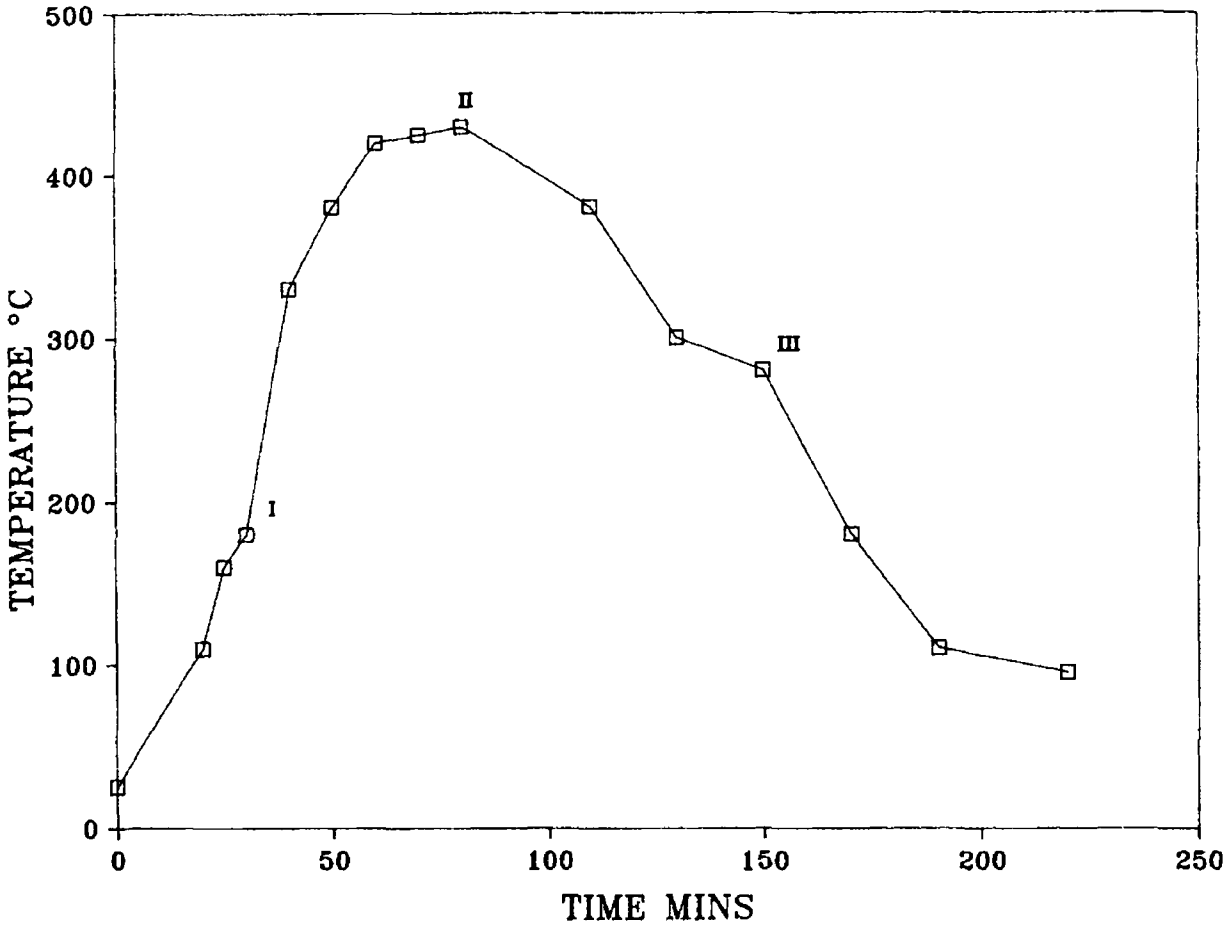

Fig 3 6 Profile of substrate temperature during TiN deposition cycle Coating conditions -2KV Ar sputter etch for 30 min - Region I, 5 min deposition of Ti with gradual introduction of N_2, 2 5 Amp magnetron current, deposition time 60 min - Region II, in-vacuo cool-down for 2 hr - Region III

Fig 3 7 The XPS survey scan indicates the presence of O, Ti, N, and C on the sample surface The relative Ti and N corrected intensities give a Ti N ratio of approximately unity

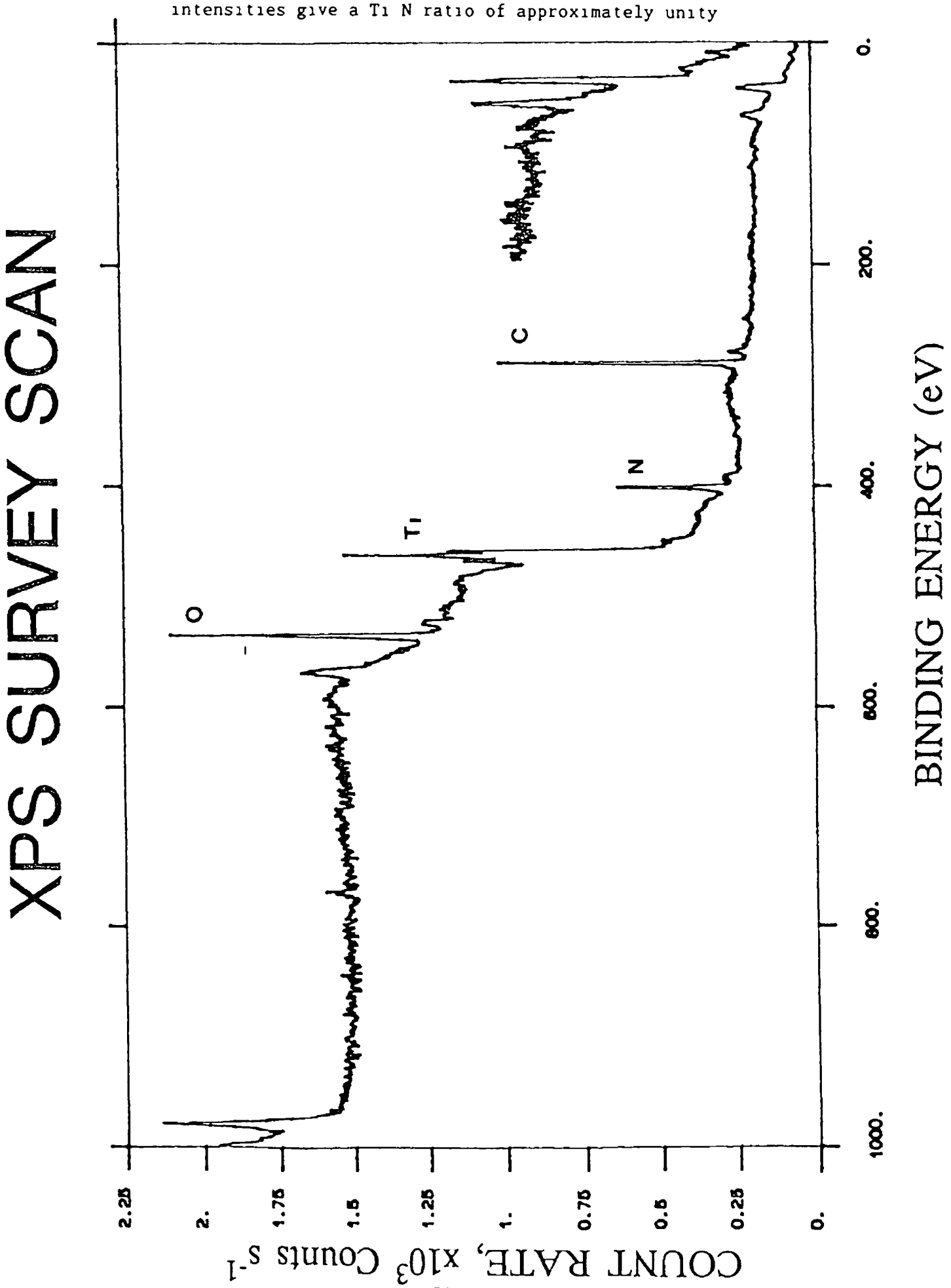

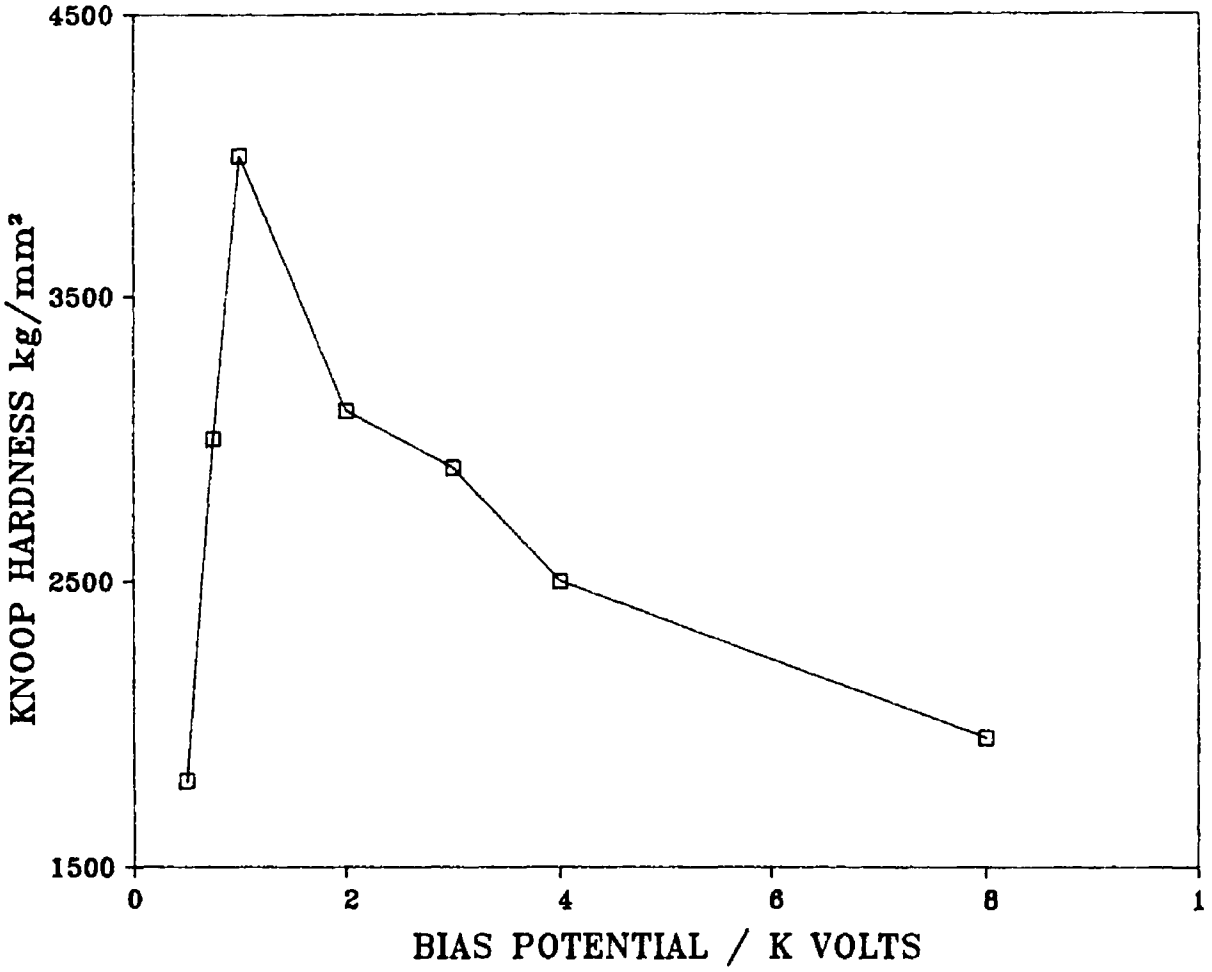

Fig 3 8 The effect of substrate bias on the Knoop Hardness of TiN films The TiN layers were produced at 0 014 mbar total pressure, at 2 5 Amp target current for 30 min The films were between 5-8 μm thick The quoted hardness values are the average of 6 readings per sample at 100 grf load (standard deviation was approx 5%)

Fig. 3.3 Two TiN films displaying regions of film delamination.

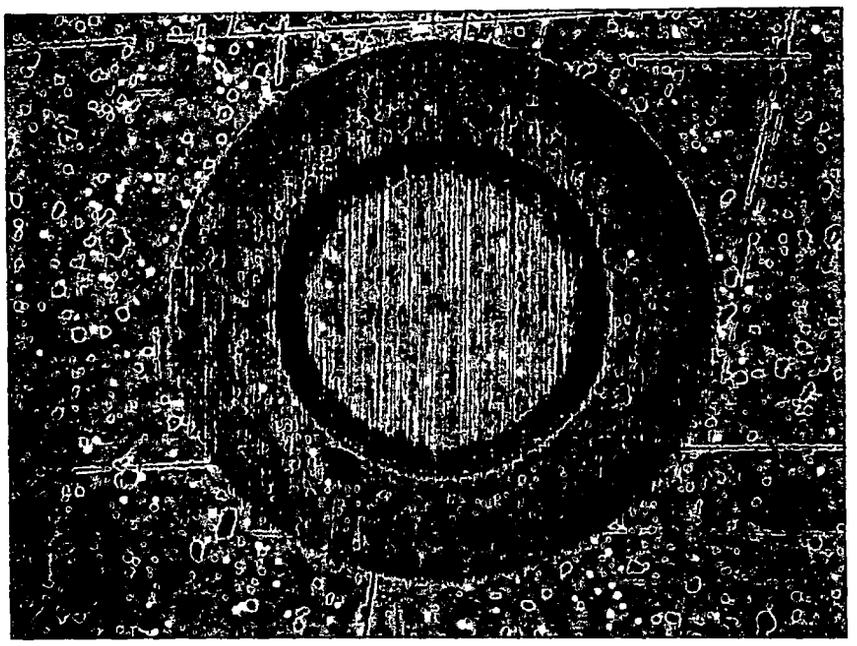

Fig 3 9 Photograph of a ball cratering depression on a TiN film Coating conditions are outlined in Fig 3 8 with -200 V bias Composite coating thickness is 5 μm x 100

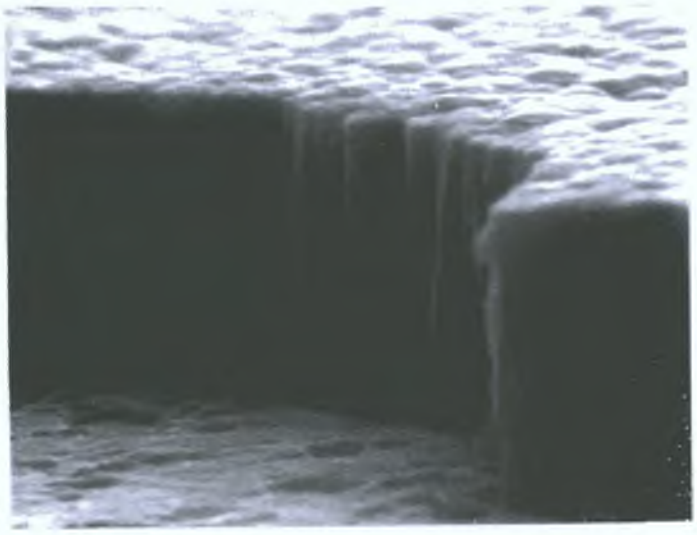

Fig. 3.10a SEM photograph of a fractured edge of a TiN film produced at -800 V bias at 0.014 mbar pressure. x 7500.

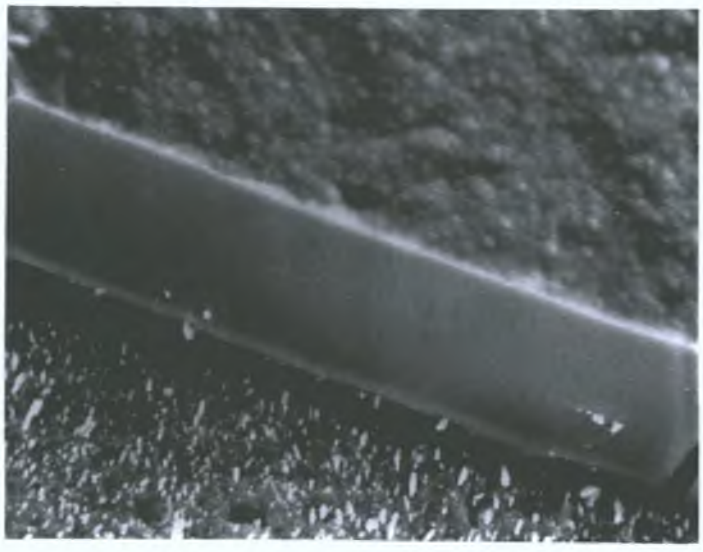

Fig. 3.10b SEM photograph of a fractured section of a TiN layer produced as outlined in Fig. 3.10a at -100 V bias. x 4500.

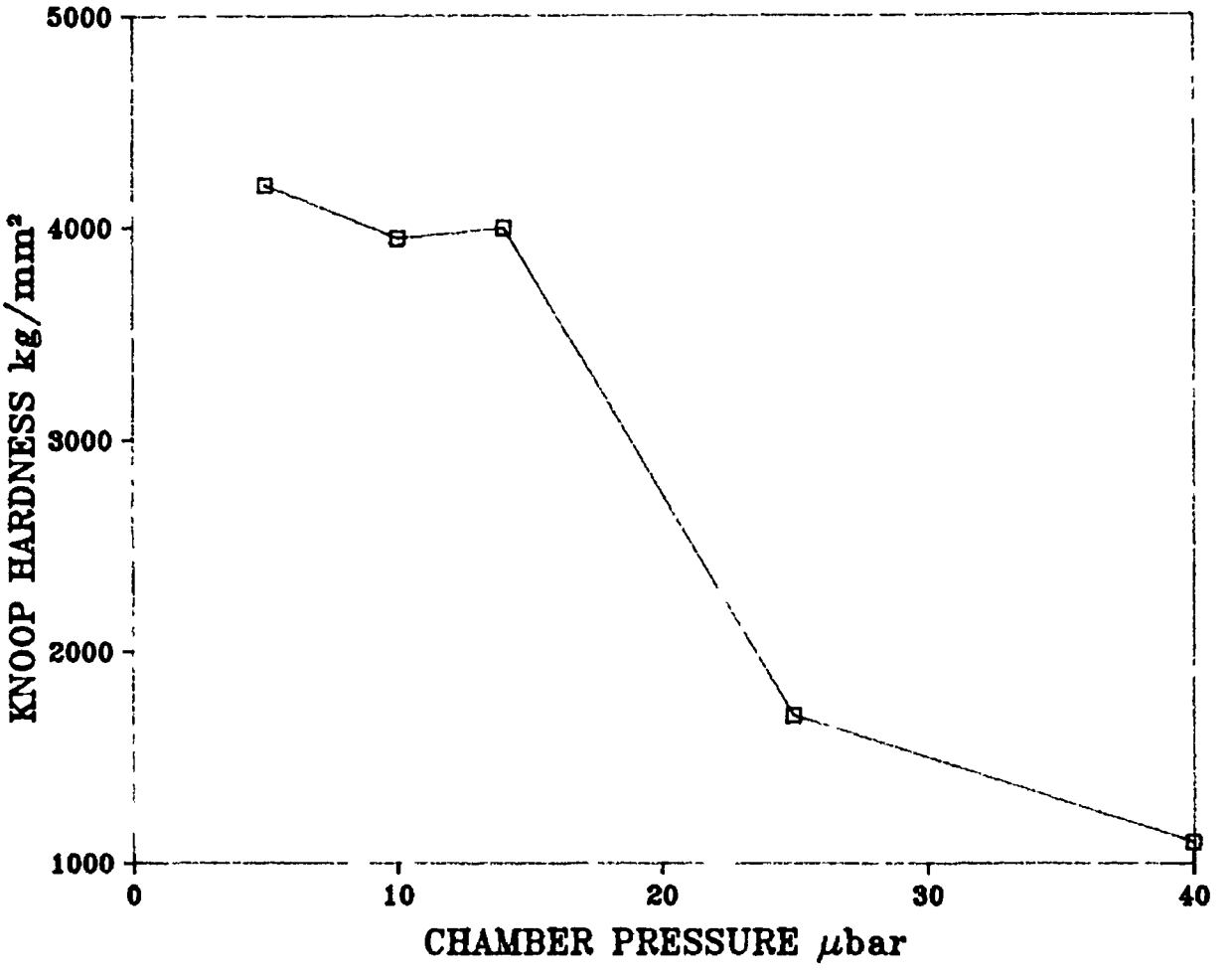

Fig 3 11 Variation of Knoop Hardness of TiN films deposited onto HSS at various gas pressures and -100 V bias The hardness values are the average of 6 readings

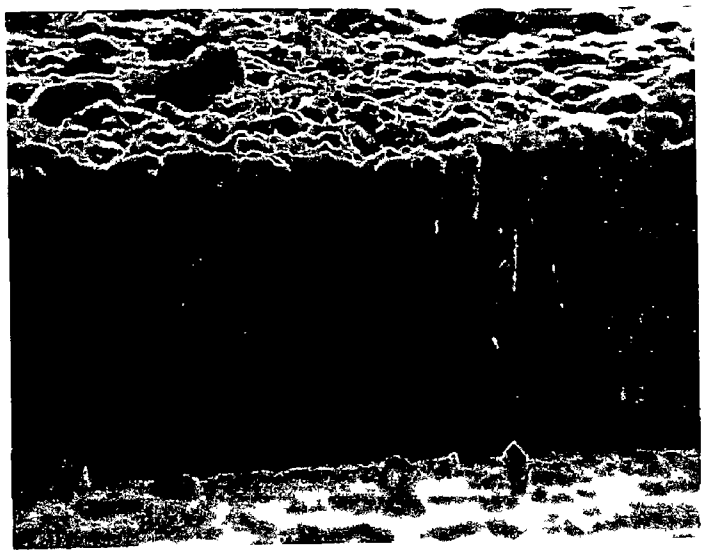

Fig 3 12 SEM micrograph of a fractured edge of a TiN film formed at 0 04 mbar and -100 V bias. x 7500.

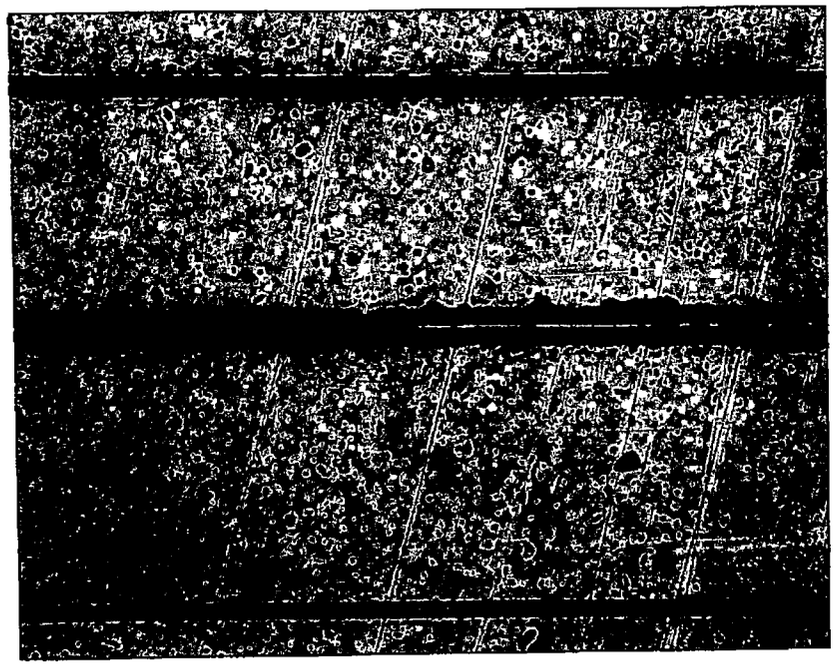

Fig 3 13 Picture of a scratch scar showing the region of adhesion failure with no evidence of "kidney shaped" crack patterns generally indicative of cohesive failure Same sample as depicted in Fig 3 9 x 50

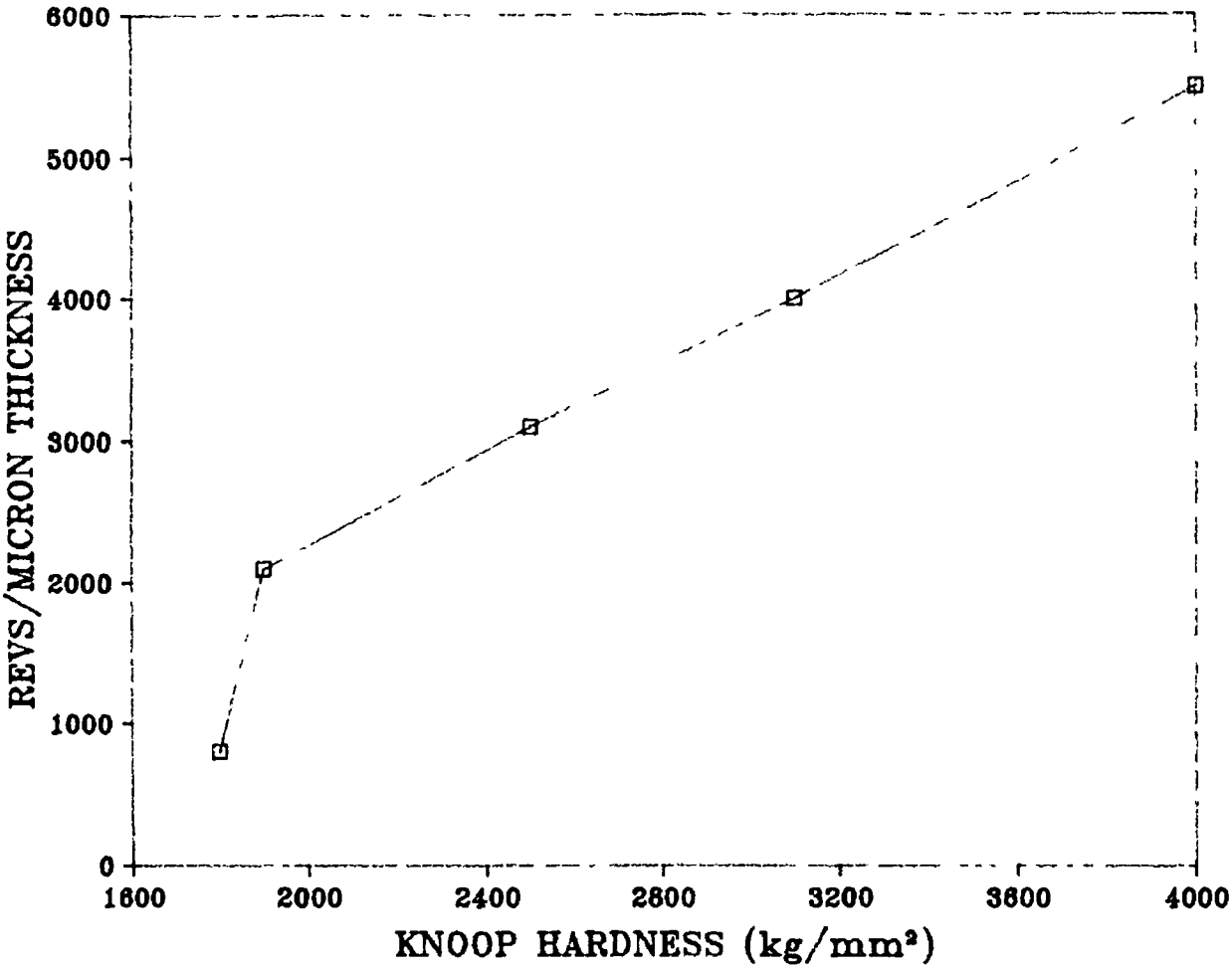

Fig 3 14 The relationship between the abrasive wear resistance and the Knoop Hardness of TiN films produced at 480°C with the ICM Abrasive wear tests conducted in an ambient solution of Al_2O_3 with the rubber wheel tester

Fig. 3.15 Wear scars produced on TiN coated HSS by the rubber wheel abrasive wear test. The TiN and Ti film have been penetrated as evidenced by the electroless copper deposit (from the $CuSO_4$ spot test) on the left hand photograph.

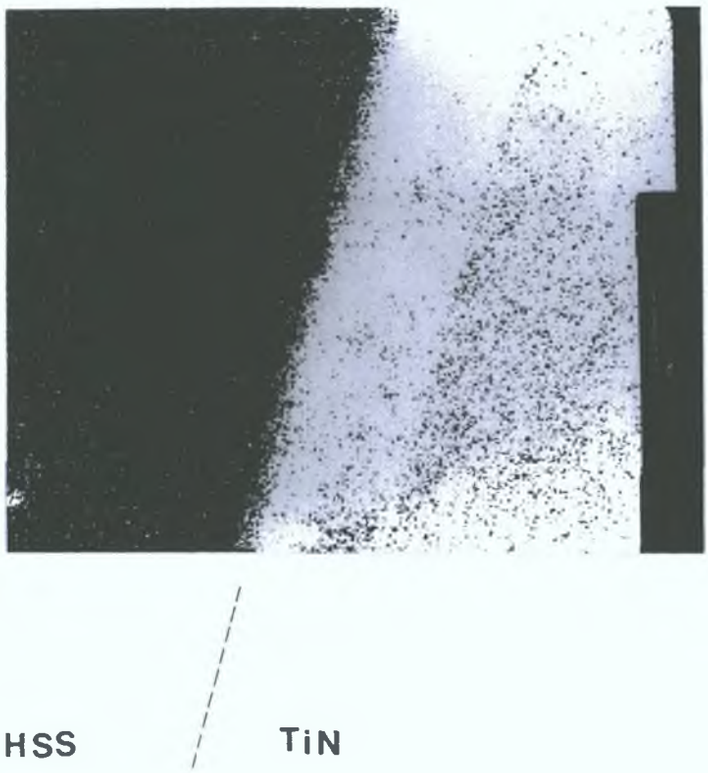

Fig. 3.16 Ti distribution density in the area localised in the interface between the HSS substrate and the TiN film. The presence of an indistinct boundary region between the TiN and the HSS is indicated. Deposition conditions were -200 V bias and 0.014 mbar pressure.

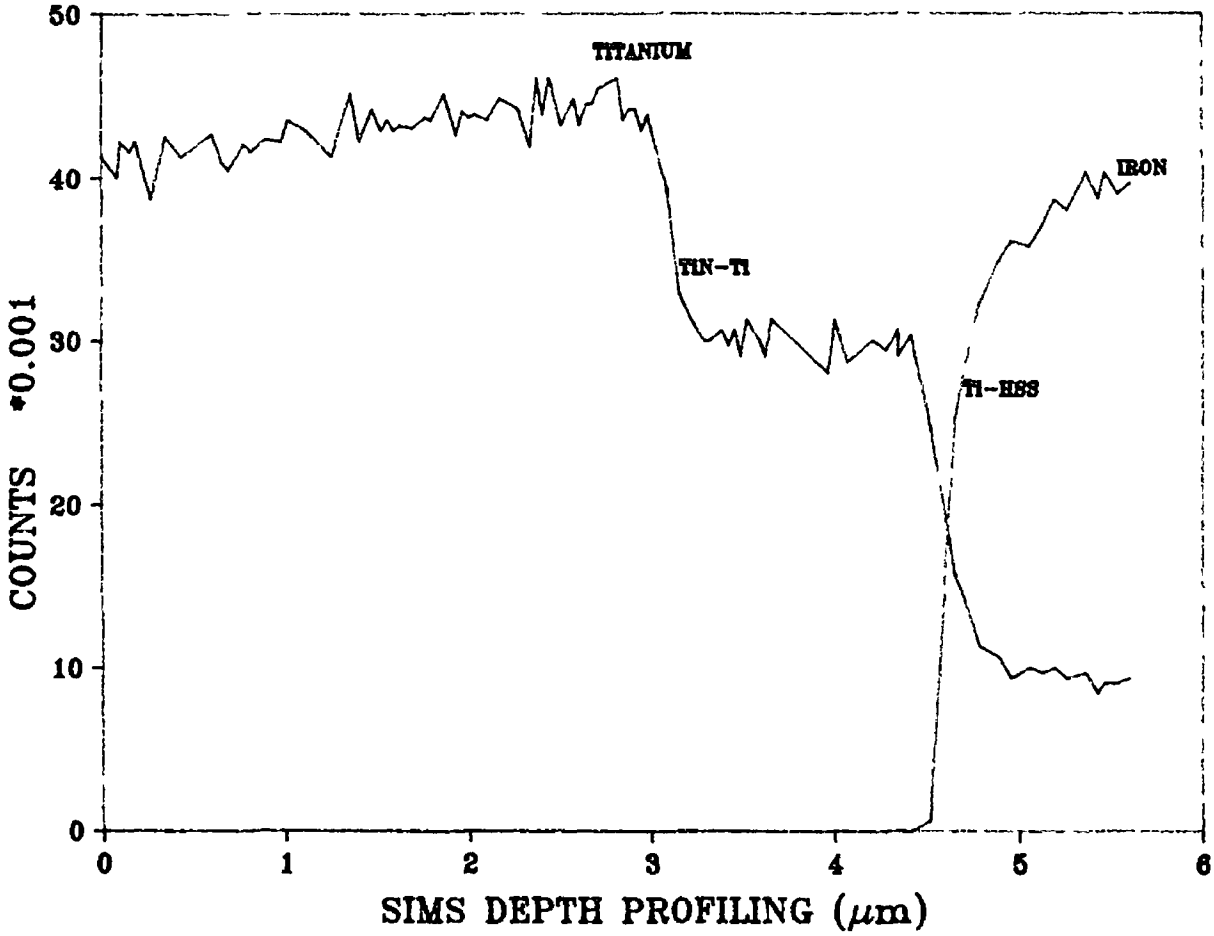

Fig 3 17 SIMS depth profile of TiN sample depicted in Fig 3 16

	HARDNESS OF HSS BEFORE TiN COATING		HARDNESS OF HSS AFTER TiN COATING	
EXP NUMBER	DIAGONAL µm	KH 100g kg/mm²	DIAGONAL µm	KH 100g kg/mm²
1	36.3	1080	36.6	1062
2	36.4	1074	36 2	1086
3	36.3	1080	36 5	1068
4	36.2	1086	36.3	1080
5	36.3	1080	36.4	1074
6	36.3	1080	36 6	1062
7	36 3	1080	36.5	1068
8	36.3	1080	36.4	1074
9	36.2	1086	36.1	1092
10	36.4	1074	36.3	1080
AVERAGE		1080		1075
DEVIATION		4		9
% DEVIATION		.35		.87

Table 3 1 Knoop hardness of M2 HSS before and after coating with TiN HSS was polished with 1 µm diamond paste on both flat surfaces and Knoop Hardness was evaluated at 100grf load The HSS was then coated with TiN at 8 µbar, -200 V bias and 2 5 Amp magnetron current for 1 hour This coating was deposited on the reverse side to that on which the initial hardness measurements were performed After cooldown, the Knoop Hardness of the HSS was evaluated at 100grf load on the same face of the substrate During the deposition process this surface rested on the substrate holder and was not coated The maximum substrate temperature during the coating was 480^{o}C

CHAPTER IV

EXPERIMENTAL RESULTS AND DISCUSSION

THE DEPOSITION OF TIN FILMS AT APPROXIMATELY 480° TO 160°C SUBSTRATE TEMPERATURE

4 1 INTRODUCTION

Magnetrons are used to routinely deposit a broad range of thin films at the research and industrial level [94-96] It is generally accepted that ion bombardment of the substrate during sputtering produces changes in the nucleation characteristics, morphology, stress and composition of the growing film Such effects are attributed to resputtering, increased deposition rate, magnetic field confinement effects, increased adatom mobility, defect formation etc , [37,65] At substrate temperatures of approx 500^{o}C, the use of indirectly cooled magnetron targets (ICM) is common At deposition rates of 0.1 μm/min the main parameter affecting substrate temperature is the radiative heat loss from the target surface. In extreme circumstances the target material may become red hot. The thermal impedance of the magnetron-target combination ultimately limits the power which can be delivered to the system The deposition of thin films at approx 0 1μm/min, with substrate temperatures of 250^{o}C (on uncooled substrates) and sufficient ion bombardment is not readily possible with ICM's The main thrust at lowering the temperature of deposition from ICM's is by reducing the magnetron input power, thereby ultimately, compromising the deposition rate In attempting to deposit at low temperatures and at high deposition rates, many investigators use the directly cooled magnetron system The ICM can be converted to a directly cooled magnetron (DCM) system by replacing the copper backing plate of the magnetron with the target material However, this simple modification to the magnetron target results, not only, in reducing the substrate deposition temperatures, but also, in changes in the operating characteristics of the magnetron, which ultimately have an influence on the film properties. This configuration provides a means of reducing the thermal impedance of the target system, increasing the deposition rate at a reduced substrate and chamber temperature. In addition, the ion bombardment to the substrate is not compromised

The operation of both directly and indirectly cooled magnetron configurations for TiN film production are compared in terms of; (i) the temperature increase in an uncooled substrate, (ii) the changes in the magnetic field of the magnetrons, (iii) the ease of target poisoning, (iv) the input power limitations, (v) the TiN deposition rates and (vi) the substrate ion current possible during ion-plating

The hardness, crystallographic orientation and chemical composition of the resulting TiN layers are analysed The XPS and XRD data reveal the presence of two titanium-nitrogen phases in films produced from the directly cooled system, with only one titanium-nitrogen phase present in films produced from the indirectly cooled device Possible reasons for such differences in film properties are addressed

4 2 RESULTS

The operating characteristics of both magnetron systems follow the empirical [97-99] current-voltage relationship, viz ,

$$I=KV^n$$

where K is a constant, I is the cathode current, V is the cathode voltage and n is an exponent which reflects the electron trapping efficiency of the plasma The graph, outlined in Fig. 4.1, indicates the values of n and K for both the ICM and DCM configuration.

The magnetron poisoning curves for both the ICM and DCM are depicted in Fig 4 2 The ICM was operated at 3A and the deposition system required 8 SCCM (standard cubic cm per min) N_2 for stoichiometric TiN production In the case of the DCM stoichiometric TiN formation necessitated the controlled admission of 15 SCCM N_2 when the target was operated at 5A It was observed that a greater tolerance in N_2 flow was permitted in the DCM mode before excessive and non-reversible target poisoning occurred The ICM system required very precise control of the N_2 partial pressure as discussed in Chapter III

The effect of altering the DC substrate bias potential, at different settings of the magnetron target current, on the substrate ion current is plotted in Fig 4 3(a) and Fig 4 3(b) As the bias potential is increased the substrate ion current gradually increases A cut-off voltage of -1000V was chosen for the ICM because higher voltages caused the discharge to extinguish. This effect was noted in the DCM at -600V In the case of the ICM, changing the magnetron current from 1A to 3A produced a change in bias current from 22mA to 46mA when the bias voltage was held constant at -600V Holding the bias voltage at -600V for the DCM and changing the target current from 1A to 3A alters the

bias current to the substrate from 50mA to 120mA Operating the ICM at 3A target current and -300V bias resulted in the Ti target becoming incandescent In this investigation the DCM Ti target reached a maximum of 50°C under the highest input power conditions. It was found that operating the ICM at 3A target current and -100V bias resulted in an equilibrium substrate temperature of 480°C These conditions were chosen to deposit the high temperature TiN layers from the ICM design

An M2 HSS steel substrate was heated to 100°C in the vacuum chamber and subjected to different magnetron target currents at various bias voltages for a period of 60 mins The resulting changes in substrate temperature are noted in Fig 4 4 for the DCM case The plateau temperatures which the substrate reached during film deposition were independent of the initial starting temperature When the substrate temperature before deposition was usually 160°C (viz , the typical substrate temperature after plasma etching) The subsequent plateau-temperatures thus generated are outlined in Table 4 1

The XPS data from the N 1s and Ti 2p transitions of TiN layers, produced from the ICM and DCM at different substrate temperatures, indicate that two types of titanium nitride are present It is evident from Fig 4 5(a) that the TiN, formed from the ICM, comprises mainly the stoichiometric TiN However, titanium nitride produced by the DCM technique exhibits two forms of nitride From the evidence of Fig 4 5(a) and Fig 4 5(b), the environment of the Ti 2p atomic orbital is similar but that of the N 1s atomic orbital is altered when deposition occurs from the ICM or the DCM This observation is also supported from XRD data tabulated in Table 4 1 TiN films produced from the DCM have a stronger TiN (111) orientation with Ti_2N phases present The TiN films, deposited from the ICM, are preferentially oriented in the (200) plane with an absence of Ti_2N phases

The Knoop hardness of the TiN films produced from the DCM configuration decreases with substrate deposition temperature, as illustrated in Fig 4 6 While the substrate temperature is the measurable variable which appears to influence the film hardness, the substrate temperature is, itself, a macroscopic parameter which is influenced by deposition rate, pressure, bias voltage, bias current, etc,. Hence, it is very

difficult to clearly identify a single reason for the change in hardness

The TiN films, produced from the DCM configuration, were wear tested in an Alumina slurry and the wear resistance is plotted against film hardness in Fig 4 7

4 3 DISCUSSION

4 3 1 Comparison of ICM and DCM Operating Conditions

The design of the magnetic field of the ICM is, essentially, unbalanced in nature Side-plumes of plasma can be readily observed originating from the perimeter of the target and extending 10-12 cm into the vacuum chamber. Upon changing targets to the DCM design, these streams of plasma become more pronounced (at given target current levels) The I/V curves of these two systems, displayed in Fig 4.1 , indicate that the electron trapping efficiency factor, n, increases from 6, in the case of the DCM, to 7 4 in the case of the ICM This difference suggests that the plasma is more confined to the ICM target whereas the plasma is more diffuse in the DCM system It is suggested that this penetration of the bulk vacuum with magnetic field lines, and the consequent plasma elongation, would enhance the levels of plasma gas ionisation experienced in this region This increased gas ionisation would contribute, in addition to the higher magnetron currents, to the increased substrate ion current density found in the DCM configuration In most thin film deposition experiments the substrates would have been surrounded by this extended DCM plasma envelope

The DCM can be operated at much higher sputtering rates (up to 0 25 μm/min) compared to the ICM system (typically 0 1μm/min). Together with high deposition rates, the control of stoichiometric TiN formation is more facile as illustrated in Fig 4 2 The sharp, transition from stoichiometric to over stoichiometric films, observed at ca. 9 SCCM N_2 with the ICM, is absent in the directly cooled device There is a continuum in N_2 flow over which golden coloured stoichiometric TiN layers can be deposited with the DCM Because of the increased sputtering rate, target poisoning is readily reversible The requirement for a high level of substrate ion current during the

deposition process is recognised [92] and was developed in Chapter III The DCM offers a greatly increased (refer to Fig 4 3) level of substrate ion current at low levels of applied bias potential. The latter phenomenon is related to the greater sputtering rates available from the DCM and the subsequent increase in the number of activated or charged gaseous species which are formed The plasma envelope developed in the DCM system concentrates gas ions and ionising electrons in the region about the substrate, thereby, increasing the substrate ion flux Increased ion fluxes at low potential minimise substrate surface damage and enhance film quality via a "surface peening" effect [95] At high sputtering rates, the ICM target glows cherry red in colour, thereby causing radiative heating of the substrate To reduce substrate temperature the ICM is operated at lower input power thus compromising deposition rates From an inspection of Fig 4 4 it is clear that the DCM can provide high rate sputtering, with appreciable substrate ion current, at low substrate temperatures The conditions employed in such processes are outlined in Table 4 1 All TiN films produced were between 5-8 μm thick.

4 3 2 TiN films Produced from ICM and DCM Systems

The orientation of the deposited films varied, as indicated in Table 1, from (200) to (111) This effect is important for tribological properties since different orientations apparently exhibit different wear properties [52] At the substrate temperatures of 480^{o}C and low deposition rates (0 1μm/min) single phase TiN with (200) preferred orientation is formed. The change in preferred orientation from (200) to (111) is observed as the deposition rate increases in broad agreement with Ref 100 The preferred orientation changes with the growth conditions and literature [100, 101] reports a change from (111) to (200) with increasing substrate ion current, whereas other workers [102] observe a change from (111) to (220) with increasing bias potential The XRD reflections, from the films produced by the DCM method, tended to be sharper indicating the presence of fine grain structure The grain size is dependent on growth parameters such as the substrate temperature and ion bombardment [52] At high substrate temperatures the adatom mobility and the rate of grain boundary migration increase, resulting in increased grain size. Increased ion

bombardment produces greater numbers of nucleation sites and greater levels of resputtering (resulting in lower adatom mobility) which can cause the grain size to decrease However, high ion currents and low bias voltages can produce larger grain sizes by increasing the energy of adatom species by momentum transfer reactions without a resputtering effect In this brief study, the interactions of substrate temperature, ion current and bias voltage could not be further elucidated

The formation of the Ti_2N phase is generally attributed to kinetic limitations and non-equilibrium growth conditions [63, 100, 103, 104] High deposition rates and/or low substrate temperatures lead to the development of film structures where Ti_2N phases are often observed [52] The combinations of high deposition rate, low substrate temperatures and high ion currents may combine to produce the kinetically more accessible rather than the thermodynamically more stable phase The Ti_2N phase was only found in the films deposited from the DCM system The Ti_2N phase was more prominent in thin films produced with high levels of ion bombardment The XRD data (Table 4 1) indicate the presence of Ti_2N phases in films produced from the DCM system which are absent in the ICM deposited film Such XRD observations are confirmed by surface XPS analyses which show the presence of two Ti-N species formed from the DCM device The TiN film formed at 480°C (see Fig 4 5) contains one TiN phase There is evidence from the O 1s XPS spectra (not diagrammed here) that a Ti-O moiety is also present in these layers particularly in the ICM deposited films The base pressure in this reactor was $5x10^{-5}$ mbar with water vapour as the main contaminant At higher substrate and chamber temperatures it is reasonable to assume that both the desorption of water from the chamber walls and reaction of water with the growing film is favoured [17] The presence of different titanium-nitrogen phases produced from the cooler DCM procedure can be understood in terms of the higher deposition rates and the reduced substrate temperatures employed

The Knoop hardness of the TiN films decreases monotonically with the substrate deposition temperature, as outlined in Fig 4.6 and Table 4 1 These films were deposited under different sputter currents, substrate ion currents and substrate bias voltages. In the case of the

DCM produced films, the Knoop hardness appears to be related to the level of both applied bias potential and ion current The reasons for the change in film hardness are complex functions of substrate temperature, deposition rate, substrate ion current and bias potential, radiative heating effects, etc, In this study it was not possible to separate the main deposition parameters affecting film hardness However, the decrease in hardness with substrate temperature is not unusual An inspection of the Thornton Diagram (Fig 1 4) reveals that the resistance to deformation is dependent on the morphology of the film which, in turn, is temperature sensitive

All TiN films investigated passed the Salt Spray Test Corrosion occurred only in areas where the film had been penetrated or at the edges of the HSS

As discussed in Appendix B, the abrasive wear law relates abrasive wear resistance directly to hardness In Fig 4 7 the wear resistance of the TiN films gradually decreases with a decrease in film hardness As the deposition process permits TiN films to be produced at lower temperatures, the wear resistance (and hardness) of the films are compromised The effectiveness of such films as wear resistant coatings is dependent on the end-use These types of TiN films find applications in the areas of corrosion resistant coatings on base metals, as electrode materials in prosthetic devices (e.g as electrodes in heart pacemakers), as coatings which preserve edge integrity on surgical needles and scalples and as wear resistant coatings when deposited onto bearings

Fig 4 1 Log/Log plot of magnetron target voltage against target current Chamber pressure was 8 μbar n=7 4 and $K=10^{-18}$ for the DCM configuration, n=6 0 and $K=4x10^{-15}$ for the ICM configuration

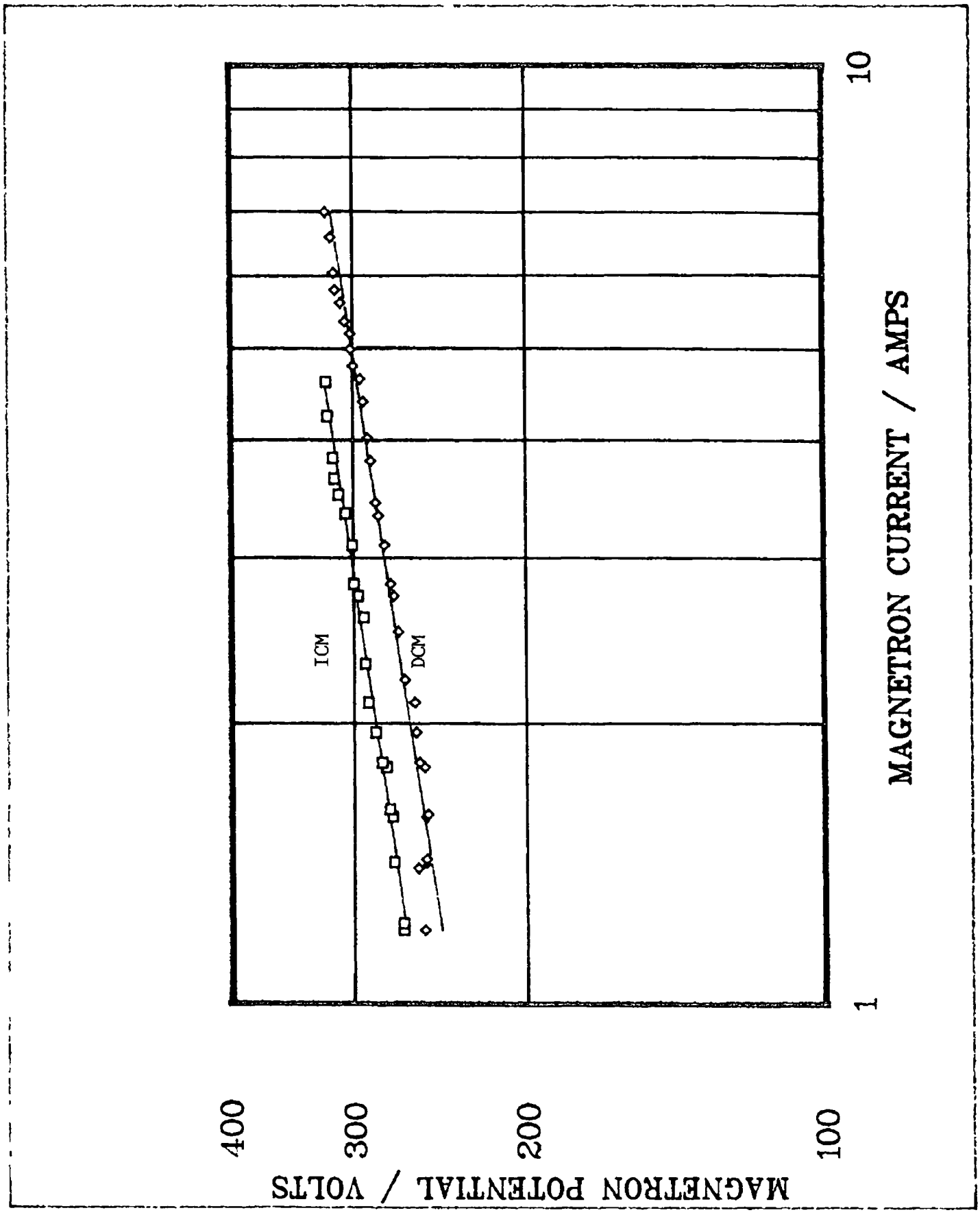

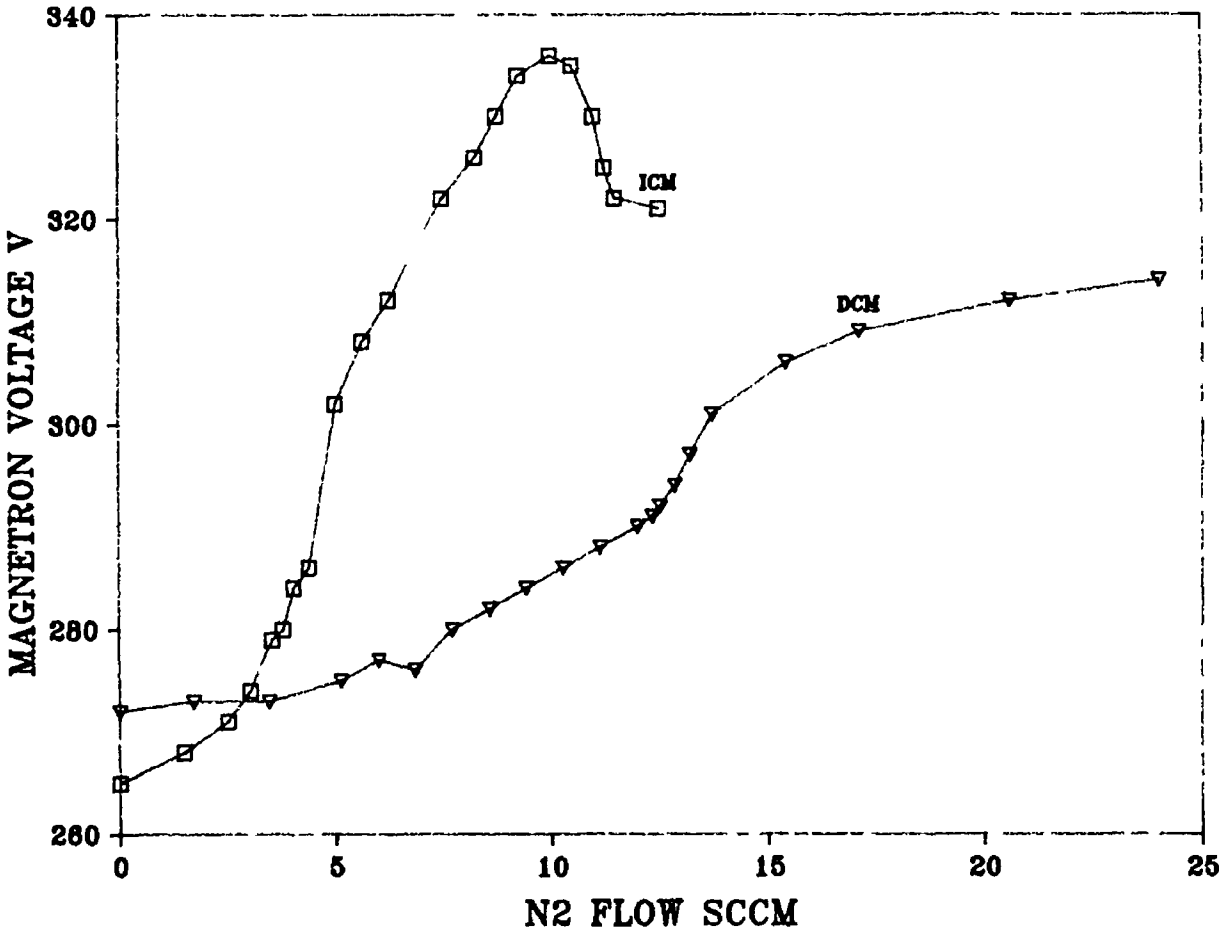

Fig 4 2 Plot of the poisoning curves obtained for TiN deposition from both ICM and DCM types The total gas pressure was 8μBar The ICM was operated at 3A total input current The DCM was operated at 5A input current The rate of admission of N_2 gas was identical for both experiments

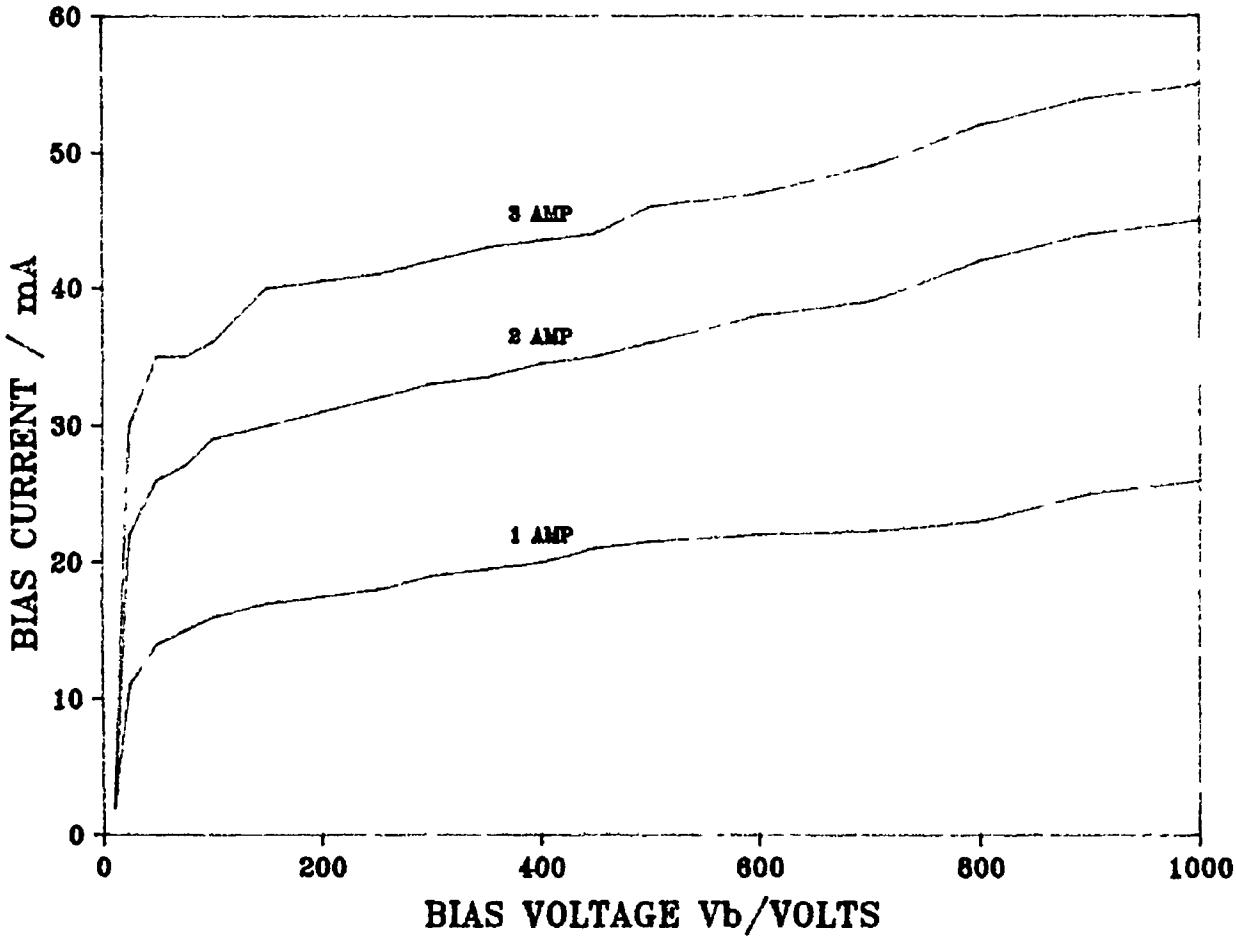

Fig 4 3a Variation of substrate bias current with substrate bias voltage (negative potential) at the various ICM magnetron current settings indicated Total pressure was 8 μbar

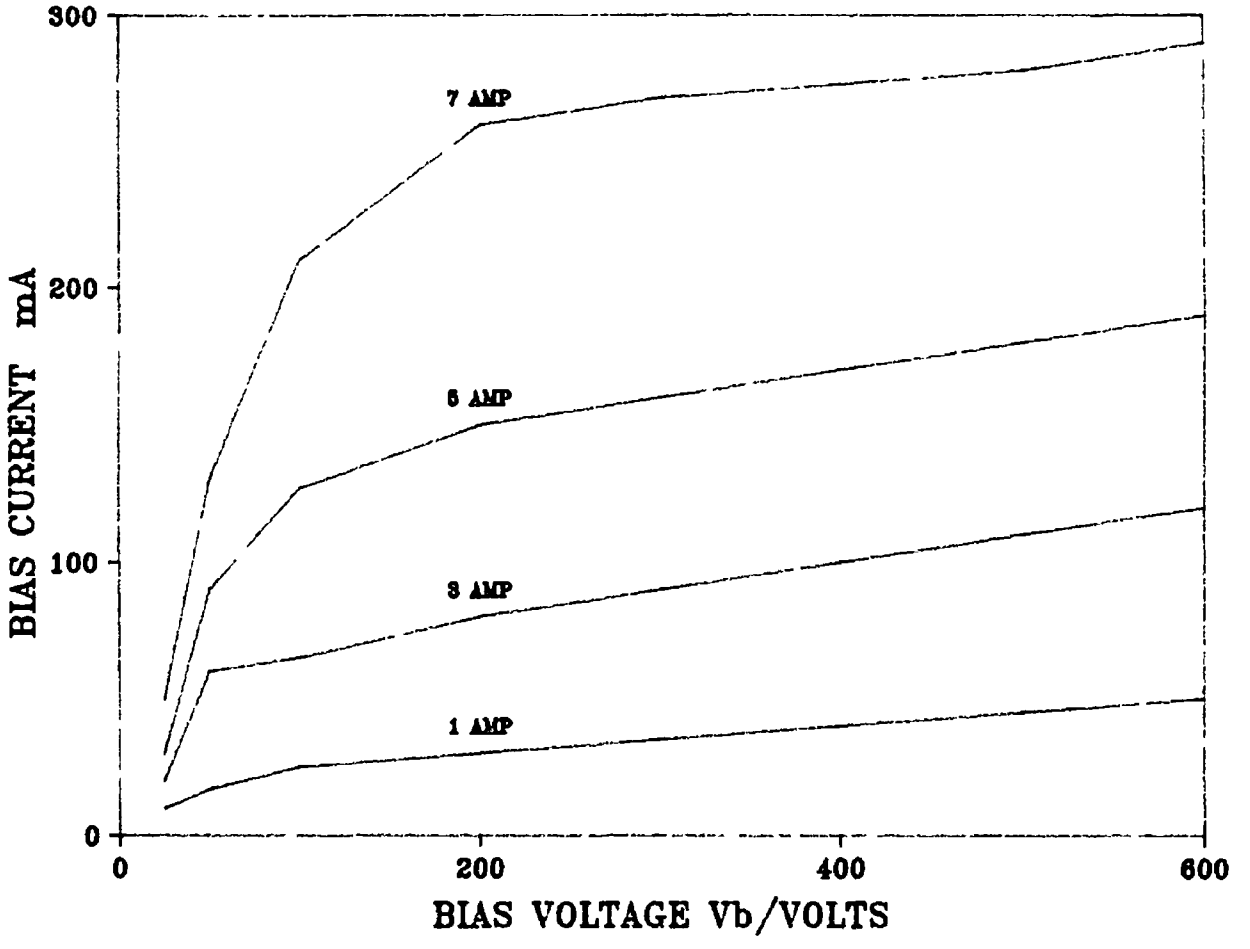

Fig 4 3b The effect on substrate bias current with applied substrate bias voltage at different settings of the DCM magnetron current indicated Experimental conditions were the same as those employed in Fig 4 3a

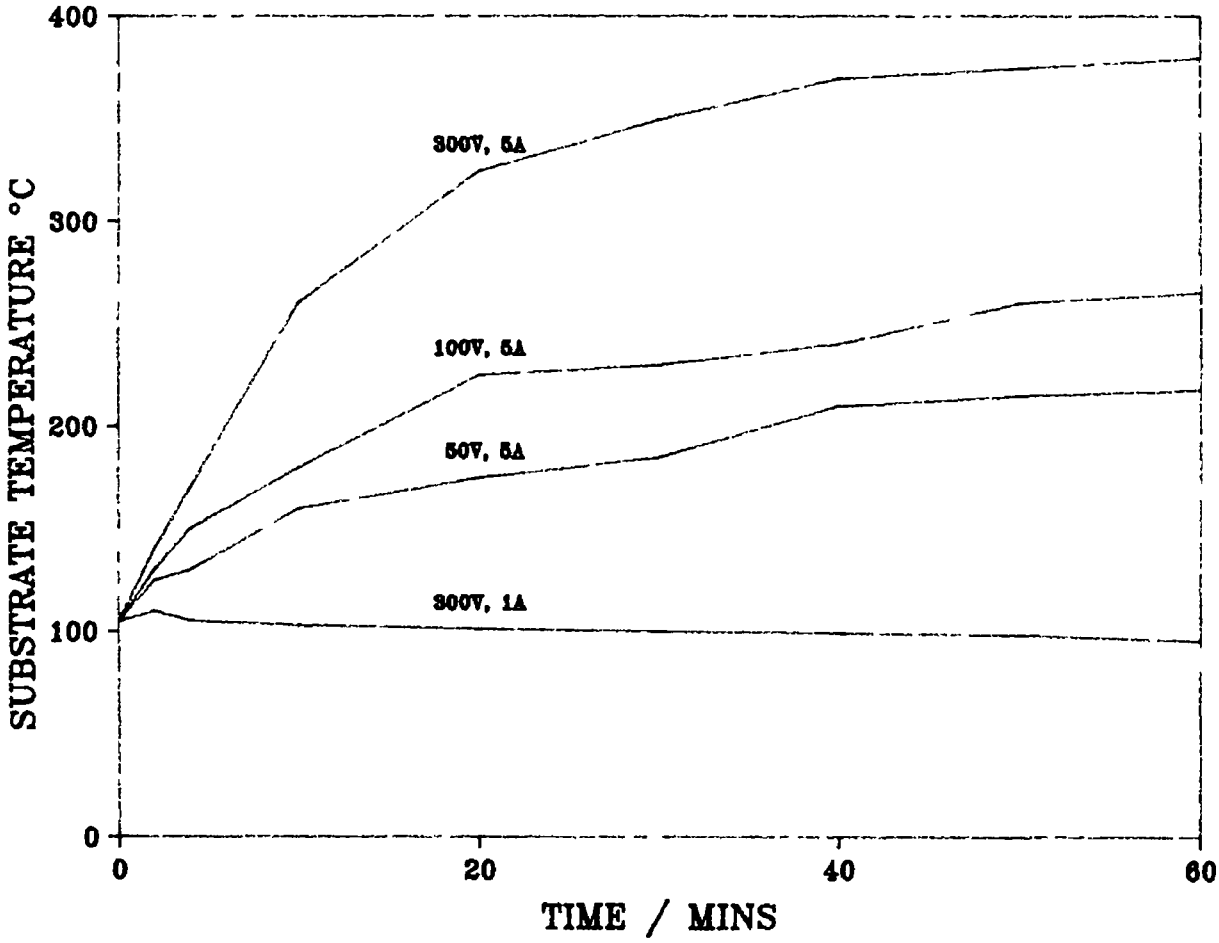

Fig 4 4 The effect of bias voltage on substrate temperature at given DCM magnetron currents during TiN deposition The substrate was initially sputter-etched to 100°C prior to deposition

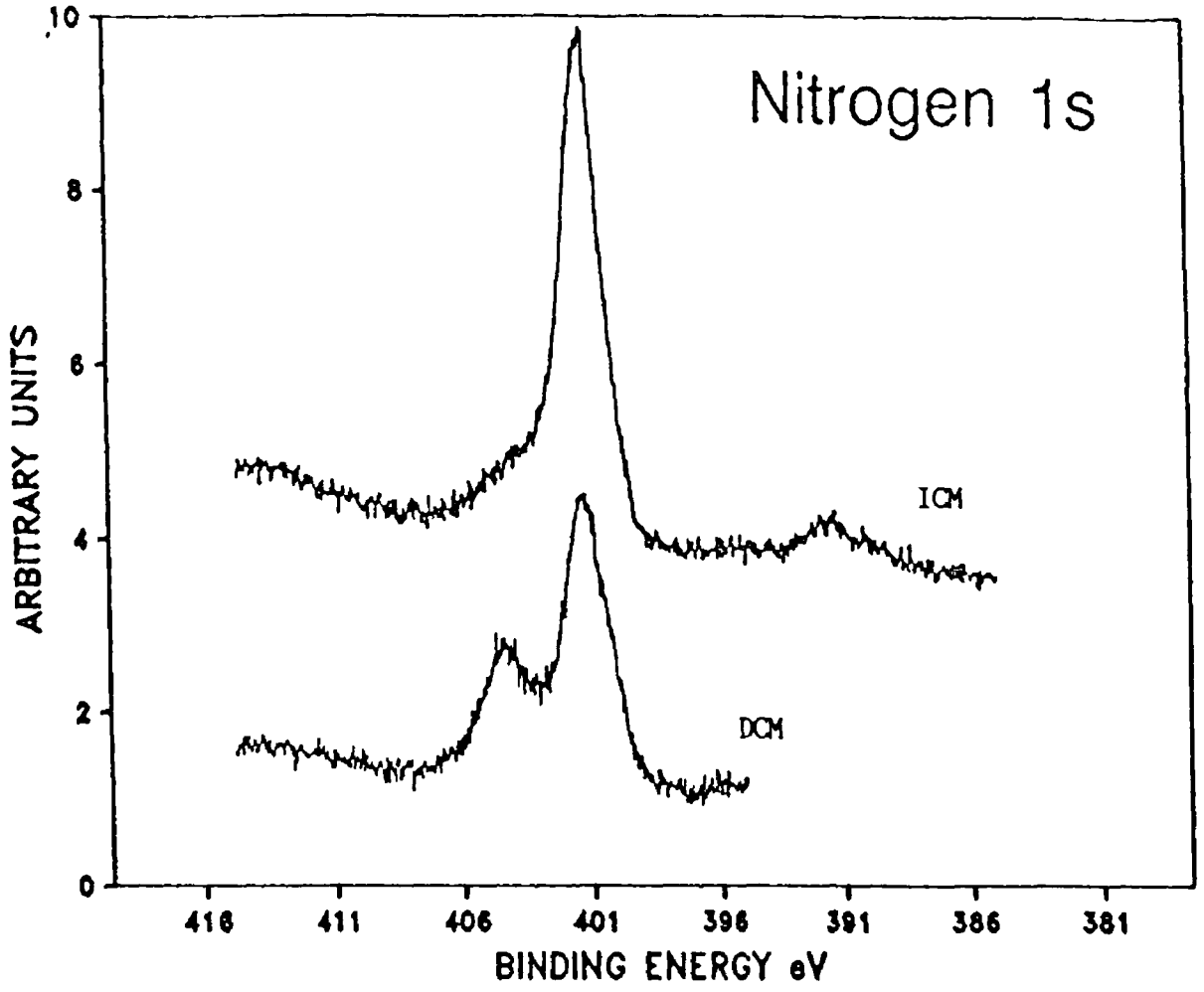

Fig 4 5a The high resolution XPS profiles of the N 1s region for the DCM (480^{o}C substrate temperature) and ICM (250^{o}C substrate temperature) are graphically compared Curve de-convolution indicates the presence of one major and one minor peak in the case of the ICM deposited films These two curves are resolved when films produced from the DCM are analysed

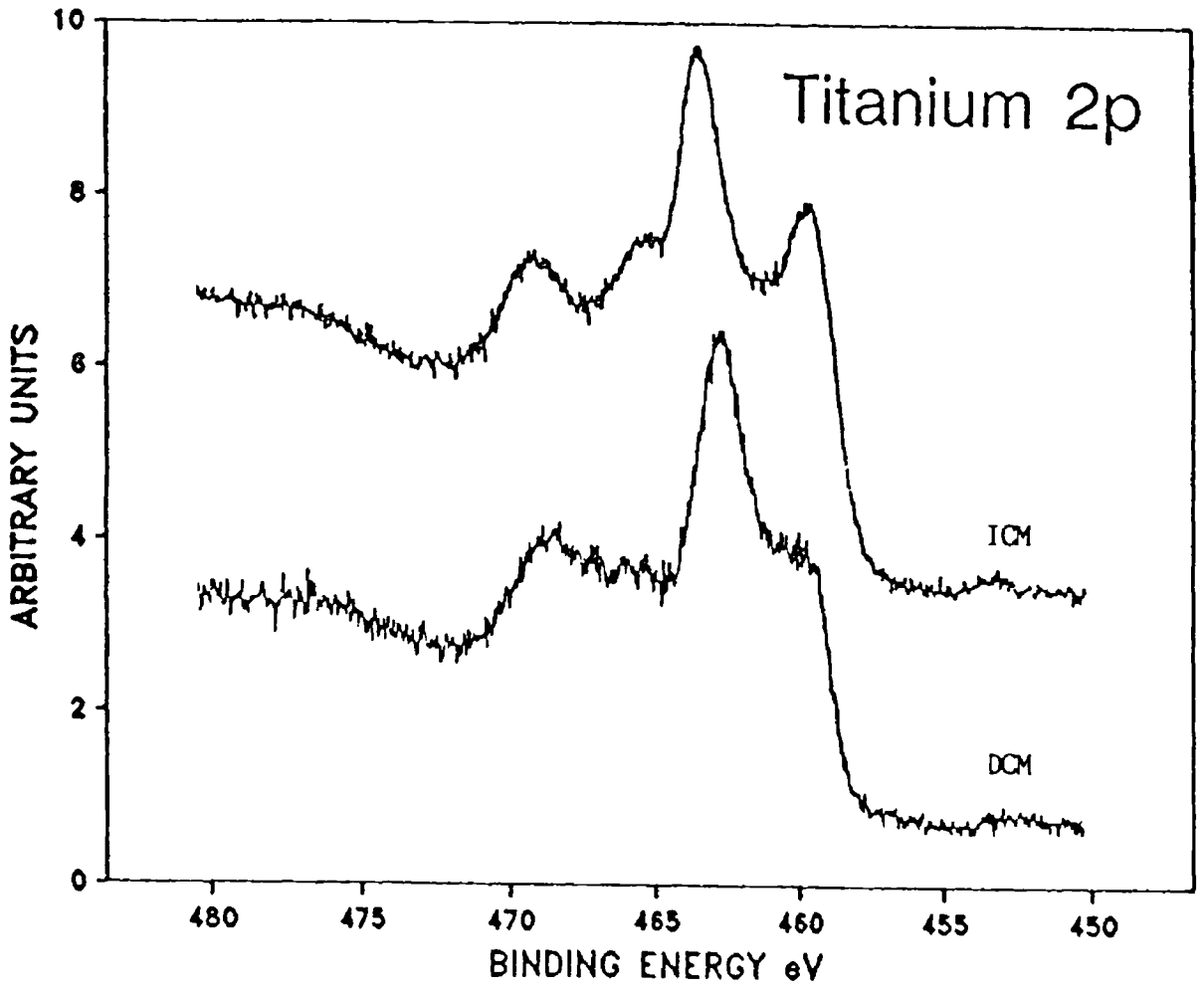

Fig 4 5b The high resolution XPS scans of the Ti 2p region are represented Curve fitting procedures indicate the presence of three Ti environments. (The simple Ti 2p region exhibits a doublet peak structure because of splitting due to the presence of Ti $2p^{1/2}$ and Ti $2p^{3/2}$)

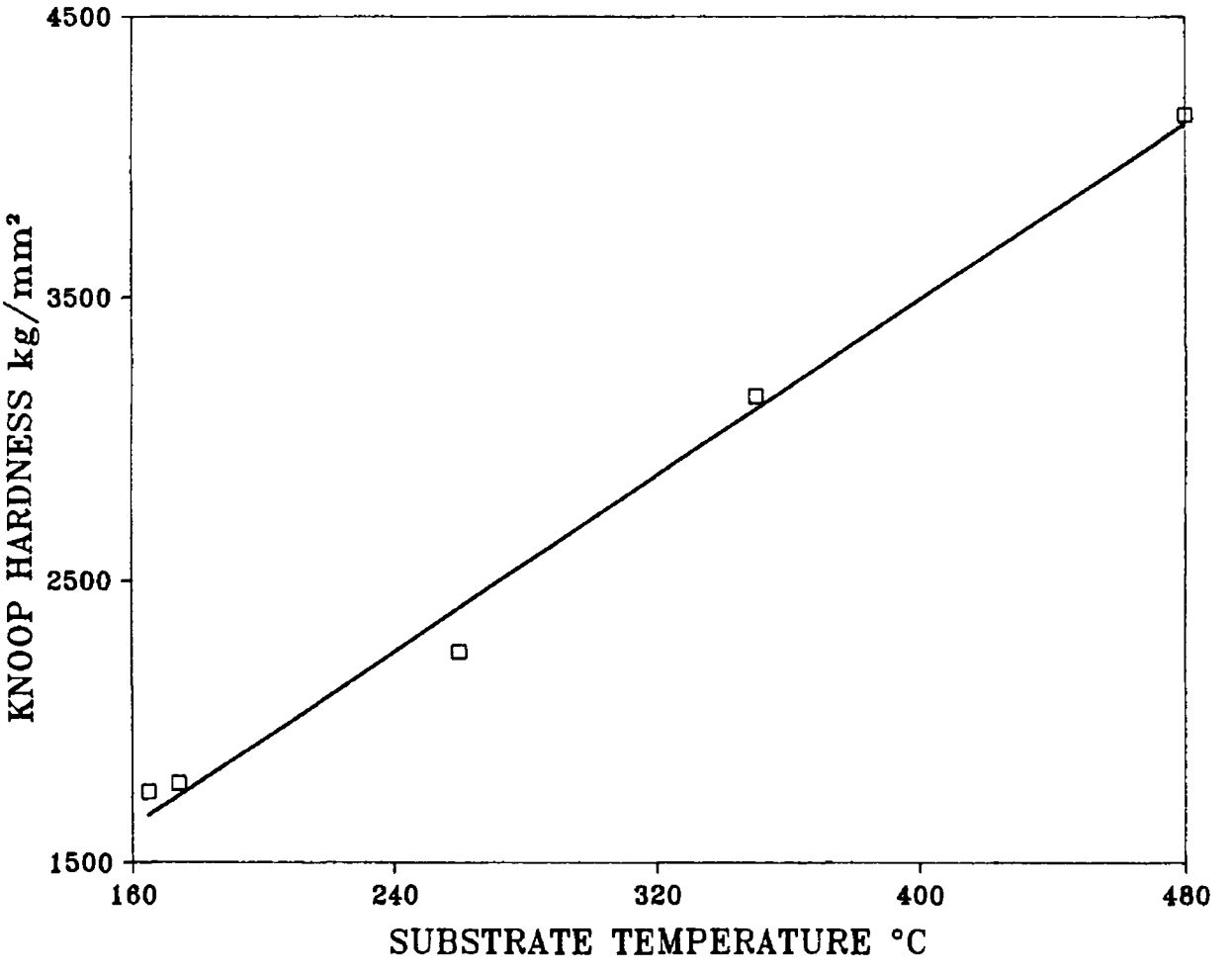

Fig 4 6 The variation of Knoop Hardness of TiN coatings with deposition temperature The quoted values are the average of 6 readings Indenter loading was 100 grf

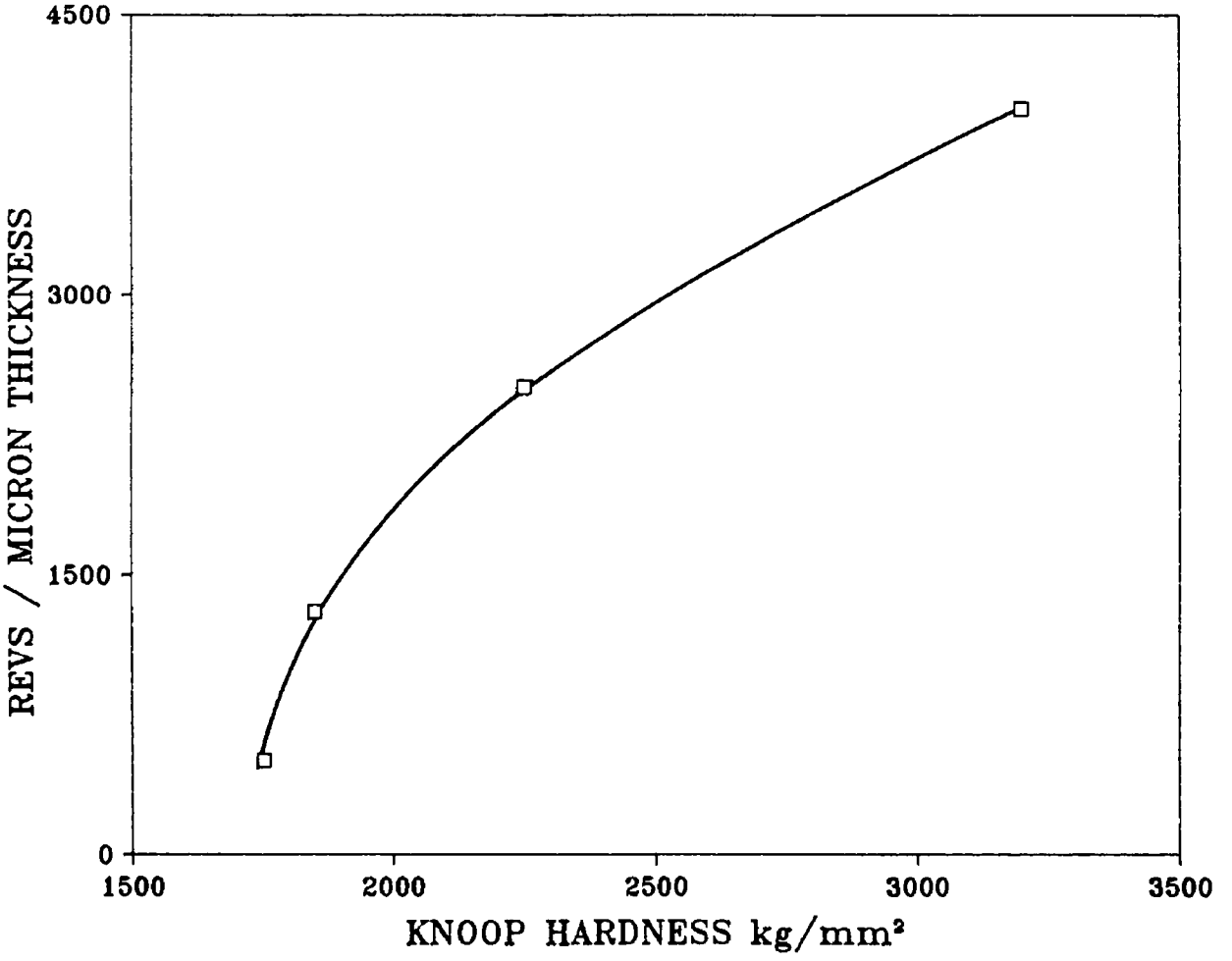

Fig 4 7 The change in abrasive wear resistance of TiN films as a function of the hardness of the coating

SAMPLE NUMBER	HK 100g	DEP TEMP °C	CURRENT BIAS VOLTS	XRD REFLECTIONS TiN				Ti2N			
				111	200	220	311	111	210	211	002
1	4203	ICM 480	3A, 100V	75	100	55	25				
2	3124	DCM 350	5A, 300V	100	37	29	-	55	29	18	37
3	2202	DCM 257	5A, 100V	100	44	68	84				
4	1815	DCM 173	5A, 50V								
5	1792	DCM 168	5A, 25V	100	26	9	64	10			

Table 4 1 Summary of data relating to deposition conditions and XRD reflections of TiN films produced from the ICM and DCM systems The values between 0-100 in the XRD reflections refer to the intensities of the peaks, normalised to the largest peak of the Ti-N phase (taking the largest reflection as 100%)

CHAPTER V

EXPERIMENTAL RESULTS AND DISCUSSION

THE DEPOSITION OF TIN FILMS ON PLASTIC AT APPROXIMATELY 100°C SUBSTRATE TEMPERATURE

5 1 INTRODUCTION

The use of decorative and functional sputtered coatings on low temperature substrates has been of considerable interest in the last few years [105, 106] Coating easily machined cheap substrate metals as substitute products for more expensive components and the decorative coating of plastic parts, especially for the transport industry, are among the current developments in low temperature coating technology Reactive magnetron sputtering as a physical vapour deposition technique has specific advantages both for the deposition of complex coating materials, enabling process temperatures to be reduced through a judicious choice of process parameters, and allowing temperature sensitive materials to be coated Ion plating is a process whereby ion bombardment of the substrate during film growth changes morphology [107, 108], crystal structure [109, 110], chemistry [111] and phase formation [112] The substrate film interface can also be significantly affected by ion bombardment in the initial stages of deposition [113]

TiN has been deposited with process parameters optimised to decrease substrate temperatures to approximately 100^{o}C, to maximise film substrate adhesion and to minimise substrate surface damage The present investigation highlights some of the experimental methods used to deposit 1μm thick Ti-TiN layers onto polycarbonate plastic for decorative purposes at approximately 100^{o}C Problems such as substrate pretreatment, film cracking and substrate deformation are also addressed

Thin films of TiN were deposited onto polycarbonate platelets at low temperatures The effect of deposition on the adhesion, stress cracking, deposition temperature and appearance of these films was studied using a designed experimental approach Substrate heating as a result of the magnetron plasma was the primary sources of high substrate temperatures during deposition TiN layer stress was reduced by decreasing magnetron deposition power and increasing deposition pressure Improved adhesion to polycarbonate was achieved by admitting 10% (by volume) of oxygen during the formation of the titanium interface region The coating of TiN onto polycarbonate improved the abrasive wear properties and the appearance of the substrate

5.2 RESULTS AND DISCUSSION

5 2.1 The Experimental Design Approach

Initial investigations into the deposition of TiN on PC have shown that stress cracking of the film and stress induced bending of the substrate are primary problems requiring solutions Layers that crack are formed from dense morphologies, with tightly knit columnar structures Increasing the amount of open columnar structure should aid stress relief [17, 92] The maximum temperature at which PC may be coated in vacuo is 120^{o}C, thereby setting an upper limit on bulk plastic coating temperature The bias voltage and current density during deposition contribute, in addition to the magnetron heating effect, to the increase in substrate temperature The thickness of both the titanium interface and the TiN layers may contribute to the level of internal stress observed in the coatings The thickness of the coating is determined by both the magnetron deposition rate and the deposition time A statistical modelling approach has been adopted as a convenient means of finding the most suitable set of operating conditions in the shortest time The approach selected has been that of orthogonal design which is well documented in the literature and is known by a variety of names, including the "Taguchi method" [114, 115] The orthogonal approach is a well-established partial factorial design where the relationships between process parameters and their resulting outputs are examined by selecting and operating at certain meaningful combinations of input level settings

The parameters chosen for the Taguchi experiment into the deposition of stress-free Ti-TiN layers are outlined as follows. The directly cooled titanium magnetron would be operated at 1A and 2A. The total pressure during deposition would be set at 8 x 10^{-3}, 10 x 10^{-3} and 15 x 10^{-3} mbar The initial deposition of the titanium interface would be of 1, 2 and 3 min duration Further layer thickening of the titanium film would take place for 10, 15 and 20 min The TiN deposition time would be 1, 2 and 3 min The RF bias during titanium and TiN deposition would be 0, 10 and 20W The plastic substrate would be RF etched for periods of 40, 60 and 80 min at 80W. Table 5 1 relates to the factors and their levels in the Taguchi experiments The 18 experiments of the Taguchi experiment were carried out and the resulting films graded

visually with respect to cracks, crazing and colour. The factors optimised for reduced stress cracking and increased wear resistance are outlined in Table 5 1 Validation studies were carried out using the optimised parameters The resulting films were golden in appearance and free from cracking However, Scotch tape tests showed that adhesion to PC had not been optimised Having achieved ability to deposit stress-free Ti-TiN layers the problem of adhesion was addressed

5 2 2 Preliminary Investigation

A preliminary investigation, prior to the designed experiment, was undertaken to identify those parameters which might have a bearing on adhesion Oxygen was added to the etching process and also during the deposition of the initial titanium layer Some improvement in adhesion was seen with oxygen (10%) added to the initial titanium layer An interface of aluminium on the plastic improved the appearance and reflectivity of the overall coating In the case of the PC substrate, etched with 80 RF power, the aluminium interface produced a film with a matt finish However, the deposit is mirror like when flat glass is the substrate Evidently the etching process increases the surface roughness of the PC It also tends to increase the adhesion of the Ti-TiN layers If the same level of RF power is used for a shorter time simultaneously with an external heat source, such that the overall maximum substrate temperature is unchanged, layer reflectivity improves but adhesion is compromised When aluminium as an interface is used in the latter case, adhesion improves and reflectivity remains unchanged

5 2 3 The Deposition of Ti-TiN on Polycarbonate

Those parameters thought to be important for improving the film substrate adhesion are as follows the inclusion of aluminium as an interface layer, the use of 10% oxygen in the initial aluminium and initial titanium layers, and the temperature prior to deposition as controlled by the duration of the 80W etch Three levels of each of the four factors were used, yielding an L9 Taguchi experiment. The factors and their levels are outlined in Table 5.2 The adhesion of

the coatings onto the plastic was tested with the Scotch tape test. The reflectivity of the overall coating was judged under the attributes bad, good and very good The optimised parameters were, a substrate temperature of 45°C before deposition, a 30 sec deposition (at 3A) of aluminium onto the PC in the absence of oxygen and the inclusion of 10% oxygen in the initial titanium layer The resultant coatings were adherent, passing Scotch tape tests The reflective Al-Ti-TiN coatings were golden coloured thin films. Another set of coated PC pieces were produced as described above but excluding the aluminium interface. Such coatings passed the tape test but were not as reflective in their finish A photograph of these films is displayed in Fig 5 1

Figure 5.2(a) shows the cross-section of the TiN coating on PC containing the aluminium interface The morphology is dense with the interface layers clearly evident. On fracturing the coated PC sample the film readily cracked The PC sample coated with Ti-TiN, using high bias when etching, was prepared for scanning electron microscopy (SEM) investigation Figure 5 2(b) shows the SEM cross-section of the matt-finished PC-Ti-TiN film. This sample did not crack on SEM preparation The matting effect is due to scattering of incident light on the rough surface The stress-relieved nature of the coating again emanates from an open morphology and rough topography Further tests were carried out on these two coatings in an attempt to understand better the relevance of the differing morphologies Test results are summarised in Table 5 3 Using the eraser method (described in Chapter II) the PC-Ti-TiN material was three times more wear resistant than the PC-Al-Ti-TiN material as outlined in Fig 5.3 In general, the wear scars produced on the Al-PC interface were cracked, indicating that spalling and delamination of the interface occurred The latter probably accounts for the poor performance of this material in wear testing experiments It was difficult to obtain any meaningful results on hardness of these films because of the plasticity of the PC substrate No significant correlations were possible between abrasive wear resistance and hardness of these deposits

It has been demonstrated that thin TiN layers can be deposited onto clear polycarbonate plastic However, the simple deposition of TiN onto PC is not readily achievable but it can be produced by the techniques outlined above The role of the interface film plays a dominant part in the overall characteristics of the multilayer film It is clear that the aluminium layer enhances the reflective and cosmetic properties of the film but compromises the thermal, chemical and environmental stability of the overall composite coating.

Fig. 5.1 Photograph: (bottom left to right), TiN-Ti-Al on PC and TiN-Ti on PC. The top row of samples is ismply the obverse of the bottom row. The reflective Al interface is clearly visible.

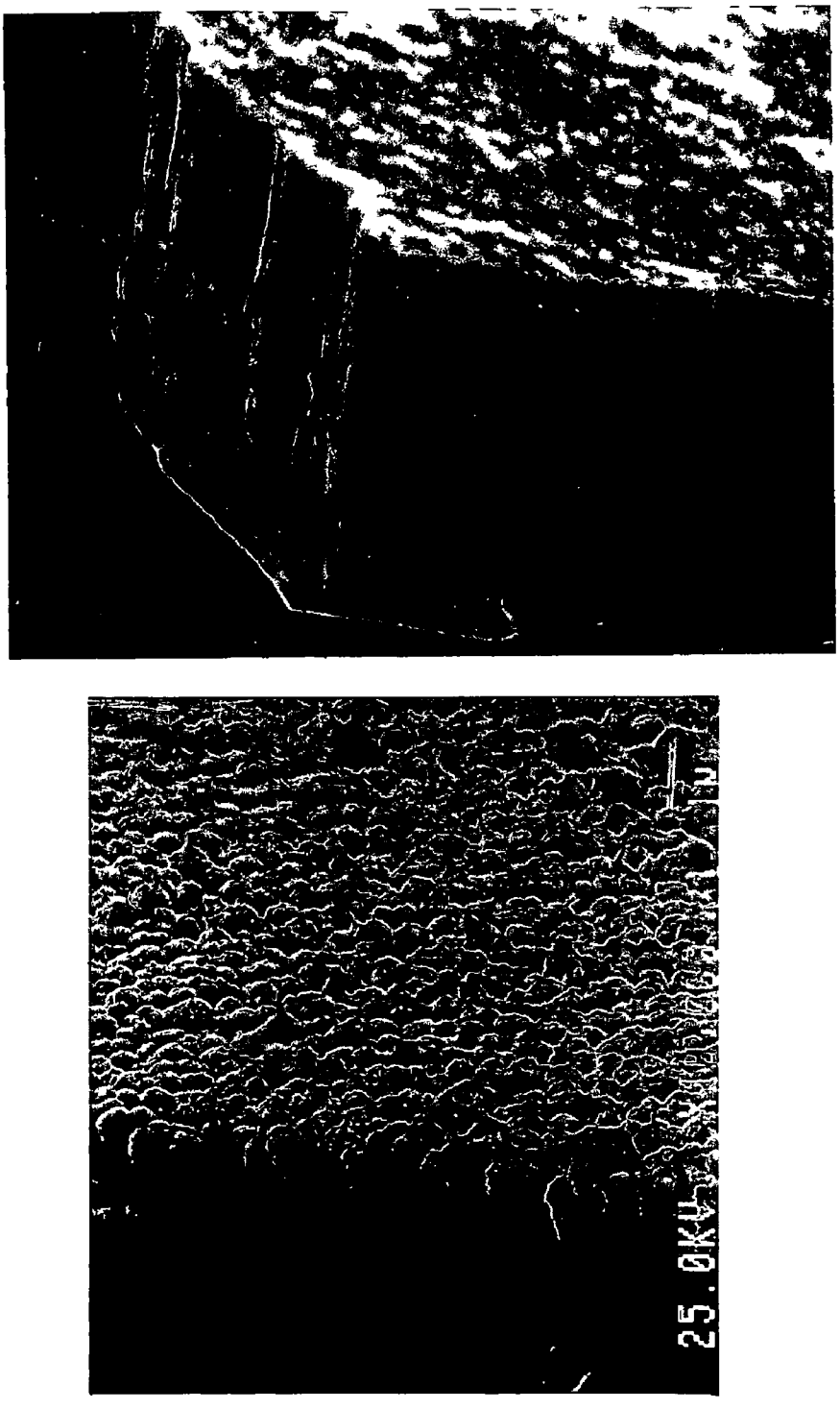

Fig 5.2 Scanning electron micrographs of cross-sections of TiN-Ti-Al on PC (upper micrograph) and TiN-Ti on PC (lower micrograph)

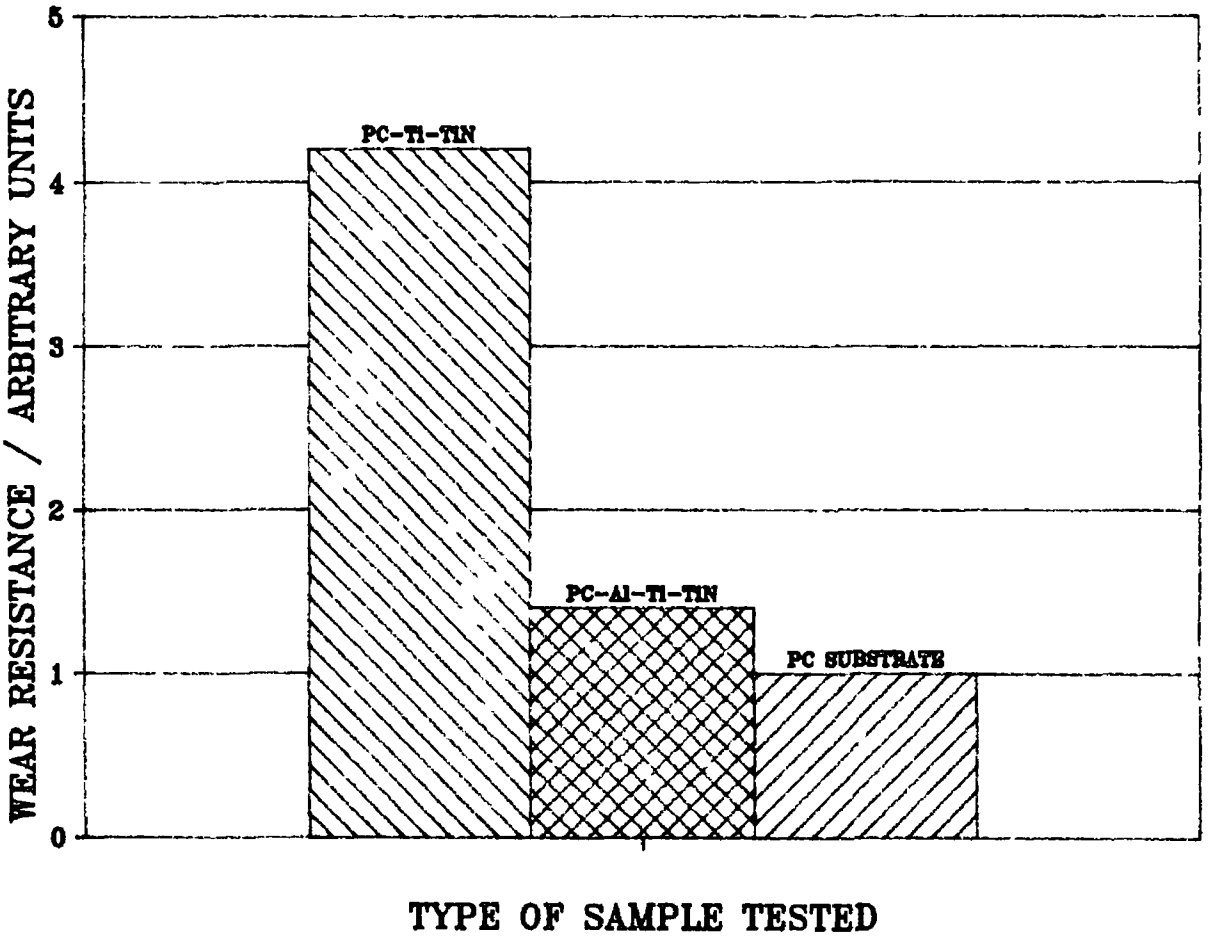

Fig 5 3 Wear resistance of PC-Ti-TiN and PC-Al-Ti-TiN films relative to the substrate PC Wear was assessed via the erasor method

EXP / FACTOR	1 ,2 ,3	4 ,5 ,6	7 ,8 ,9	10,11,12	13,14,15	16,17,18
A	1 ,1 ,1	1 ,1 ,1	1 ,1 ,1	2 ,2 ,2	2 ,2 ,2	2 ,2 ,2
B	1 ,1 ,1	2 ,2 ,2	3 ,3 ,3	1 ,1 ,1	2 ,2 ,2	3 ,3 ,3
C	00,10,20	00,10,20	00,10,20	00,10,20	00,10,20	00,10,20
D	00,10,20	00,10,20	10,20,00	20,00,10	10,20,00	20,00,10
E	10,15,20	15,20,10	10,15,20	20,10,15	20,10,15	15,20,10
F	8 ,10,15	10,15,8	15,8 ,10	10,15,8	8 ,10,15	15,8 ,10
G	1 ,2 ,3	3 ,1 ,2	2 ,3 ,1	2 ,3 ,1	3 ,1 ,2	1 ,2 ,3
H	40,60,100	100,40,60	100,40,60	40,60,100	60,100,40	60,100,40

A = MAGNETRON CURRENT IN AMPS
B = TiN DEPOSITION PERIOD IN MINS
C = RF BIAS (WATTS) DURING TiN DEPOSITION
D = RF BIAS (WATTS) DURING Ti DEPOSITION
E = Ti DEPOSITION PERIOD IN MINS
F = TOTAL PRESSURE x(0.001) MBAR
G = INITIAL Ti DEPOSITION TIME (MINS)
H = INITIAL PERIOD (MINS) FOR 80W RF ETCH

USING THE ERASER TEST AND A VISUAL INSPECTION ON CRAZING THE OPTIMISED PARAMETERS DETERMINED ARE THE FOLLOWING.

A = MAGNETRON CURRENT 1 AMP
B = TiN DEPOSITION PERIOD 1 MIN
C = 10W RF BIAS DURING TiN DEPOSITION
D = ZERO RF BIAS DURING Ti DEPOSITION
E = Ti DEPOSITION PERIOD 15 MINS
F = TOTAL PRESSURE 015 MBAR
G = INITIAL Ti DEPOSITION TIME 2 MINS
H = INITIAL PERIOD OF 60 MINS FOR 80W RF ETCH

Table 5 1 Taguchi array for Ti-TiN on polycarbonate

EXP / FACTOR	1	2	3	4	5	6	7	8	9
A	43°C	43°C	43°C	65°C	65°C	65°C	80°C	80°C	80°C
B	0%	0%	10%	0%	0%	10%	0%	0%	10%
C	0%	10%	25%	10%	25%	0%	25%	0%	10%
D	15 SEC	0 SEC	30 SEC	30 SEC	15 SEC	15 SEC	0 SEC	30 SEC	15 SEC

A = SUBSTRATE TEMPERATURE BEFORE Ti DEPOSITION
B = LEVEL OF OXYGEN IN INITIAL AL LAYER (V/V)
C = LEVEL OF OXYGEN IN INITIAL Ti LAYER (V/V)
D = TIME FOR AL DEPOSITION (3 AMPS)

USING THE ERASER TEST AND A VISUAL INSPECTION ON COSMETICS THE OPTIMISED PARAMETERS DETERMINED ARE THE FOLLOWING·

A = SUBSTRATE TEMPERATURE BEFORE Ti DEPOSITION OF 43°C
B = ZERO LEVEL OF OXYGEN IN INITIAL AL LAYER (V/V)
C = 10% (V/V) OXYGEN IN INITIAL Ti LAYER
D = 30 SEC OF AL DEPOSITION (3 AMPS)

Table 5 2 Taguchi array for Ti-TiN on polycarbonate focusing on improving adhesion of the layer to the plastic

PHYSICAL TESTING

Ti/TiN	LOW	POROUS COLUMNAR	+	+	+	+	+
Al/Ti/TiN	HIGH	DENSE COLUMNAR	+	-	-	+	-
TESTING PROCEDURE	REFLECTIVITY	MORPHOLOGY	SCOTCH TAPE	WEAR	WATER 100°C	CO2 ICE	LIQUID NITROGEN

RESISRANCE AGAINST CHEMICAL ATTACK

Ti/TiN	-	-	+	+	+	+
Al/Ti/TiN	-	-	-	+	+	-
TESTING PROCEDURE	NaOH 20% W/W	CH3COOH CONC	SALT SPRAY	HCl CONC	H2SO4 CONC	HNO3 CONC

"+".....TEST PRESENTED NO EFFECT ON LAYERS

"-".....TEST HAD DETRIMENTAL EFFECT ON LAYERS

Table 5 3 Summary of test results

CHAPTER VI

CONCLUSIONS

The deposition of stoichiometric TiN films on HSS at 420-480°C, using the indirectly cooled magnetron configuration, has been achieved. The adhesion of the TiN to the steel is improved by the formation of a graded interface The latter is generated, firstly, by the overlap of the pretreatment etch with the initial phase of Ti formation. In the second instance, the feedback control mechanism facilitates the generation of a graded interface at the Ti/TiN boundary by slowly admitting the N_2 gas to the appropriate level SEM, EPMA and dynamic SIMS investigations provide evidence for the existence of such interfaces The computer controlled feedback system permits the deposition of stoichiometric TiN films by maintaining a constant partial pressure of N_2 gas in the chamber. This level of nitrogen gas is ascertained from the magnetron poisoning curves The bias voltage and total pressure affect the hardness of the films The wear resistance of the films is influenced by the hardness of the TiN layers and, hence, consequently by the bias voltage and total pressure during deposition (at these substrate temperatures and deposition rates)

The influence of the type of magnetron (i.e. ICM or DCM) target configuration was investigated with a view to depositing TiN at approx 250°C on an uncooled steel substrate The limitations of the ICM, in this application, were identified as (i) large radiative heating effect on the substrate, (ii) insufficiently high levels of ion current to the biased substrate and (iii) in order to deposit at low substrate temperatures, reduced target power was necessary, which consequently reduced the sputtering rate The DCM configuration allowed deposition of adherent, stoichiometric TiN films at approximately 250°C The advantages of the DCM were. (i) low substrate deposition temperature, (ii) high deposition rates, (iii) high substrate ion currents at low bias potentials and (iv) compared to the ICM device, control of target poisoning and stoichiometric TiN production was facile The operating characteristics of the ICM and DCM configuration were different, particularly, in the case of the magnetic field confinement of the target The changes in the magnetic field of the DCM permit the greater levels of ion current observed, compared to the ICM The TiN films produced at the lower substrate temperature by the DCM method were different than those produced by the higher ICM configuration. In particular TiN films produced from the DCM device were softer and

contained both TiN and Ti_2N phases whereas only single phase TiN was observed in the case of films formed from the DCM configuration. The ability to deposit TiN at reduced substrate temperatures was achieved through the use of the DCM

The DCM technique was then employed to deposit a golden coloured TiN film on clear polycarbonate plastics using a designed experimental approach The stresses in the TiN layer were reduced by reducing magnetron power and increasing deposition pressure which resulted in an open film morphology The adhesion of the film to the plastic was improved by (i) the use of an aluminium interface layer and (ii) the addition of oxygen to the initial phase of the Ti deposit prior to TiN deposition A reflective coating was deposited with method (i) above, but a matt-finished film resulted from deposition method (ii) Results of physical and chemical testing of these films indicated that the Al-Ti-TiN layers were not as robust as the set of Ti-TiN films However, both types of coating afforded the PC plastic some wear protection

RECOMMENDATIONS FOR FURTHER WORK

The following achievements have been outlined in this thesis·

(a) Deposition of hard, wear resistant TiN on HSS at 480^{o}C

(b) Control of TiN stoichiometry

(c) Control of graded interface formation

(d) Deposition of TiN at 250^{o}C approximately

(e) Deposition of Ti-TiN layers on plastic at 100^{o}C approximately

The trend in modern thin film deposition is towards lower substrate deposition temperatures, more adherent films and films with given preferred orientations Based on the investigations presented here, certain future work can be identified At present, the reactive deposition of indium-tin-oxide with surface conductivity approx 1 ohm/square, on substrates heated to 70^{o}C is difficult. In this application substrates would include clear plastic and glass Clearly, many of the deposition methods outlined in this thesis would be useful for such investigations In another development, piezo-electric films, with preferred crystal orientation perpendicular to the substrate surface, are required on metal and ceramic substrates High deposition rates and consistent crystal texture are required The results from the DCM target system suggest that this configuration may be useful for the above application.

The work to date has been on flat 2 dimensional substrates, these investigations should be extended to substrates with 3 dimensional geometry

The control feedback system may allow the high rate deposition of aluminium oxide, titanium dioxide or silicon dioxide from a metal magnetron target.

REFERENCES

1 W R Grove, Phil Trans Roy Soc London, 142, (1952), 87
2 L Holland "The Vacuum Deposition of Thin Films", J Wiley & Sons, Inc , New York, 1956
3 L I Maissel, "Physics of Thin Films", Vol 3, Academic Press Inc , New York, 1966
4 K L Chopra, "Thin Film Phenomena", McGraw-Hill, New York, 1969
5 A S Penfold, Thin Solid Films, 171, (1989), 99
6 S Rossnagel, Thin Solid Films, 171, (1989), 125
7 L I Maissel and R Glang "Handbook of Thin Film Technology", McGraw-Hill Publications, 1970, Chapter 2
8 F F Chen "Introduction to Plasma Physics", Plenum Press, 1974
9 M Nelkon and P Parker "Advanced Level Physics", Heinemann, London, 1977
10 S Hofmann, Thin Solid Films, 191, (1990), 335
11 W D Munz and J Gobel. Surf Eng Vol 3 No 1, (1987), 47
12 P W Atkins "Physical Chemistry", Arrowsmith, Bristol, 1978
13 J A Venables, G D T Spiller and M Hanbucken, Rep Prog Plys 47, (1984), 399
14 R E. Thin in "Physics of Thin Films", Ed. G Hass, Academic Press, Vol 1, 1963
15 K L Chopra and M R Roundlett, J Appl Phys , 39, (1968), 1874
16 J.A Thornton, Ann Rev. Mat Sci , 7, (1977), 239
17 J A Thornton, J, Vac Sci Technol , Vol 11 No 4, (1974), 666
18 D W. Hess, J Vac Sci. Technol , A8(3), (1990), 1677
19 R D Arnell and D G Teer, Thin Solid Films, 84, (1981), 281.
20 D G Teer and B L. Delcea, Thin Solid Films, 54, (1978), 295
21 D M Mattox and G J Kominiak, J Vac Sci Technol , 9, (1972), 528
22 H E Winter and E J Kay, J Appl Phys , 38, (1967), 3928
23 D M Mattox, J Vac Sci Technol , 10, (1973), 41
24 M Lardon, R Buhl, H Singer, H K Puliter and E Moll, Thin Solid Films, 54, (1978), 317
25 J A Thornton and D W Hofmann, Thin Solid Films, 171, (1989), 5
26 D S Rickerby, B A Bellamy and A M Jones, Surf Eng , Vol 3 No 2, (1987), 138
27 A J Perry and M Jagner, Thin Solid Films, 171, (1989), 197
28 F M d'Heurle and J M E Harper, Thin Solid Films, 171, (1989), 81
29 E Klokholm and B S Berry, J Electrochem Soc , Vol 115, No 8, (1968), 823

30 A G. Evans, G B Crumley and R E Demaray, Materials Research Society Symposia Proceedings, Vol 54, (1983), 193

31 H K Pulker, "Coatings on Glass", Elsevier, Amsterdam, 1984

32 B M Kramer, Thin Solid Films, 108, (1983), 117

33 C Quaryhaegens, L M Stals, M Van Strappen and L DeSchepper, Thin Solid Films, 197, (1991), 37

34 D M Mattox in, "Deposition Technologies for Films and Coatings", Ed R F Bunshah, 1988

35 H K Pulker, A J Perry and R Berger, Adhesion and Surface Technology, 14, (1981), 25

36 G J Kominiak and D M Mattox, Thin Solid Films, 40, (1977), 141

37 J E Sundgren and H T G Hentzell, J Vac Sci Technol , A4(5), (1986), 2259

38 E A. Almond, Vacuum, 34, (1984), 835

39 M Kornmann, H Schackner, R Funk and B Lux, J Cryst Growth, 28, (1975), 259

40 T Takahashi and H Mamiya, J Cryst Growth, 26, (1974), 203

41 W A Brainard and D R Wheeler, Thin Solid Films, 63, (1979), 363

42 U Helmersson, B O Johansson, B E Sundgren, H T G Hentzell and P Billgren, J Vac Sci Technol , A3(2), (1985), 308

43 J Valli, U. Makela, A Matthews and V Murawa, J Vac Sci. Technol , A3(6), (1985), 2411

44 M Van Strappen, B Malliet, L DeSchepper, L M Stals, J P Celis and J Roos, 7th IPAT Meeting, Geneva, Ed CEP Consultants, Edinburgh, 1989, 209-212

45 R L Hatschek, American Machinist Special Report, 752, (1983), 128

46 M Wittmer, B Studer and H. Melchior, J Appl Phys , 52, (1981), 5722

47 M A Nicolet, Thin Solid Films, 52, (1978), 415.

48 T Shikama, H Araki, M Fuitsuka, M Fukutomi, H Shinno and M Okada, Thin Solid Films, 106, (1983), 185

49 A Mumtag and W H Class, J Vac Sci Technol , 20, (1982), 345

50 E Valkonem, T Karlsson, B. Karlsson and B O Johansson in "Thin Film Technologies", Proc Soc Photo-Opt Instrum Eng , (1983), 401

51 L E Toth "Transition Metal Carbides and Nitrides", Academic Press, New York, 1971

52 J E Sundgren, Thin Solid Films, 128, (1985), 21.

53 K Nakamura, K Inagava K Tsurvoka and S Komiya, Thin Solid Films, 40, (1977), 155

54 A Matthews and D G Teer, Thin Solid Films, 73, (1980), 367

55 W Fleisher, D Schulze, R Wilberg, A Lunk and F Schrade, Thin Solid Films, 63, (1979), 347

56 M K Hibbs, B O Johansson, J E Sundgren and U Helmesson, Thin Solid Films, 122, (1984), 115

57 J L Vossen and J J Cuomo in "Thin Film Processes" Ed J L Vossen and W Kern, Academic Press, 1978

58 R Manory, Surf Eng Vol. 3 No 3, (1987), 233

59 W D Munz, D Hofmann and K Hartig, Thin Solid Films, 96, (1982), 79.

60 R McNulty and M Ahern, Donnelly Mirrors Ltd , Confidential Report No 31, 1988

61 R P Howson, A G Spencer, K Oka and R.W Lewin, J Vac Sci Technol , A7(3), (1989), 1230

62 S Schiller, G Beisler, S Schneider and W Sieber, Thin Solid Films, 83, (1981), 253

63 W D Sproul, P J Rudnik and C A Gogal, Thin Solid Films, 171, (1989), 171

64 L Maissel and R. Glang, "Handbook of Thin Film Technology", McGraw-Hill, New York, 1970. p 1 22

65 B Window and N Savvides, J. Vac Sci Technol , A4(2), (1986), 196.

66 H Boving and R Rocchi, Societe Suisse De Chronometrie, Communication 14, 22/23, Sept 1978

67 A Thomas, Surf Eng Vol 3 No 2, (1987), 117

68 M Nishibori and K Kinosita, Thin Solid Films, 48, (1978), 325

69 Metals Handbook Vol II, Nondestructive Inspection and Quality Control, 8th Edition, 1976 The American Society for Metals

70 P J Burnett and D S Rickerby, Surface Eng , 3, No 1 , (1987), 69

71 P F Bowden and D Tabor, "Friction and Lubrication of Solids", Oxford Claredon Press, Part II, 1964

72 B Lawn and R Wilshaw, J Materials Science, 10, (1975), 1049

73 H Bueckle, Metall Reviews, 4, (1959), 49

74 "Microindentation Techniques in Materials Science and Engineering", ASTM Specification Publication No 889, Philadelphia, PA/USA, 1986

75 V E Lysaght and A DeBellis, "Hardness Testing Handbook - American Chain and Cable Co Inc ", 1969-1974, p 87

76 M Tagaki, N Nishibori and K Kinosita, Thin Solid Films, 51, (1978), 13
77 R D Arnell, Surface and Coating Technology, 43/44, (1990), 674
78 A Matthews and A R Lefkow, Thin Solid Films, 126, (1985), 283
79 W D Sproul, Thin Solid Films, 107, (1983), 143
80 W D Sproul, Thin solid Films, 118, (1984), 279
81 M Kodama and R F Bunshah, Thin Solid Films, 96, (1982), 53
82 M Wittmer, J Vac Sci Technol , A3, (1985), 1797
83 R Manory and A Gill Plating Surf Finishes, 13, (1986), 68
84 A Okamoto and T Serikawa, Thin Solid Films, 137, (1986), 143
85 Robert B Ross, "Metallic Materials Specification Handbook", Published by E & F N Spon Ltd , 1980
86 B Jonsson and S Hogmark, Thin Solid Films, 114, (1984), 257
87 P J Burnett and D S Rickerby, Thin Solid Films, 148, (1987), 41
88 P A Steinmann, Y Tardy and H E Hintermann, Thin Solid Films, 154, (1987), 333
89 A J Perry, Thin Solid Films, 107, (1983), 167
90 J Valli, J Vac Sci Technol , A4, (1986), 3007
91 A J. Perry, Surf Eng , 2, (1986), 183
92 H Freller and H P Lorenz, "Plasma Surface Engineering", Vol 2, (1988), 687
93 R D Arnell in " Tribology Principles and Design Applications", Macmillan, 1990
94 J S Chapin, Res Dev 25, (1974), 37
95 R K Waits, in "Thin Film Processes", J L Vossen and W Kern (eds), Academic Press, New York, 1978, 75
96 J A Thornton, J Vac Sci Technol , 15, (1978), 171
97 J A Thornton and A Penfold in J L Vossen and W Kern (eds), "Thin Film Processes", Academic Press, New York, 1978, 76
98 S L Rohde, I Petrov, W D Sproul, S A Barnett, P J Rudnick and M E Graham, Thin Solid Films, 193/194, (1990), 117
99 T Van Vorous, Solid State Technol , 12 (1976), 62
100 H M Gabriel, in T Takagi (ed), Proc Int Ion Engineering Congr , Kyoto, Sept 12-16, (1983), 1311
101 A Matthews and H A Sundquist, in T Takagi (ed), Proc Int Ion Engineering Congr , Kyoto, Sept 12-16, (1983), 1325
102 M Kobayashi and Y Doi, Thin Solid Films, 54, (1978), 67

103 B O Johansson, J E Sundgren, J E Green, A Rockett and A Barnett, J Vac Sci Technol , A(3), (1985), 303

104. M H. Francombe, in J W Matthews (ed), Epitaxial Growth, Academic Press, New York, 1975

105 O Knotek, M Atzor and F Jungblut, in "Plasma Surface Engineering", Vol 1, 1988, p 579

106 H Erhart, S Bastian and H Petersen, in "Plasma Surface Engineering", Vol 1, 1988, p 603

107 D G Teer and R D Arnell, Recent Developments in Surface Coating and Modification Processes, Tribology Group of the Institute of Mechanical Engineers, London, 1985, p 21

108 D G Teer and P A Higham, Thin Solid Films, 58, (1979), 121

109 S Aisenburg and J Chabot, J Appl Phys , 42, (1971), 2953

110 C Weissmantal, Thin Solid Films, 63, (1979), 315

111 R Bunshah and A C Raghuran, J Vac Sci Technol , 9, (1972), 1385

112 L J Zilko and J E Green, J Appl Phys , 51, (1981), 1549

113 R F Bunshah, Thin Solid Films, 107, (1983), 21

114 G Z Yin and D W Jillie, Solid State Technol , 5, (1987), 127

115 T M Pang, M Scherei, B Heinz, C Williams and G N Chaput, J Vac Sci Technol , A7(3), (1989), 1254

116 H R Koening and L I Maissel, IBM J Res Dev 14, (1970), 168

117 H S Butler and G S Kino, Phys Fluids, 6, (1963), 1346

118 G S Anderson, W.N Mayer and G K Wehner, J Appl Phys 37, (1966), 574

119 I V Kragelsky, M N Dobychin and V S. Kombalov in "Friction and Wear" Pergamon Press Ltd ISBN 0-08-025, 461-1, 1977

120 D H Buckley in "Surface Effects in Adhesion, Friction Wear and Lubrication" Elsevier Scientific Publishing Company, ISBN 0-444-4 1966-7, 1981

121 M M Khrushcov and M A Babichev "Investigation of the Wear of Metals" Acad Sci USSR, Moscow p 351, 1960

122 P J Mutton and J D Watson, Wear, 48, (1978), 385

123 R Cortellucci Wear. 47, (1978), 397

124 A D Sarkar, Friction and Wear, 1980, (Academic Press).

125 J G A Bitter, Wear, 6, (1963), 5

126 G P Tilly, Wear, 23, (1973), 87

127 G L Sheldon and A Kanhere, Wear, 21, (1972), 195

128. H H Uhlig, J Appl Mech , 21, (1954), 401

129. R C D Richardson, Wear, 11, (1968), 245

130 R P Steijn "Sliding Wear and Metal Transfer under Unlubricated Conditions" Trans ASME, Ser D. 18, No 159, 67-77

131 A K Vijh, Wear, 39, (1976), 173

APPENDIX A

GLOW DISCHARGE PHENOMENA RELEVANT TO DIODE SPUTTERING

A 1 THE DC GLOW DISCHARGE

An understanding of the processes that occur within the self sustained glow discharge is vital for the design and interpretation of sputtering experiments Argon gas is mainly used for such purposes, and the predominant collision process responsible for charge carrier generation is that which occurs between a fast electron (whose kinetic energy >15 76 eV, the ionisation energy for Ar) and a neutral Ar atom, viz ,

$$Ar + e^-(fast) \longrightarrow Ar^+ + e^-(slowed) + e^-(slow) \qquad A.1\ 1$$

In the presence of an electric field the two slow electrons produced are accelerated and engage in further ionising collisions This avalanche effect results in the generation of an abundance of positive ions and electrons which are able to migrate through the gas discharge and thereby carry current The avalanche is known as gas breakdown, and is marked by an abrupt drop in the voltage required to carry a given current, Fig A 1 The luminous regions are called the negative glow and positive column, their colour spectrum being typical of the excitation gas The gas discharge can be visualised as consisting of an aggregate of relatively fast mobile electrons, and relatively slow, immobile ions and gas atoms The Crook's dark space, Fig A 1, consists of an abundance of positive ions, combined with a relative sparcity of electrons In this region, the cathodic potential has electrostatically repulsed the mobile electrons leaving behind the positive ions In effect, the cathode voltage is screened off by the positive ion cloud, resulting in a large potential drop across this region The latter description combined with the low potential drop across the remainder of the tube, Fig A 1, imply that the glow regions are excellent conductors The so-called plasmas tend, on average, to be electrically neutral, containing an equal concentration of positive and negative charge and unable to support an electric field gradient A typical DC gas discharge used in a sputtering process will contain a concentration of N_1, of 10^9 to 10^{10} ions per cm^3 and an equal number of electrons in the plasma region At 60 mbar pressure, the unexcited gas contains $N_o \sim 2 \times 10^{15}$ atoms cm^{-3} thus the fractional degree of ionisation is of the order of $N_1/N_o \sim 5 \times 10^{-6}$ which is very dilute

The large voltage drop which occurs across the cathode dark space causes the acceleration of positive ions which enter this region by diffusion from the negative glow This ion bombardment causes an atom-by-atom ejection of the cathode (or target) material The sputtering process occurs by virtue of momentum transfer between the impacting ion and the target lattice atom, Fig A 2 The incoming inert ion is Auger neutralised and may recoil from the target surface with appreciable energy The sputtered atom leaves the target surface with 3 to 10 eV of energy (compared to the thermal evaporation situation where evaporated atoms have 0 03 eV) The neutralised bombarding ion and sputtered target atom are deposited on the substrate surface, placed so as to intercept the coating flux In general, most target materials are polycrystalline and so a randomisation of trajectories of sputtered atoms takes place

Several other events occur at the cathode surface The bombarding ions dissipate in excess of 90% of their kinetic energy in the form of heat (which necessitates water cooling of the target) The rapid deceleration of the bombarding ions upon striking the cathode results in the emission of a broad spectrum electromagnetic radiation, whose shortest wavelengths are given by,

$$\lambda = hc/eV \qquad A\ 1\ 2$$

where V is the dark-space sheath voltage , h is Plancks' constant and c is the speed of light

The events which occur in the dark space involving the slow electrons consist of ionisation of the gas atoms accompanied by further generation of electrons which are subsequently accelerated (i e secondary electrons) At the edge of the dark space an abundance of electrons and positive ions exist This negative glow region comprises particles undergoing excitation collisions resulting in luminescence This plasma region can be considered as

"a quasineutral gas of charged and neutral particles which exhibit collective behaviour"

The motion of particles in plasmas exhibit Maxwellian velocity distributions where the most probable velocity C_o is given by,

$$C_o = (2kT/m)^{1/2} \qquad \text{A 1 3}$$

since a high velocity particle can be characterised as having a high "temperature" (viz , $C_o \propto T^{1/2}$) plasmas are typically described by their electron, ion and neutral atom temperatures The average kinetic energy of a gas is related to the absolute temperature, T, by

$$\frac{mC^2}{2} = 3/2\ kT \qquad \text{A 1 4}$$

If, for example, the kinetic energy of the electrons in a plasma is 1 eV then the electron temperature of that plasma (i e 1 eV - $^3/_2$ kT) is 11,600^o K A typical sputtering plasma would have the following characteristic temperatures, T_e, electron temperature > 25,000^{o}K, T_i, ion temperature = 500^{o}K, T_o, neutral gas temperature = 300^{o}K

DC discharges are inefficient in their use of high energy electrons to cause enhanced ionisation, produce low sputtering rates of 10 to 500 Å/min and generate unnecessary substrate heating from the high energy electrons The high energy secondary electrons can be manipulated by magnetic fields In the 1930's magnetically confined discharges - magnetron discharges - were introduced, and are discussed more fully in the Introduction

A 2 LOW FREQUENCY AC GLOW DISCHARGES

Low frequency AC glow discharges are not often used for sputtering At frequencies up to 50KHz, ions are sufficiently mobile to enable a complete DC discharge to form at each electrode on each AC half-cycle Thus this type of discharge is similar to a DC discharge with both electrodes being alternatively sputtered

A 3 RADIOFREQUENCY (RF) GLOW DISCHARGES

At AC frequencies above 50KHz electrons oscillating in the glow space acquire sufficient energy to cause ionising collisions, thus both reducing the dependence of the discharge on secondary electrons and lowering the gas breakdown voltage [116] In addition, the electrodes may be both insulators and conductors since the RF voltages can be transmitted through any type of impedance At typical RF frequencies of 5-30 MHz, a pulsating, negative voltage can develop on an electrode which is capacitively coupled to the RF generator Due to the substantial differences in mobilities between the ions and electrons, the I-V characteristics of an RF glow discharge resemble those of a rectifier, (Fig A 3) [117] Upon application of the RF potential through the capacitor, an initially high electron current flows to the electrode On the next half cycle only a small ion current can flow The voltage on the electrode surface must self-bias negatively until the net current is zero, since no charge can travel tnrough the capacitor The average DC value of this negative self bias potential is almost equal to the peak RF voltage applied [118] The electrode potential redistribution is understood by considering the equation which relates the ion flux through the sheath (i.e the difference between the floating potential and the plasma potential) to the voltage which develops across the sheath Assuming a space charge limited current, then the ion flux J, is given by the Langmuir-Child relation

$$J_1 = (K\ V^{3/2})/(\sqrt{m}D^2) \qquad \text{A 3 1}$$

where V is the potential across the sheath, D is the sheath length, m is the ion mass and K is a constant If the current density of ions is equal at both electrodes then

$$\frac{V_1^{2/3}}{D_1^2} = \frac{V_2^{3/2}}{D_2^2} \qquad \text{A 3 2}$$

where D_1, D_2 and V_1, V_2 refer to the respective potential differences and the sheath lengths associated with two electrodes of areas A_1 and A_2 The sheath region is associated with a large potential drop and

limited conductivity and can be regarded as having a capacitance given by,

$$C = k\ A/D \qquad A\ 3\ 3$$

where, K is the dielectric constant across the sheath Since the quantity of charged passed = V_1C_1 or V_2C_2, then

$$V_1/V_2 = C_2/C_1 \qquad A\ 3\ 4$$

Rewriting Equn A 3.4 from Equn A 3 3 yields

$$\frac{V_1}{V_2} = \frac{A_2/D_2}{A_1/D_1} = \frac{A_2}{A_1}\ \frac{D_1}{D_2} \qquad A\ 3\ 5$$

Substituting this into Equn A 3 1 gives

$$\frac{V_1^{3/2}}{V_2^{3/2}} = \frac{D_1^{2}}{D_2^{2}} = \frac{(A_1V_1)^2}{(A_2V_2)^2} \qquad A\ 3\ 6$$

or

$$\frac{V_1}{V_2} = \frac{(A_2)^4}{(A_1)^4} \qquad A\ 3\ 7$$

In actual practice, the larger electrode comprises the entire sputtering chamber which has a common electrical ground with the RF generator The smaller target electrode develops a large sheath potential and sputters vigorously, whereas the chamber develops a small sheath potential insufficient to cause sputtering

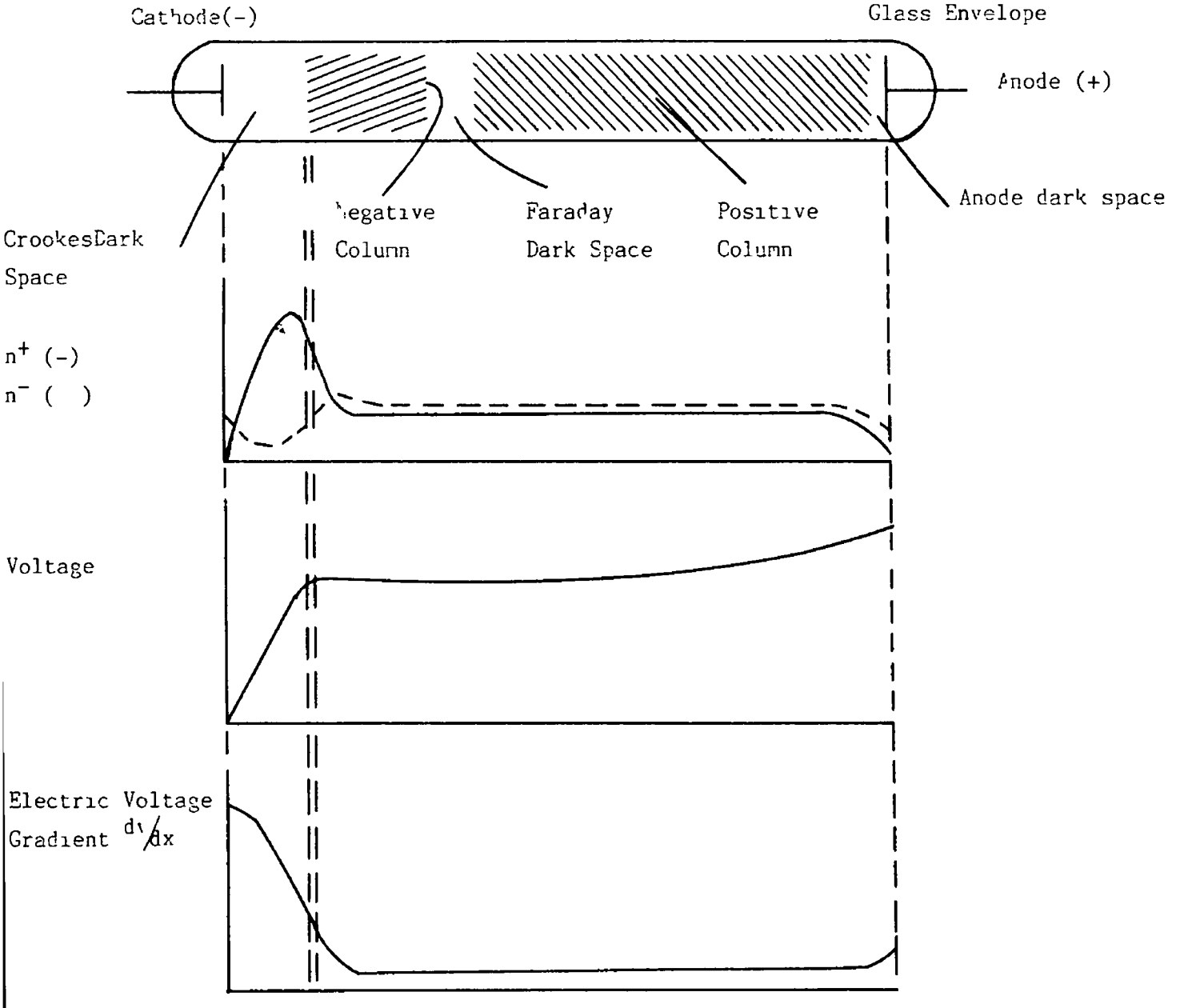

Fig A 1 Schematic representation of a DC glow discharge showing (i) the variation in the number of ions (n^+) and electrons (n^-) with distance from the cathode, (ii) variation of voltage and (iii) variation in the voltage gradient across the discharge (-dv/dx is the electric field E)

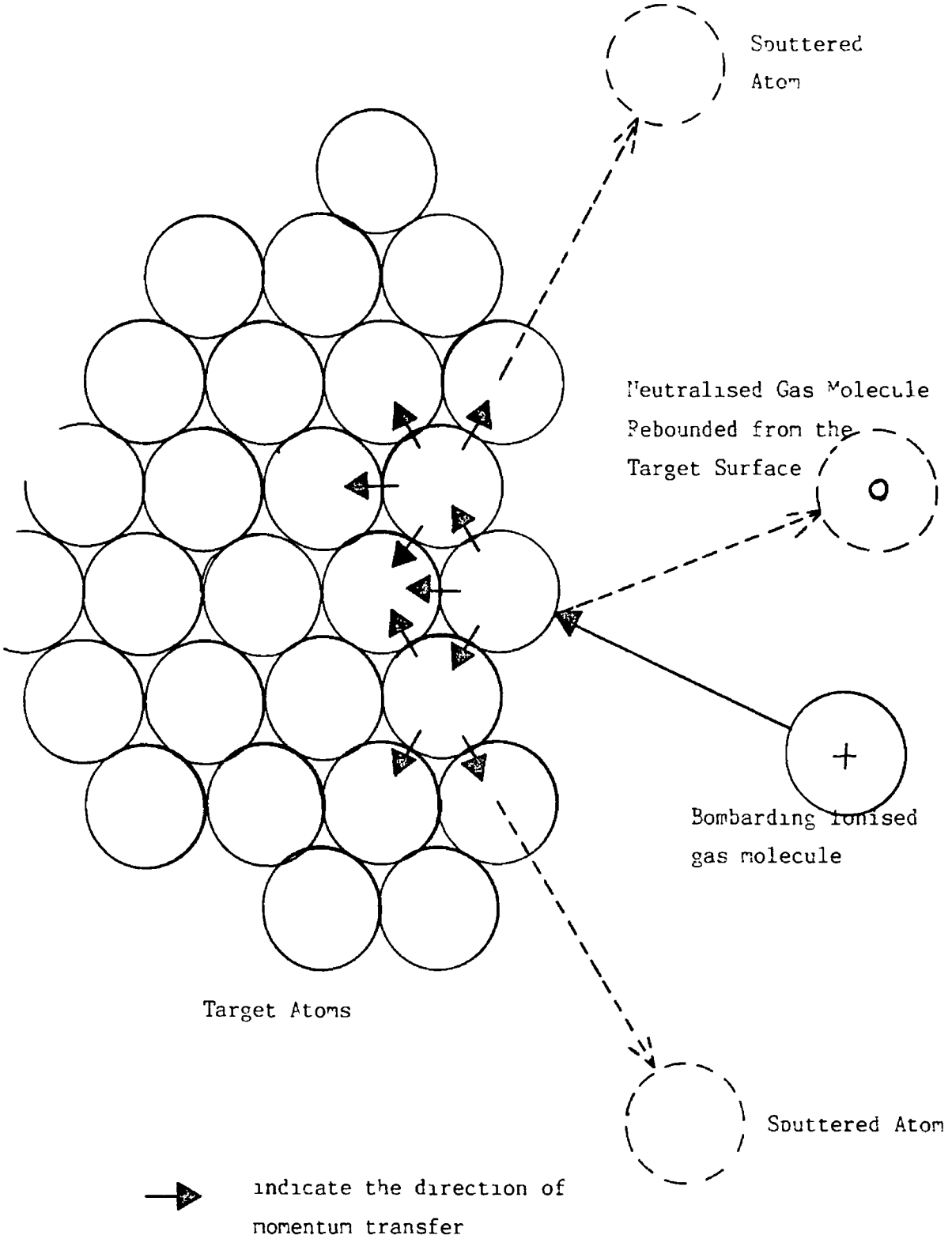

Fig A 2 Collision process responsible for sputtering and fast neutral generation.

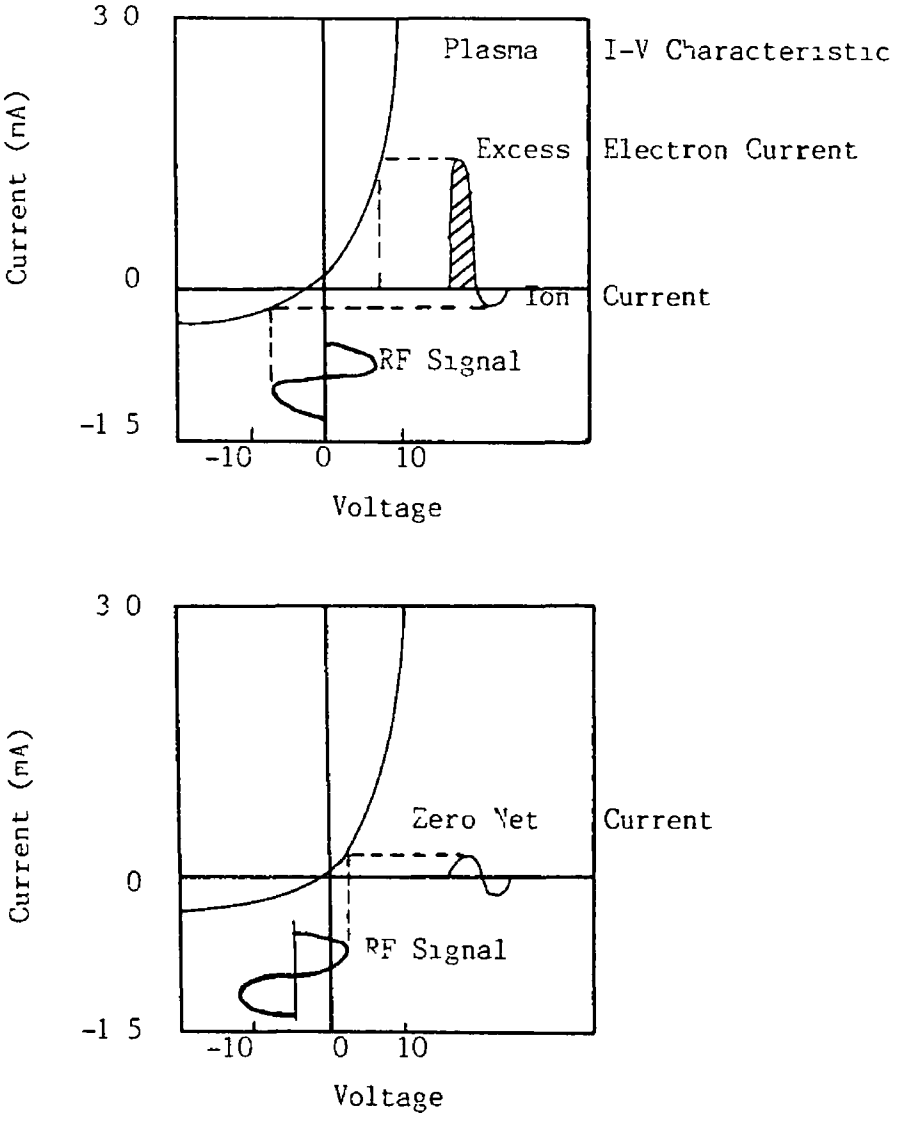

Fig A 3 The formation of a pulsating negative sheath on a capacitively coupled surface in an RF glow discharge

APPENDIX B

AN OVERVIEW OF WEAR PHENOMENA EXPERIENCED IN TRIBOLOGICAL SYSTEMS WITH PARTICULAR REFERENCE TO ABRASIVE WEAR

B 1 TYPES OF WEAR

Wear is the removal of material from one or both of two surfaces in contact It occurs when solid surfaces are in relative sliding, rolling, or rubbing movement [119] The most common types of wear are adhesive, abrasive, corrosive, erosive, fatigue, fretting and cavitation To reduce wear in practical tribological devices it is important to understand and appreciate the various wear mechanisms

B 1 1 Adhesive Wear

When two solid surfaces are placed in solid-state contact, bonding across the interface generally occurs [120] This bonding can be weak when it is simply a physical attraction of one body for another (i e Van der Waal's attraction) It can also be extremely strong e g. where chemical bonding occurs When a load is applied to the two surfaces in contact the probability of strong bonding occurring is enhanced Even with the most effective lubrication, contact occurs through the lubricating films if the forces applied are sufficiently large When two atomically clean surfaces are placed in contact, the attractive forces of the solids for each other are sufficient to produce extremely strong bonds as a result of the electronic interaction of the solid surfaces in the clean state When the surfaces are clean, the entire real area of contact undergoes adhesion. Where the surfaces are covered with a film, whether it is simply a contaminating surface film or a lubricating film, the amount of adhesion decreases In cases where adhesion occurs at the interface and tangential motion is imposed on the surfaces to cause one to move relative to the other, shear takes place rupturing the adhesive bonds at the interface in order to accomplish the tangential motion In practice the bonds seldom rupture at the interface, instead, the bonds of the cohesively weaker material break The latter transfers to the cohesively stronger material This results in adhesive wear [119]

B 1 2 Abrasive Wear

Abrasive wear [75, 120] occurs in practical mechanical operations such as grinding, cutting, and machining The fundamental mechanism involved in the abrasive process is shown schematically in Fig B 1(a) There are generally two methods by which abrasion and abrasive wear can take place The first mode, frequently encountered in industrial material removal processes such as cutting, grinding, and machining an abrasive grit is embedded in a matrix The abrasive grit begins to cut or skive a groove in the workpiece surface and to remove material from the workpiece Generally the grit is a material of high cohesive strength, e g , SiC The second mechanism [119] involves high cohesive strength material (such as silicon dioxide, aluminium oxide, or silicon carbide) becoming trapped as individual particles between two surfaces (as indicated in Fig B 1(b)) Trapped between surfaces A and B is a relatively hard, high atomic density, high cohesive energy material that skives or cuts material from both surfaces

In the study [121, 122] of the abrasive wear process, the properties of the abrasive are as important as the properties of the material being removed The physical characteristics and the chemical composition of the abrasive influence its interactions with the workpiece material Abrasives, in addition to simply removing material from a solid surface, results in that surface having a considerable amount of strain energy The interaction of the abrasive with the solid surface can produce surface cracking even in brittle materials where plastic deformation is less likely The energy supplied to the interface is dissipated in the formation of cracks as opposed to the generation of dislocations Dislocations associated with those materials that are sufficiently ductile to undergo deformation Correlations [71] have been found between the particle size of the abrasive and the depth of damage observed in the abraded material As the particle size of the abrasive increases the depth of damage in the surface is deeper A cohesively weaker material experiences a greater depth of damage than a cohesively stronger material

Polymers are extremely susceptible to abrasive wear because of their relatively weak cohesive strength compared to most other solids. The particle size has an influence on the abrasive wear characteristics of

the polymer [123] The larger the abrasive particle, the greater the amount of material removed from the polymer surface

B 1 3 Corrosive Wear

Corrosive wear occurs when the environment interacts with the surfaces in solid-state contact to produce reaction products that affect the wear characteristics of the materials in sliding, rubbing, or rolling contact [120] This environmental interaction can occur by a number of mechanisms Where the mechanical components are in dry sliding, oxygen from the air or the gaseous species present in the particular environment can interact with the solid surface, the resulting reaction products can cause corrosive wear In addition, the presence of excessive quantities of extreme pressure or anit-wear additives or other chemical agents in lubrication systems can bring about corrosive wear at the interface Even with conventional liquid lubricants, high temperatures can cause excessive reaction of dissolved oxygen in oils with the solid surfaces resulting in corrosive attack of any labile elements present

Corrosive wear is not entirely detrimental The concept of extreme pressure and anti-wear additives is based on the premise that the additive interacts with the solid surface to form reaction products similar to those produced in the corrosive wear situation Typically in the anti-wear and anti-seizure situation the organometallic additive containing S, P, or Cl are intended to decompose and then react at the solid surfaces to form inorganic chloride, sulphide or phosphide films which prevent metal to metal contact

The friction coefficients of the materials in contact influence the corrosive wear The higher the coefficient of friction the greater the amount of energy dissipated at the interface and the greater the surface temperature becomes, thus promoting surface reactivity In addition, the higher the ambient pressure of the gaseous or liquid species which interact with the solid surface, the greater probability of surface reactions occurring

B 1 4 Erosive Wear

Erosive wear is defined as the process of material removal from a surface subjected to impingement attack by solid or liquid media, being particulate in nature for the former and in the form of droplets for the latter [119] Various investigations [119, 120] have attempted to relate the basic properties of materials to their erosive wear behaviour For metals. the binding energy appears to be related to erosive wear resistance The cohesively strongly bonded metals are more resistant to erosive wear than the cohesively weaker bonded metals Polymers are extremely prone to deformation and although cohesively weaker than metals display good erosive wear resistant properties Ceramics experience less erosive wear than metals or polymers [121] The rate of erosive wear depends on the velocity of attack, the angle of impingement and the prior diameter of th impinging particles [124-127]

B 1 5 Fatigue Wear

Fatigue wear occurs by the repeated application of stress which leads to the production of surface and subsurface cracks generating wear particles and resulting in the loss of material from solid surfaces This process can occur in such devices as roller bearings where a crack is observed to initiate either subsurface or in the surface region, the subsurface crack gradually migrates to the surface and liberates a wear particle In relatively homogeneous materials, the initiation of the fatigue cracks can be assisted by dislocation mechanisms. The accumulation of dislocations along the slip or cleavage plane results in the generation and growth of the surface originated fatigue crack. Dislocations can also act in the development of subsurface initiated cracks because of their coalescence to the solid surface with repeated stress cycles, particularly where strain occurs in the material

B 1 6 Fretting

Fretting occurs when surfaces are in oscillatory or reciprocating motion where the amplitude of the oscillation is relatively small Initially the rubbing of two solid surfaces in solid-state contact generally produces a failure because of the adhesive wear in the

materials Adhesive wear debris is generated at the interface which becomes oxidised in the environment because of the excess energy stored in the particle The environment plays a very important role on the wear observed for surfaces which undergo fretting Uhlig [128] has developed a wear law and proposes that fretting wear is proportional to the total number of cycles, the frequency of oscillation and the load

B 1 7 Cavitation

Cavitation wear is the loss of material-surfaces as a result of a stream of liquid containing entrapped gas bubbles impinging the solid surface The impinging liquid brings the gaseous bubbles to the surface at relatively high velocities The bubbles strike the solid surface and collapse on impact Their collapse imposes shock waves on the solid surface and results in the liberation of material from the surface Cavitation wear produces a roughening of the surface similar to the effect of an etchant It is frequently observed, on impellers and propellers where the liquids have impacted near the hub and the vanes

B 2 CHARACTERISTICS OF THE ABRASIVE WEAR PROCESS

In wear the act of rupture is localised in a small volume of material which is removed from the rubbing zone in the form of wear particles The magnitude of the wear is usually judged from the decrease in dimensions of the body in a direction perpendicular to the sliding surface A typical plot of wear versus time of operation indicates the presence of a three stage wear process The first stage, termed running-in wear, is a non-equilibrium stage of the wear process, and represents only a small proportion of the total time of operation of the junction It is characterised by the specific wear rate dQ/dL (where Q is the wear and L the length of the wear track). which falls with time during sliding contact The second stage of the wear process, which is the longest, is characterised by constant values of the wear rate, i e , dQ/dL = constant The third stage, called catastrophic wear, is characterised by increasing wear rate and is not applicable to rubbing surfaces In steady-state conditions of wear the real contact area is constant at any point in time [119] It is assumed that the volume of material δV removed from the surface as wear

particles is proportional to the real contact area, Ar, i e ,

$$\delta V = Ar \qquad B\ 2\ 1$$

The mass wear intensity Ig or volume wear intensity Iv for a rubbing pair are defined [124] as

$$Ig = \delta G/L \qquad B\ 2\ 2$$

$$Iv = \delta V/L \qquad B.2.3$$

where δG and δV are the change in mass and change in volume of the worn material along a sliding part L

A simple abrasive wear law [126] can be obtained by considering the interaction of a hard conical asperity of apex angle, 2θ, penetrating a solid to a depth, h, under a load, δW

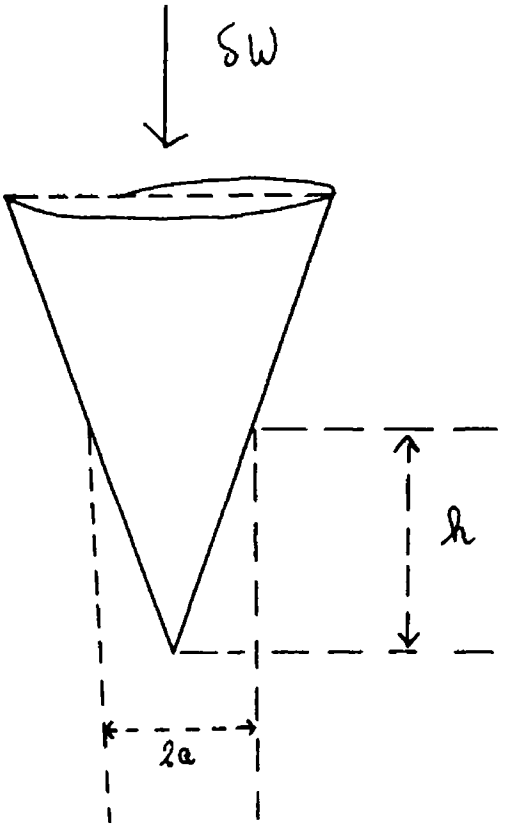

The cone pushes a wall of material ahead of it, producing a volume of wear debris If the length traversed is dL, the volume dV which is removed is

$$dV = \tfrac{1}{2}\, 2a\, h\, dL \qquad \text{B 2 4}$$

where 2a is the diameter of the indentation Since h = a cot (θ),

$$dV = a^2\, dL\, \mathrm{Cot}(\theta) \qquad \text{B 2 5}$$

The load is supported by only half the basal area πa^2 If H is the hardness of the indented material

$$\tfrac{1}{2}\pi a^2 = \delta W/H \text{ or } a^2 = 2\delta W/\pi H \qquad \text{B 2 6}$$

Substituting this value of a^2 into Equation B 2 6

$$dV = \{(2\delta W/\pi H)\, \mathrm{Cot}(\theta)\}\, dL \qquad \text{B 2 7}$$

The rate at which material is removed is dV/dL and

$$dV/dL = (\delta W/H)\ (0\ 63\mathrm{Cot}\ \theta) \qquad \text{B 2 8}$$

By analogy, in the case of the whole surface being abraded by many cones, supporting a total load W, then

$$V/L = (0\ 63\mathrm{Cot}\theta)\ (W/H) \qquad \text{B 2 9}$$

According to this simple abrasive wear law the wear resistance of a material is directly proportional to the load applied and inversely proportional to its hardness Also for a cone, the larger the semi-apex angle θ, the smaller the rate of wear This can be explained since a cone with a larger value of θ is more blunt and a sharp cutting edge is essential for improving ploughing efficiency

When used as an abrasive an initially sharp grit will become blunt because of wear It is commonly perceived that a hard abrasive will retain its sharpness longer than a softer abrasive However, hardness is not always an accurate guide to abrasive wear ability, and for example, quartz is known to be more aggressive than diamond in certain

circumstances [124] Richardson [129] suggests that a ratio Hm/Ha be used to predict the abrasive wear efficiency of grits where Hm is the hardness of the abraded material and Ha is that of the abrasive If the ratio is large, the rate of wear is small but not zero since the may have soft micro-constituents, and also repeated attacks remove surface layers of the abraded material by a fatigue mechanism The ratio Hm/Ha for a steel being abraded by quartz is 0 95 and the latter is known to wear the former successfully Experiments [129] with certain combinations suggest that when the ratio Hm/Ha <0 8, the victim undergoes rapid abrasive wear When Hm/Ha >0 8 a situation of soft abrasive wear is experienced and the abraded material should not undergo abrasive wear when Hm/Ha greater than or equal to unity

Khruschov and Babicher [121] quote the Vickers Hardness (HV) as a parameter capable of characterising the yield stress, Pt. Using pure metals and annealed alloys (with Sn-Pb as standard) they found that

$$H \text{ standard}/H \text{ sample} = \varepsilon = 0\ 127\ HV \qquad B\ 2\ 10$$

It was established that Equation B 2 10 is not universal and that the method of hardening influenced the abrasive wear life For example, it was found that ε varies in a complex fashion for quenched and tempered steels [121] The elastic modulus E was also used as a criterion against which abrasive wear can be evaluated [130] For a wide range of materials, i e , metals, alloys, minerals and solid compounds Khrushchov [121] showed that

$$\varepsilon = (0\ 49\ 10^{-4}\ E^{1\ 3}) \qquad B\ 2\ 11$$

This equation cannot be applied to heat treated steels since E is a structurally insensitive parameter and is virtually independent of heat treatment conditions, whereas heat treatment has a significant effect on the wear resistance of steels Accordingly, E cannot be regarded as a universal criterion of wear resistance

Whereas much emphasis is placed on the hardness of the component and of the abrasives together with the sharpness of their cutting edges, the

effect of particle size does not become obvious in theoretical treatments of abrasive wear processes in metals and non metals Experiments show that up to a certain size, the wear rate rises in a linear fashion with increasing diameter of the abrading particles Characteristically, for a particular friction couple, there is a critical particle diameter beyond which the size of the abradants is ineffective The reasons for the latter are somewhat nebulous In the process of abrading thin films on substrates the diameter of the grit must be of the order of the thickness of the film [19]

An overall increase in abrasive wear resistance with hardness has been reported [121] but this is not in proportion to the hardness values as dictated by the wear laws Wear processes in materials are very complex phenomena and neat trends with variables are not always attainable As far as hardness of the material which is being abraded is concerned it can be stated that abrasive wear resistance increases with increasing hardness

Since both the bond energy and the melting point are measures of cohesive forces in the solid state, there is evidence to demonstrate [131] that abrasive wear resistance can be correlated with bond strength at an atomic level The reason for such encouraging correlations lies in the non-dependence of the bond energy on the presence of small quantities of other elements, however, the latter may influence the hardness of the material

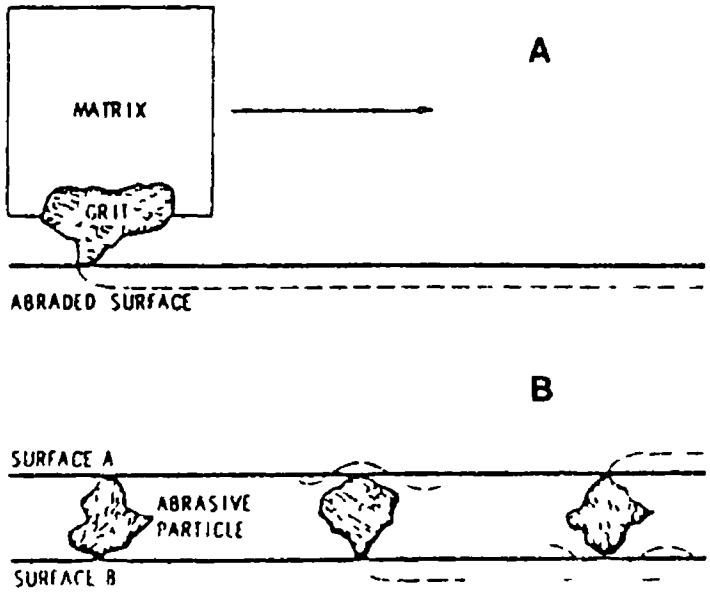

Fig B 1 Abrasive wear mechanism.

PUBLISHED WORK

"The Deposition of TiN at less than 150°C by Reactive Magnetron Sputter Ion Plating" M J Ahern Surface and Coating Technology, 43/44, (1990), 279

"The Role of Deposition Parameters and Adhesion Effects on the Formation of TiN Films on High Speed Steel" M J. Ahern and M S J Hashmi, J Material Processing Technology, Submitted, 1991

"On the Reactive Sputtering of TiN at 450°C Substrate Temperature", M J Ahern and M S J Hashmi, 11th International Conference on Production Research, August 1991, (Ed Prof Ming, Dept of Precision Machinery and Instrumentation, University of Science and Technology of China, Hafai) to be published, 1991

"Comparison of Operating Conditions and TiN Films Produced from Both Directly and Indirectly Cooled Magnetron Targets", M J Ahern and M.S J Hashmi, Surface and Coating Technology, accepted for publication, 1992

"Low Temperature Vacuum Deposition Process", Irish Patent Application No 1186/90